DISSERTATION

PROBABILISTIC FOUNDATION OF NONLOCAL DIFFUSION AND FORMULATION AND ANALYSIS FOR ELLIPTIC PROBLEMS ON UNCERTAIN DOMAINS

Submitted by

Nathanial J. Burch

Department of Mathematics

In partial fulfillment of the requirements

For the Degree of Doctor of Philosophy

Colorado State University

Fort Collins, Colorado

Summer 2011

Doctoral Committee:

Advisor: Donald Estep

Jennifer Hoeting
Richard Lehoucq
Patrick Shipman
Simon Tavener

ABSTRACT

PROBABILISTIC FOUNDATION OF NONLOCAL DIFFUSION AND FORMULATION AND ANALYSIS FOR ELLIPTIC PROBLEMS ON UNCERTAIN DOMAINS

In the first part of this dissertation, we study the nonlocal diffusion equation with so-called Lévy measure ν as the master equation for a pure-jump Lévy process. In the case $\nu \in L^1(\mathbb{R})$, a relationship to fractional diffusion is established in a limit of vanishing nonlocality, which implies the convergence of a compound Poisson process to a stable process. In the case $\nu \notin L^1$, the smoothing of the nonlocal operator is shown to correspond precisely to the activity of the underlying Lévy process and the variation of its sample paths. We introduce volume-constrained nonlocal diffusion equations and demonstrate that they are the master equations for Lévy processes restricted to a bounded domain. The ensuing variational formulation and conforming finite element method provide a powerful tool for studying both Lévy processes and fractional diffusion on bounded, non-simple geometries with volume constraints.

In the second part of this dissertation, we consider the problem of estimating the distribution of a quantity of interest computed from the solution of an elliptic partial differential equation posed on a domain $\Omega(\boldsymbol{\theta}) \subset \mathbb{R}^2$ with a randomly perturbed boundary, where $\boldsymbol{\theta}$ is a random vector with given probability structure. We construct a piecewise smooth transformation from a partition of $\Omega(\boldsymbol{\theta})$ to a reference domain Ω in order to avoid the complications associated with solving the problems on $\Omega(\boldsymbol{\theta})$. The domain decomposition formulation is exploited by localizing the effect of the randomness to boundary elements in order to achieve a computationally efficient Monte Carlo sampling procedure. An a posteriori error analysis for the approximate distribution, which includes a deterministic error for each sample and a stochastic error from the effect of sampling, is also presented. We thus provide an efficient means to estimate the distribution of a quantity of interest via a Monte Carlo sampling procedure while also providing a posteriori error estimates for each sample.

TABLE OF CONTENTS

LIST OF FIGURES

LIST OF ALGORITHMS

1. INTRODUCTION

The field of applied mathematics concerns itself with the use of mathematical and statistical methods and models in various science, engineering, and industrial applications. Unfortunately, as famously stated by George Box,

> "All models are wrong, some are useful,"

so that a rigorous analysis of the validity of the model is in order. In other words, every practical application of mathematical and statistical models is accompanied by uncertainty and this uncertainty must be quantified and reduced wherever possible. Common instances where uncertainties arise include the estimation of parameters from data, augmenting the problem with simplifying assumptions, finite sampling of the input and parameter spaces, and obtaining outputs using a numerical method. This dissertation concerns two parts, with each addressing an important problem in the field of uncertainty quantification. Namely, in Part I, we study nonlocal diffusion as a model for diffusion processes in which the classical diffusion model is invalid and, in Part II, we investigate the effect of uncertainty in the domain on which a partial differential equation (PDE) is posed on a quantity of interest (QOFI) computed from the solution. Part I consists of Chapters 2-6, whereas Part II consists of Chapters 7-9. The final chapter, Chapter 10, includes a brief conclusion.

1.1 Probabilistic Foundation of Nonlocal Diffusion

Historically, diffusion processes have been modeled by the classical diffusion equation,

$$u_t(x,t) = c\Delta u(x,t). \tag{1.1.1}$$

The model (1.1.1) relies on the classical balance law,

$$\frac{\partial u}{\partial t} + \nabla \cdot q = 0,$$

which states that the rate of change in the density $u(x,t)$ at x is due to a change in flux at x, and an assumption that the flux q satisfies Fick's first law,

$$q = -c\nabla\, u.$$

However, it has been observed experimentally that many diffusion processes do not obey the classical model, e.g., contaminant flow in groundwater [28], sporadic movement of foraging spider monkeys [62], dynamic motions in proteins [51], turbulence in fluids [43], and dynamics of financial markets [47]; see [42] for a review of other such applications. Consequently, when the underlying assumption of Fick's first law is questionable, alternate models for diffusion must be considered [6, 53]. One alternative is the fractional diffusion equation

$$u_t(x,t) = -c(-\Delta)^{\alpha/2}u(x,t), \quad \alpha \in (0,2], \tag{1.1.2}$$

which arises via a generalization of Fick's first law; see [59]. Another viable alternative to the classical diffusion model is the nonlocal diffusion equation,

$$u_t(x,t) = \int_{\mathbb{R}} \big(u(y,t) - u(x,t)\big)\nu(x-y)\,\mathrm{d}y, \tag{1.1.3}$$

where ν is positive and assumed to be symmetric. The integral operator on the right-hand side of (1.1.3) represents nonlocal diffusion because the rate of diffusion associated with $u(x,t)$ depends upon points $y \neq x$.

The work of [3, 26, 36] allows for the consideration of volume-constrained nonlocal diffusion, which are the nonlocal analogs of classical boundary value problems. The volume-constrained problems have been studied in various contexts; see [21, 22, 29]. In [36], the authors provide variational formulations, which then give rise to a conforming finite element method with discontinuous basis functions. The relationship between (1.1.2) and (1.1.3) in the limit of vanishing nonlocality establishes that numerical solutions of fractional diffusion on bounded domains can be approximated.

A useful perspective when studying diffusion processes is that of a stochastic process and its master equation, i.e., the deterministic equation that governs the time evolution of the probability density function describing the process. Each of the models (1.1.1)–(1.1.3) are the master equations for particular Lévy processes. A Lévy process L_t is characterized by the Lévy-Khintchine decomposition in terms of the characteristic function,

$$\varphi_{L_t}(\xi) = \exp\left(\left(ib\xi - \frac{c\xi^2}{2} + \int_{\mathbb{R}} \left(e^{i\xi x} - 1 - i\xi x I_{\{|x|<\delta\}}\right)\nu(x)\,\mathrm{d}x\right)t\right).$$

Specifically, (1.1.1) is the master equation for Brownian motion, (1.1.2) is the master equation for a centered and symmetric stable process, and (1.1.3) is the master equation for a pure jump

process. When $\nu \in L^1(\mathbb{R})$, the latter is a Markovian continuous time random walk (CTRW), that is, a compound Poisson process. Non-Markovian CTRWs, also for $\nu \in L^1(\mathbb{R})$, can be studied via the appropriate master equation as well, e.g., the master equation for a particular renewal-reward process is the Cattaneo-Vernotte equation

$$u_t(x,t) + \frac{\tau}{2} u_{tt}(x,t) = \int_{\mathbb{R}} \big(u(y,t) - u(x,t)\big)\nu(x-y)\,\mathrm{d}y. \tag{1.1.4}$$

To understand sample paths and statistics of a given process, one often relies on many realizations of the process and then constructing a density estimate μ_N from the simulations. Unfortunately, simulating the process can become expensive, or may even be impossible. Consequently, there are many advantages to having both the corresponding master equation and the ability to find numerical solutions. Most notable is that statistics of the given process are readily available once the numerical approximation u_h of the density is obtained and do not rely on costly simulations.

Part I is presented in Chapters 2-6 and is organized as follows. Chapter 2 gives an overview of the diffusion equations (1.1.1)–(1.1.3) and introduces them as the master equations for stochastic processes. In Chapter 3, which is published work of the author [21], we obtain numerical solutions to the volume-constrained nonlocal diffusion equation and study the relationship to classical and fractional diffusion as diffusion is localized. Chapter 4, which is a manuscript in preparation for journal submission by the author, introduces the nonlocal Cattaneo-Vernotte equation and investigates properties of solutions and the effect of relaxation time. In Chapter 5, which is published work of the author [22], we present density estimates from simulations of the underlying stochastic processes to (1.1.3) and (1.1.4) with volume constraints and compare them to the corresponding numerical solutions of the master equation. Chapter 6, which is a manuscript in preparation for journal submission by the author, considers exit-time distributions of a general class of Lévy processes with volume constraints.

1.2 Formulation and Analysis for Elliptic Problems on Uncertain Domains

Many natural phenomena are modeled by PDE boundary value problems and, given a fixed set of input data into the model, e.g., boundary conditions, parameters, and coefficients, much effort has been expended to obtain efficient and accurate outputs. Traditionally, the input data are given in a deterministic fashion. However, the inability to accurately measure parameters, inhomogeneities,

and deviations from a deterministic set of input data have deemed stochastic descriptions of the model more appropriate in the presence of such uncertainties.

The case when uncertainties are present in the coefficients of a PDE model has received much attention from numerous disciplines. A typical formulation of such a problem reads: find $w(x;\boldsymbol{\theta})$ such that

$$\begin{cases} -\nabla\cdot(a(x;\boldsymbol{\theta})\nabla w(x;\boldsymbol{\theta})) = f(x;\boldsymbol{\theta}), & x\in\Omega, \\ \qquad\qquad w(x;\boldsymbol{\theta}) = 0, & x\in\partial\Omega, \end{cases} \tag{1.2.1}$$

where $\boldsymbol{\theta}$ is a random vector with some given probability structure. The ensuing demand for rigorous mathematical and statistical theory to accommodate the applications has been met; see [8, 11, 12, 13, 20, 33, 34, 69]. Some commonly used tools include Karhunen-Loeve expansions, generalized Polynomial Chaos, and stochastic collocation.

Much less attention, however, has been given to the case when the physical domain is uncertain, though this problem is equally practical in its application. In fact, given a sufficiently fine spatial resolution, the physical domain on which any model is posed is uncertain [67], e.g., due to manufacturing imperfections, the inability to obtain accurate measurements, or the approximation of the geometry from a discrete set of data points. The model problem is: find $w(x;\boldsymbol{\theta})$ such that

$$\begin{cases} -\nabla\cdot(a(x)\nabla w(x;\boldsymbol{\theta})) = f(x), & x\in\Omega(\boldsymbol{\theta}), \\ \qquad\qquad w(x;\boldsymbol{\theta}) = 0, & x\in\partial\Omega(\boldsymbol{\theta}), \end{cases} \tag{1.2.2}$$

where $\boldsymbol{\theta}$ is a random variable with some given probability structure and $\Omega(\boldsymbol{\theta})\subset\mathbb{R}^2$ is a stochastic polygonal domain. Specific applications of such problems include transport in tubes with rough boundaries [65], aerodynamic studies in the design of wind turbines [23], heat diffusion across irregular and fractal-like surfaces [16, 19], structural analysis studies [55], acoustic scattering on rough surfaces [56, 68], seismology and oil reservoir management [13], various civil and nuclear engineering studies [11], chemical transport in rough domains [20], and understanding the effect of geometric variability on the electromechanical behavior of nanostructures [7].

Often, only a few statistics on the output, rather than the entire solution, are desired. For instance, one might consider estimating the distribution of a QOFI computed from the solution of (1.2.2) via

$$Q(w;\boldsymbol{\theta}) = \int_{\Omega(\boldsymbol{\theta})} w(x;\boldsymbol{\theta})\psi(x)\,\mathrm{d}x,$$

where ψ is uniquely determined by the QOFI. To estimate the distribution of $Q(w;\boldsymbol{\theta})$, standard Monte Carlo sampling techniques are employed, which necessitate understanding the numerical error for every realization of $\boldsymbol{\theta}$. Such sampling methods face several significant challenges: a naive approach will require constructing a mesh of the domain for each realization of $\boldsymbol{\theta}$; the variational formulation requires a basis of test functions that depend on $\boldsymbol{\theta}$; and it is not clear how to perform an error analysis for multiple problems across different domains and different meshes as the error estimates will depend on $\boldsymbol{\theta}$ in some unknown way. Consequently, new tools must be developed for problems with stochastic domains. The most popular approach is to transform the problem from the stochastic domain to a deterministic domain, which moves the dependence on $\boldsymbol{\theta}$ from the domain to the coefficients and data.

Motivated by the use of transformations to a deterministic reference domain in [70] and classical isoparametric finite element analysis, we transform the problem (1.2.2) to a PDE with stochastic coefficients posed on Ω, much like (1.2.1), via a piecewise smooth mapping on a partition of Ω. Constructing this mapping takes little additional computational effort and, since all the resulting problems are posed on Ω, allows for an intuitive comparison of results and errors across all realizations of $\boldsymbol{\theta}$. Further, exploiting the domain decomposition formulation by localizing the effect of randomness to the boundary subdomains and performing a Neumann expansion, an efficient Monte Carlo sampling approach can be implemented that requires no re-meshing of the domain. Further, an a posteriori error analysis for each realization of $\boldsymbol{\theta}$ is available, as is an a posteriori error analysis for the approximate distribution of the QOFI.

Part II is presented in Chapters 7-9 and is organized as follows. In Chapter 7, we give an overview of stochastic computations in PDE models with random coefficients. Chapter 8, which is a manuscript in preparation for journal submission by the author, formulates elliptic problems on a stochastic domain, describes the piecewise smooth transformation to a reference domain, and presents well-posedness results of both the untransformed and transformed problems. Chapter 9, which will be included in said manuscript, presents a Monte Carlo sampling procedure and a posteriori error analysis in the estimation of the distribution of a QOFI computed from solutions of an elliptic PDE posed on a stochastic polygonal domain.

Part I

Probabilistic Foundation of Nonlocal Diffusion

2. A SURVEY OF THE UNDERLYING STOCHASTIC PROCESSES OF DIFFUSION EQUATIONS

We introduce models for diffusion, e.g., classical, fractional, and nonlocal, as the master equations for different stochastic processes. The classical diffusion equation is the master equation, i.e., Fokker-Planck equation, for a Wiener process, whereas the fractional and nonlocal diffusion equations are the master equations for a centered and symmetric stable process and a Lévy jump process, e.g., a Markovian CTRW. Non-Markovian CTRWs, e.g., renewal-reward processes, can also be studied via the appropriate master equation, which is demonstrated by considering the nonlocal Cattaneo-Vernotte equation.

2.1 Wiener Processes and Classical Diffusion

The first study of classical diffusion is often credited to Adolf Fick, who in 1855 introduced Fick's first law of diffusion. We begin with the mass balance law,

$$\frac{\partial u}{\partial t} + \frac{\partial q}{\partial x} = 0,$$

which states that a time change in density $u(x,t)$ at x is due to a change in flux, q, at x. Determining q in general, however, is nontrivial. Classically, it is assumed that density flows from regions of high density to those of low density, with the magnitude of this flux proportional to the density gradient. That is, we assume Fick's first law

$$q = -c\frac{\partial u}{\partial x},$$

so that we arrive at the classical diffusion equation, Fick's second law,

$$u_t(x,t) = cu_{xx}(x,t). \tag{2.1.1}$$

It was later understood that the classical diffusion equation governs a particle undergoing Brownian motion. Interestingly, Brownian motion was given its first detailed account long before Fick's laws

of diffusion by Robert Brown in 1827. Brown witnessed pollen grains, and then later other inorganic fine particles like glass and even dust from the Sphinx, exhibiting irregular motion when suspended in water. In 1905, Einstein derived the classical diffusion equation in his investigations of Brownian motion. The first stochastic differential equation describing Brownian motion, i.e., the Langevin equation, is credited to Paul Langevin in 1908.

More specifically, Einstein presented the integrodifference equation [30],

$$u(x,t+\tau) = \int_{\mathbb{R}} u(x-s,t)\phi(s)\,\mathrm{d}s, \tag{2.1.2}$$

which has several aliases, e.g., Einstein's master equation, the Chapman-Kolmogorov equation, and the Smoluchowski equation. Subtracting $u(x,t)$ from each side of (2.1.2) gives

$$u(x,t+\tau) - u(x,t) = \int_{\mathbb{R}} \big(u(x-s,t) - u(x,t)\big)\phi(s)\,\mathrm{d}s. \tag{2.1.3}$$

We expand both the left hand and right hand sides of (2.1.3) to obtain

$$\frac{\partial u}{\partial t} + \frac{\tau}{2}\frac{\partial^2 u}{\partial t^2} + \cdots = \frac{\mathbb{E}(S^2)}{2\tau}\frac{\partial^2 u}{\partial x^2} + \frac{\mathbb{E}(S^4)}{4!\tau}\frac{\partial^4 u}{\partial x^4} + \cdots, \tag{2.1.4}$$

where

$$\mathbb{E}(S^k) = \int_{\mathbb{R}} s^k \phi(s)\,\mathrm{d}s.$$

We assume the hydrodynamic scaling of time and space, i.e.,

$$\lim_{\tau\to 0} \frac{\mathbb{E}(S^2)}{2\tau} = c,$$

and that

$$\mathbb{E}(S^{2k}) = \mathrm{o}(\tau), \quad k \geq 2.$$

We then take $\tau \to 0$ in (2.1.4) to obtain (2.1.1).

The Fourier transform of (2.1.1) gives

$$\widehat{u}_t(\xi,t) = -c\xi^2 \widehat{u}(\xi,t). \tag{2.1.5}$$

Solving (2.1.5) with initial condition $u(x,0) = \delta(x)$,

$$\widehat{u}(\xi,t) = \exp(-c\xi^2 t),$$

which yields the fundamental solution of (2.1.1), denoted with $g(x,t)$,

$$g(x,t) = \frac{1}{\sqrt{4\pi ct}}\exp\left(-\frac{x^2}{4ct}\right). \tag{2.1.6}$$

We note that $\widehat{u}(\xi,t)$ is the characteristic function of a scaled Wiener process, $\sqrt{2c}W_t$. Further, evident from (2.1.6), given that a particle begins at the origin, its position after time t is a zero-mean Gaussian random variable with variance $2ct$. For (2.1.1) and an arbitrary initial condition $u(x,0) = u_0(x)$, $u(x,t)$ is the convolution of u_0 with the fundamental solution g, i.e.,

$$u(x,t) = (g * u_0)(x,t) = \frac{1}{\sqrt{4\pi ct}}\int_{\mathbb{R}} \exp\left(-\frac{(x-y)^2}{4ct}\right) u_0(y)\,\mathrm{d}y. \tag{2.1.7}$$

Rewriting (2.1.7),

$$u(x,t) = \int_{\mathbb{R}} g(y,t)u_0(x-y)\,\mathrm{d}y,$$

gives that $u(x,t)$ is the expectation of the initial density of particles at position $x-y$ that have diffused to position x during time t through Brownian motion.

The classical diffusion equation is a special case of a Fokker-Planck equation,

$$u_t(x,t) = \frac{\partial^2}{\partial x^2}\left(\frac{1}{2}\sigma^2(x,t)u(x,t)\right), \tag{2.1.8}$$

which describes the time evolution of the probability density function of the state X_t of an It$\bar{\text{o}}$ stochastic differential equation [57]

$$\mathrm{d}X_t = \sigma(X_t,t)\mathrm{d}W_t. \tag{2.1.9}$$

In the special case of a constant diffusion coefficient, i.e., $\sigma(x,t) = \sqrt{2c}$, (2.1.9) reduces to

$$\mathrm{d}X_t = \sqrt{2c}\mathrm{d}W_t \tag{2.1.10}$$

and (2.1.8) simplifies to the classical diffusion equation (2.1.1).

2.2 Centered and Symmetric Stable Processes and Fractional Diffusion

An alternate model for diffusion is of interest when the underlying assumption of classical mass balance and Fick's first law are questionable. See, for instance, the papers [6, 53] for discussions and citations to the literature.

One alternative is the anomalous diffusion model given by the fractional diffusion equation

$$u_t(x,t) = -c(-\Delta)^{\alpha/2}u(x,t), \quad \alpha \in (0,2]. \tag{2.2.1}$$

with

$$\mathcal{F}\left\{(-\Delta)^{\alpha/2}\, v\right\} := |\xi|^{\alpha}\widehat{v}. \tag{2.2.2}$$

Anomalous diffusion represents a multiscale model for diffusion; see [63]. The fractional diffusion (2.2.1) for $\alpha \in (1,2]$ arises via a generalization of Fick's first law using a fractional derivative operator; see [59]. Fractional gradient and divergence operators are discussed in [48] and the fractional Laplacian can be obtained through composition of these operators. Fourier transforming (2.2.1) gives

$$\widehat{u}_t = -c|\xi|^{\alpha}\widehat{u}. \tag{2.2.3}$$

Since the characteristic function of a centered and symmetric α-stable process S_t^{α} is given by

$$\varphi_{S_t^{\alpha}}(\xi) = \exp\left(-c|\xi|^{\alpha}t\right),$$

the fundamental solution to (2.2.1) is the characteristic function of a centered and symmetric α-stable process S_t^{α}.

2.3 General Lévy Processes and Nonlocal Diffusion

The most general type of diffusion to satisfy the so-called positive maximum principle [18, pg. 9] are of the form

$$u_t(x,t) = qu(x,t) + b\frac{\partial u}{\partial x}(x,t) + \frac{c}{2}\frac{\partial^2 u}{\partial x^2}(x,t) + \int_{\mathbb{R}} \big(u(y,t) - u(x,t)\big)\nu(y-x)\,\mathrm{d}y. \tag{2.3.1}$$

In this section, we show that (2.3.1) (minus the reaction term) is the master equation for a general Lévy process. The main focus of our attention will be on the integral operator, which is the master equation for a jump process.

The distribution F of a random variable X is said to be infinitely divisible if, $\forall n \in \mathbb{N}$, there exists $\widetilde{X}_i \overset{iid}{\sim} \widetilde{F}_i$ such that $\sum_{i=1}^{n} \widetilde{X}_i \overset{d}{=} X$. Such random variables are prevalent and include those with Gaussian, Cauchy, exponential, Poisson, and gamma distributions. The Lévy-Khintchine formula provides a characterization of infinitely divisible random variables via a decomposition of the

characteristic function. That is, the distribution of a random variable L is infinitely divisible *if and only if* there exists

$$b \in \mathbb{R}, \quad c \in R_{\geq 0}, \tag{2.3.2a}$$

and a measure ν satisfying

$$\nu(\{0\}) = 0 \quad \text{and} \quad \int_{\mathbb{R}} \left(1 \wedge |x|^2\right) \nu(\mathrm{d}x) < \infty. \tag{2.3.2b}$$

such that

$$\varphi_L(\xi) = \exp\left(ib\xi - \frac{c\xi^2}{2} + \int_{\mathbb{R}} \left(e^{i\xi x} - 1 - i\xi x I_{\{|x|<\delta\}}\right) \nu(\mathrm{d}x)\right), \tag{2.3.3}$$

where $\delta > 0$ is arbitrary and often taken to be equal to one.

A process L_t that has an infinitely divisible distribution for each t is a Lévy process. Further, the Lévy-Itō decomposition states that for any triplet (b, c, ν) satisfying (2.3.2) there is a probability space on which a Lévy process L_t composed of four independent processes (constant drift bt, Brownian motion $\sqrt{c}W_t$, compound Poisson process Y_t, and square integrable martingale Z_t), i.e.,

$$L_t = bt + \sqrt{c}W_t + Y_t + Z_t,$$

exists. Moreover, such a Lévy process has a characteristic function given by

$$\varphi_{L_t}(\xi) = \exp\left(\left(ib\xi - \frac{c\xi^2}{2} + \int_{\mathbb{R}} \left(e^{i\xi x} - 1 - i\xi x I_{\{|x|<\delta\}}\right) \nu(\mathrm{d}x)\right) t\right). \tag{2.3.4}$$

For simplicity, we will consider triplets of the form $(0, 0, \nu)$, since the cases with $b \neq 0$ and $c \neq 0$ have been well-studied. We also write $\nu(\mathrm{d}x) = \nu(x)\mathrm{d}x$, and consider two choices of ν:

1. ν is symmetric, i.e.,

$$\nu(-x) = \nu(x), \quad \forall x \neq 0, \tag{2.3.5a}$$

2. ν is *not* symmetric and admits a finite mean, i.e.,

$$\int_{\mathbb{R}} |x|\nu(x)\,\mathrm{d}x < \infty. \tag{2.3.5b}$$

In either of these cases, there is no need for the compensator $i\xi x I_{\{|x|<\delta\}}$ so that (2.3.4) with $b = c = 0$ reduces to

$$\varphi_{L_t}(\xi) = \exp\left(\left(\int_{\mathbb{R}} \left(e^{i\xi x} - 1\right) \nu(x)\,\mathrm{d}x\right) t\right). \tag{2.3.6}$$

We introduce the notation $\widehat{u}(\xi,t) = \varphi_{L_t}(\xi)$ so that differentiating (2.3.6) gives

$$\widehat{u}_t(\xi,t) = \left(\int_{\mathbb{R}} \left(e^{i\xi x} - 1\right) \nu(x)\,\mathrm{d}x\right) \widehat{u}(\xi,t).$$

Inverse Fourier transforming yields the master equation for $L_t = Y_t + Z_t$,

$$u_t(x,t) = \int_{\mathbb{R}} \big(u(y,t) - u(x,t)\big)\nu(y-x)\,\mathrm{d}y. \tag{2.3.7}$$

We further split into cases by distinguishing the cases $\nu \in L^1(\mathbb{R})$ and $\nu \notin L^1(\mathbb{R})$. In the former case, we introduce the *probability density function* ϕ and the mean wait-time λ such that

$$\phi(z) = \frac{1}{\lambda}\nu(z). \tag{2.3.8}$$

In this case, the Lévy process is a compound Poisson process,

$$Y_t = \sum_{k=1}^{N_t} R_k, \tag{2.3.9}$$

where $R_k \overset{iid}{\sim} \phi$ and the Poisson process N_t has intensity $1/\lambda$. Consequently, the master equation for Y_t reduces to

$$u_t(x,t) = \frac{1}{\lambda}\int_{\mathbb{R}} \big(u(y,t) - u(x,t)\big)\phi(y-x)\,\mathrm{d}y \tag{2.3.10}$$

In the latter case, i.e., $\nu \notin L^1(\mathbb{R})$, L_t is a square integrable jump martingale, but not a compound Poisson process. For $\nu \notin L^1(\mathbb{R})$, we understand (2.3.7) as a distribution.

We now show that the master equation for nonlocal diffusion with $\nu \in L^1(\mathbb{R})$ is a special case of the master equation for an arbitrary CTRW,

$$u_t(x,t) = \int_0^t \Lambda(t-t')\int_{\mathbb{R}} \big(u(y,t') - u(x,t')\big)\phi(x-y)\,\mathrm{d}y\,\mathrm{d}t', \tag{2.3.11}$$

where

$$\widehat{\Lambda}(s) = \frac{s\widehat{\omega}(s)}{1-\widehat{\omega}(s)}, \tag{2.3.12}$$

ϕ is the step density, and ω is the wait-time density. Note that when wait-times are exponential, $\Lambda(t-t') = \frac{1}{\lambda}\delta(t-t')$ and (2.3.11) reduces to (2.3.10), which implies that (2.3.10) is the master equation for a Markovian CTRW, namely, a compound Poisson process.

2.4 Renewal-Reward Process and Nonlocal Diffusion with Relaxation

Different choices of Λ in (2.3.11) give rise to non-Markovian CTRWs. In practice, Λ will be determined from data. For the particular choice of Λ such that

$$\Lambda(t-t') = \frac{1}{\beta}\frac{2}{\tau}\exp\left(-\frac{t-t'}{\tau/2}\right), \tag{2.4.1}$$

we obtain the nonlocal Cattaneo-Vernotte equation

$$u_t(x,t) + \frac{\tau}{2}u_{tt}(x,t) = \frac{1}{\beta}\int_{\mathbb{R}}\big(u(y,t)-u(x,t)\big)\,\phi(x-y)\,\mathrm{d}y, \tag{2.4.2}$$

where u is some field, e.g., temperature or probability, ϕ is a symmetric function, i.e., $\phi(x-y) = \phi(y-x)$, and $\beta \geq 2\tau > 0$. The assumption (2.4.1) is tantamount to

$$\omega(t) = \begin{cases} \dfrac{t}{\tau^2}\exp\left(-\dfrac{1}{\tau}t\right), & \beta = 2\tau, \\ \dfrac{2}{\sqrt{\beta(\beta-2\tau)}}\exp\left(-\dfrac{t}{\tau}\right)\sinh\left(\dfrac{\sqrt{\beta(\beta-2\tau)}}{\beta\tau}t\right), & \beta > 2\tau. \end{cases} \tag{2.4.3}$$

We will show in Chapter 4 that (2.4.2) is the master equation for a non-Markovian CTRW, namely a renewal-reward process

$$Y_t = \sum_{k=1}^{N_t} R_k, \tag{2.4.4}$$

where the wait-times are *not* exponentially distributed and $R_k \overset{iid}{\sim} \phi$. The parameter β represents the mean wait-time between steps and $\tau/2 > 0$ is a relaxation time. The nonlocal Cattaneo-Vernotte equation (2.4.2) is also a model for nonlocal hyperbolic heat conduction.

We contrast (2.4.2) to the classical Cattaneo-Vernotte equation,

$$w_t + \frac{\tau}{2}w_{tt} = aw_{xx}, \tag{2.4.5}$$

where $\tau/2 > 0$ is again a relaxation time and $a > 0$ is the diffusion coefficient. The equation (2.4.5) is a model for diffusion that admits finite speeds of propagation, specifically $\sqrt{2a/\tau}$. When w is a temperature field, (2.4.5) is a model of hyperbolic heat conduction [45].

3. CLASSICAL, NONLOCAL, AND FRACTIONAL DIFFUSION EQUATIONS ON BOUNDED DOMAINS

This chapter is taken directly from published work by the author found in [21]. We compare the solutions of one-dimensional volume-constrained problems corresponding to classical, fractional and nonlocal diffusion on bounded domains. The latter two diffusions are viable alternatives for anomalous diffusion, when Fick's first law is an inaccurate model. In the case of nonlocal diffusion, a generalization of Fick's first law in terms of a nonlocal flux is demonstrated to hold. A relationship between nonlocal and fractional diffusion is also reviewed, where the order of the fractional Laplacian can lie in the interval $(0, 2]$. The contribution of this paper is to present volume-constrained problems for nonlocal diffusion including a variational formulation that leads to a conforming finite element method using piecewise discontinuous shape functions. Several examples are given where the effect of nonlocality is studied. The relationship between nonlocal and fractional diffusion explains that the numerical solution of volume-constrained problems, where the order of the fractional Laplacian can lie in the interval $(0, 2]$, is possible.

3.1 Introduction

The one-dimensional form of Fick's second law

$$w_t = cw_{xx}, \quad c > 0, \tag{3.1.1}$$

postulates the diffusion in time undergone by the scalar field w representing the particle density. An alternate model for diffusion is of interest when the underlying assumption of classical mass balance and Fick's first law, e.g.,

$$\begin{cases} w_t = -q_x, \\ \\ q = -cw_x, \end{cases}$$

respectively, are questionable. See, for instance, the papers [6, 53] for discussions and citations to the literature. One alternative is the anomalous diffusion model given by the fractional diffusion equation

$$v_t = -c\,(-\Delta)^{\alpha/2}\, v, \quad 0 < \alpha \leq 2, \tag{3.1.2}$$

with

$$(-\Delta)^{\alpha/2}\, v := \mathcal{F}^{-1}(|\xi|^{\alpha}\widehat{v}\,), \tag{3.1.3}$$

where

$$\widehat{v}(\xi) := \mathcal{F}(v)(\xi) = \int_{\mathbb{R}} v(s)e^{-i\xi s}\,\mathrm{d}s$$

denotes the Fourier transform of a function v and $\mathcal{F}^{-1}$ denotes the inverse Fourier transform. Anomalous diffusion represents a multiscale model for diffusion; see [63]. The fractional diffusion (3.1.2) for $\alpha \in (1, 2]$ arises via a generalization of Fick's first law using a fractional derivative operator; see [59]. Fractional gradient and divergence operators are discussed in [48] and the fractional Laplacian can be obtained through composition of these operators.

The paper [26] demonstrates that the asymptotic behavior for a solution of (3.1.2) is given by the solution of the integrodifferential equation

$$u_t(x,t) = \frac{1}{\lambda}\int_{\mathbb{R}} \big(u(y,t) - u(x,t)\big)\,\phi(y-x)\,\mathrm{d}y, \quad t \geq 0, \tag{3.1.4}$$

where ϕ is a symmetric function, i.e., $\phi(y-x) = \phi(x-y)$, $\phi \geq 0$, $\lambda > 0$, and $\int_{\mathbb{R}} \phi(s)\,\mathrm{d}s = 1$. The integral operator on the right-hand side of (3.1.4) represents nonlocal diffusion because the rate of diffusion associated with $u(x,t)$ depends upon points $y \neq x$. The rate of diffusion is the difference in the rate at which u enters x at time t, or $\frac{1}{\lambda}\int_{\mathbb{R}} u(y,t)\,\phi(y-x)\,\mathrm{d}y$, and the rate at which u departs x at time t, or $\frac{1}{\lambda}u(x,t)$. This suggests that the asymptotic behavior for a solution of a volume-constrained problem corresponding to the nonlocal equation (3.1.4) is also fractional, and indeed, selecting ϕ as a Lévy stable density, demonstrates this relationship. The nonlocal equation (3.1.4) also represents a model for peridynamic heat conduction [17] .

We now briefly establish a relationship of (3.1.4) to its underlying stochastic process. Consider the compound Poisson process.

$$Y_t = \sum_{k=1}^{N_t} R_k, \tag{3.1.5}$$

where $R_k \overset{iid}{\sim} \phi$ and the Poisson process N_t has intensity $1/\lambda$. Recalling that the characteristic function of the compound Poisson process is given by

$$\widehat{u}(\xi,t) = \varphi_{Y_t}(\xi) = \exp\left(\frac{1}{\lambda}\left(\widehat{\phi}(\xi) - 1\right)t\right) \tag{3.1.6}$$

establishes said relationship.

The purpose of this paper is to compare the solutions of the initial value volume-constrained problems corresponding to (3.1.1) and (3.1.4) using a conforming finite element method on several nonlocal diffusion problems. The nonlocal volume-constrained problems augment (3.1.4) with Dirichlet and Neumann volume constraints. The finite element method for (3.1.4) depends upon the variational formulation presented in [36]. The relationship between nonlocal and fractional diffusion explains that the numerical solution of volume-constrained problems, where the order of the fractional Laplacian lies in the interval $(0, 2]$, is possible; for example, the recent paper [61] only considers the order $1 < \alpha \leq 2$. Convergence and stability analysis of a finite difference method for (3.1.4) are investigated in [15]. The former paper investigates (3.1.4) on the real line, while the analysis in the latter paper considers the nonlocal p-Laplacian diffusion equation with nonlocal Neumann boundary conditions and compactly supported ϕ.

This chapter is organized as follows. Section 3.2 discusses relationships among classical, fractional and nonlocal diffusion. In particular, the nonlocal diffusion equation (3.1.4) leads to a generalization of Fick's first and second laws, and a relationship between nonlocal and fractional diffusion is reviewed. Section 3.3 reviews nonlocal volume-constrained problems and their variational counterparts. The volume constraints given generalize the notion of Dirichlet and Neumann boundary conditions. The finite element formulation, properties of nonlocal diffusion, and three numerical examples are given in Section 3.4.

3.2 Nonlocal Flux, Fick's First Law, and Fractional Diffusion

A relationship is now established between the classical and nonlocal diffusion equations (3.1.1) and (3.1.4), respectively, by examining the nonlocal flux implied by the latter equation and Fick's first law. The key to this relationship are the two lemmas given in [46, 54] due to Noll. The first lemma provides a formula for a flux,

$$p(x,t) = -\frac{1}{2}\int_{\mathbb{R}}\int_0^1 \big(u(x+(1-\mu)z,t) - u(x-\mu z,t)\big) z\phi(z)\,\mathrm{d}\mu\,\mathrm{d}z, \tag{3.2.1}$$

such that

$$\begin{aligned}\frac{\partial}{\partial x}p(x,t) &= \frac{1}{2}\int_{\mathbb{R}}\int_0^1 \frac{\mathrm{d}}{\mathrm{d}\mu}\Big(\big(u(x+(1-\mu)z,t) - u(x-\mu z,t)\big)\phi(z)\Big)\,\mathrm{d}\mu\,\mathrm{d}z \\ &= -\frac{1}{2}\int_{\mathbb{R}} \big(u(x+z,t) - u(x,t) + u(x-z,t) - u(x,t)\big)\phi(z)\,\mathrm{d}z\end{aligned}$$

and, since $\phi(z) = \phi(-z)$,

$$u_t = -\frac{1}{\lambda} p_x.$$

The hypothesis for the application of the lemma is the antisymmetry of the integrand of (3.1.4). The second lemma grants, with $a < b$, that

$$\frac{1}{\lambda}\int_a^b \int_{\mathbb{R}} \big(u(y,t) - u(x,t)\big)\, \phi(y-x)\, \mathrm{d}y\, \mathrm{d}x = \frac{1}{\lambda}\int_a^b \int_{\mathbb{R}\setminus(a,b)} \big(u(y,t) - u(x,t)\big)\, \phi(y-x)\, \mathrm{d}y\, \mathrm{d}x,$$

because

$$\frac{1}{\lambda}\int_a^b \int_a^b \big(u(y,t) - u(x,t)\big)\, \phi(y-x)\, \mathrm{d}y\, \mathrm{d}x = 0,$$

a statement that there is no diffusion exchange within (a,b).

Evidently, the nonlocal diffusion equation (3.1.4) has replaced the classical flux $q = -cu_x$ with the nonlocal flux p. The flux p is nonlocal because points $z \neq x$ are involved, in contrast to the classical, local, flux that would only require the point x at time t, or $u_x(x,t)$. Therefore,

$$\begin{aligned}\frac{1}{\lambda}\int_a^b \int_{\mathbb{R}\setminus(a,b)} \big(u(y,t) - u(x,t)\big)\, \phi(y-x)\, \mathrm{d}y\, \mathrm{d}x &= \frac{\mathrm{d}}{\mathrm{d}t}\int_a^b u(x,t)\, \mathrm{d}x \\ &= -\int_a^b \frac{\partial p(x,t)}{\partial x}\, \mathrm{d}x \\ &= -\big(p(b,t) - p(a,t)\big).\end{aligned}$$

In words, the time rate of change of diffusion over the interval (a,b) is not only equal to the flux p into (a,b) at points b and a, but also the rate at which u diffuses from outside of (a,b) into (a,b) at time t.

We now demonstrate how the nonlocal flux p (3.2.1) can be approximated by u_x. Let $\varepsilon > 0$, $\lambda = \varepsilon^2$, define the radial symmetric density ϕ_ε by

$$\begin{cases} \phi_\varepsilon(s) := \dfrac{1}{\varepsilon}\phi(s/\varepsilon), \\ \displaystyle\int_{\mathbb{R}} s^{2k}\phi(s)\, \mathrm{d}s < \infty, \quad k = 0, 1, 2 \ldots \end{cases} \tag{3.2.2}$$

and denote

$$0 < c := \frac{1}{2}\int_{\mathbb{R}} s^2 \phi(s)\, \mathrm{d}s,$$

given the symmetric density ϕ.[1] A formal expansion implies that

$$\begin{aligned}\frac{1}{\lambda}p(x,t) &= -\frac{1}{2}\int_{\mathbb{R}}\int_0^1 \frac{1}{\varepsilon^2}\left(u_x(x,t)z^2 + \sum_{k=2}^{\infty}\frac{1}{k!}z^{k+1}\frac{\partial^k u(x,t)}{\partial x^k}\right)\phi_\varepsilon(z)\,\mathrm{d}\mu\,\mathrm{d}z \\ &= -cu_x(x,t) + \frac{1}{\varepsilon^2}\sum_{k=2}^{\infty}\frac{\partial^{2k-1}u(x,t)}{\partial x^{2k-1}}\frac{1}{(2k-1)!}\int_{\mathbb{R}} z^{2k}\phi_\varepsilon(z)\,\mathrm{d}z \\ &= q(x,t) + \sum_{k=2}^{\infty}\frac{\partial^{2k-1}u(x,t)}{\partial x^{2k-1}}\frac{\varepsilon^{2(k-1)}}{(2k-1)!}\int_{\mathbb{R}} z^{2k}\phi(z)\,\mathrm{d}z.\end{aligned}$$

Under the assumption that the above expansion is valid, and ε is sufficiently small, classical mass balance and Fick's first law is generalized to

$$\begin{cases} u_t = -p_x, \\ \\ p = -cu_x + \mathrm{O}(\varepsilon^2). \end{cases}$$

Note that the nonlocal diffusion equation (3.1.4) does not explicitly require continuity, let alone differentiability, of u, in contrast to the two derivatives of w needed for the classical diffusion equation (3.1.1). The effect of the density ϕ_ε as ε decreases is to "localize" the diffusion of (3.1.4). Indeed, defining

$$\psi(y-x) := \delta(y-x) + c\frac{\partial^2}{\partial x^2}\delta(y-x), \tag{3.2.3}$$

where $\delta(\cdot)$ denotes the Dirac delta distribution, or generalized function, implies, along with integration by parts, that

$$\int_{\mathbb{R}}\big(u(y,t)-u(x,t)\big)\psi(y-x)\,\mathrm{d}y = cu_{xx}(x,t),$$

when $u(x,\cdot)$ and $u_x(x,\cdot)$ decay sufficiently fast to zero at $\pm\infty$.

A relationship between fractional (3.1.2) and nonlocal diffusion (3.1.4) is now reviewed. The Fourier transform of (3.1.4) results in

$$\widehat{u}_t(\xi,t) = \frac{1}{\lambda}(\widehat{\phi}(\xi)-1)\widehat{u}(\xi,t). \tag{3.2.4}$$

The authors of [26] assume that as $\xi \to 0$

$$\widehat{\phi}(\xi) = 1 - a|\xi|^\alpha + \mathrm{o}(|\xi|^\alpha), \quad a > 0, \tag{3.2.5}$$

with $0 < \alpha \leq 2$, where $\mathrm{o}(|\xi|^\alpha) \to 0$ faster than ξ. In particular, because

$$\widehat{\psi}(\xi) = 1 - c|\xi|^2,$$

[1] The assumption on the density ϕ implies that the odd moments must be zero.

where ψ is given by (3.2.3), the assumption (3.2.5) recovers the classical diffusion equation when $\alpha = 2$ and $a = c\lambda$. When $0 < \alpha \leq 2$, then (3.2.4) and (3.2.5) give

$$\widehat{u}_t(\xi, t) = \frac{1}{\lambda}(\widehat{\phi}(\xi) - 1)\widehat{u}(\xi, t) \tag{3.2.6}$$

$$= -\frac{a}{\lambda}|\xi|^\alpha \widehat{u}(\xi, t) + \mathrm{o}(|\xi|^\alpha) \tag{3.2.7}$$

and application of the inverse Fourier transform with (3.1.3) grants

$$u_t = -\frac{a}{\lambda}\left(-\Delta\right)^{\alpha/2} u + \mathcal{F}^{-1}\left(\mathrm{o}(|\xi|^\alpha)\right).$$

In words, the assumptions (3.2.5) demonstrate that nonlocal diffusion is approximately that given by the fractional diffusion (3.1.2) as $\xi \to 0$. See Theorem 1 in [26] for further information. A specific case demonstrating this relationship between fractional and nonlocal diffusion is drawn by appealing to the theory of Lévy stable processes. For instance, a Lévy stable density ϕ with stability index satisfies (3.2.5). The nonlocal diffusion equation therefore represents a model for anomalous diffusion.

3.3 Nonlocal Volume-Constrained Problems

The previous section discussed relationships among classical, fractional, and nonlocal diffusion equations in absence of boundary conditions. While boundary conditions are well-understood for classical diffusion, the same cannot be said for fractional and nonlocal diffusion. For instance, the paper [32] establishes an abstract variational formulation for the fractional advection dispersion equation with homogeneous Dirichlet boundary conditions in terms of fractional derivatives. The results of [32] immediately apply to the fractional Laplacian equation with homogeneous Dirichlet boundary conditions, however, only the case $1 < \alpha \leq 2$ for the order of the fractional Laplacian is considered. We now present classical and variational formulations for the nonlocal diffusion volume-constrained problem on a bounded interval where $0 < \alpha \leq 2$.

The paper [26] also presents formulations for the nonlocal diffusion equation with homogeneous Dirichlet or Neumann volume constraints. We study the time evolution of a field u on a bounded domain Ω, thus $x \in \Omega$. Note that (3.1.4) can be rewritten as

$$\begin{aligned} u_t(x,t) = &\frac{1}{\lambda}\int_\Omega \big(u(y,t) - u(x,t)\big)\phi_\varepsilon(x-y)\,\mathrm{d}y \\ &+ \frac{1}{\lambda}\int_{\mathbb{R}\setminus\Omega} \big(u(y,t) - u(x,t)\big)\phi_\varepsilon(x-y)\,\mathrm{d}y. \end{aligned} \tag{3.3.1}$$

The homogeneous nonlocal Dirichlet volume constraint constrains the field u via

$$u(y,t) = 0, \quad y \in \mathbb{R} \setminus \Omega, \tag{3.3.2a}$$

while, for the homogeneous nonlocal Neumann volume constraint,

$$\frac{1}{\lambda} \int_{\mathbb{R}\setminus\Omega} \big(u(y,t) - u(x,t)\big)\phi_\varepsilon(x-y)\,\mathrm{d}y = 0, \quad x \in \Omega, \tag{3.3.2b}$$

which is a statement that the rate of diffusion exchange between Ω and $\mathbb{R} \setminus \Omega$ is zero. The analysis given at the end of Section 3.2 then implies that an approximation to the fractional Laplacian equation with either homogeneous Dirichlet or Neumann volume constraints with $0 < \alpha \leq 2$ is available.

Our numerical experiments consider $\Omega = (0,1)$ and both the nonlocal homogeneous Dirichlet volume-constrained problem, where (3.3.1) and (3.3.2a) combine to give

$$\begin{cases} u_t(x,t) = \dfrac{1}{\lambda} \displaystyle\int_{\mathbb{R}} \big(u(y,t) - u(x,t)\big)\phi_\varepsilon(x-y)\,\mathrm{d}y, & x \in (0,1), \\ u(x,t) = 0, & x \in \mathbb{R} \setminus (0,1), \\ u(x,0) = u_0(x), & x \in (0,1), \end{cases} \tag{3.3.3a}$$

and the nonlocal homogeneous Neumann volume-constrained problem, where (3.3.1) and (3.3.2b) combine to give

$$\begin{cases} u_t(x,t) = \dfrac{1}{\lambda} \displaystyle\int_0^1 \big(u(y,t) - u(x,t)\big)\phi_\varepsilon(x-y)\,\mathrm{d}y, & x \in (0,1), \\ u(x,0) = u_0(x), & x \in (0,1). \end{cases} \tag{3.3.3b}$$

Here, ε is a positive number representing the nonlocality, $\lambda = c\varepsilon^\alpha$, and the symmetric density function ϕ_ε is defined

$$\phi_\varepsilon(s) := \frac{1}{\lambda}\phi(s/\varepsilon), \tag{3.3.4}$$

where ϕ is a specified symmetric probability density function that satisfies

$$\widehat{\phi}(\xi) = 1 - c|\xi|^\alpha + \mathrm{o}\,|\xi|^\alpha, \quad c > 0.$$

If ϕ is zero outside a closed and bounded interval centered at zero, which implies $\alpha = 2$ in (3.3.4), then solutions of (3.3.3a) and (3.3.3b) approximate those of the classical homogeneous Dirichlet and Neumann volume-constrained problems

$$\begin{cases} v_t(x,t) = v_{xx}(x,t), & x \in (0,1), \\ v(0,t) = v(1,t) = 0, & \\ v(x,0) = u_0(x), & x \in (0,1) \end{cases} \tag{3.3.5a}$$

and

$$\begin{cases} v_t(x,t) = v_{xx}(x,t), & x \in (0,1), \\ v_x(0,t) = v_x(1,t) = 0, & \\ v(x,0) = u_0(x), & x \in (0,1), \end{cases} \tag{3.3.5b}$$

respectively, as $\varepsilon \to 0$ for smooth $u(x,t)$; see [1, 2] for details.

The results in [36] provide the variational formulation associated with (3.3.3a) and (3.3.3b). Define the bilinear form

$$B_I(u,v) := \frac{1}{2}\int_I \int_I \big(u(y,t) - u(x,t)\big)\big(v(y) - v(x)\big)\,\phi_\varepsilon(x-y)\,\mathrm{d}y\,\mathrm{d}x, \tag{3.3.6}$$

where I is an open interval such that $I \subseteq \mathbb{R}$. Then, the nonlocal Green's first identity [36, Section 4][2] leads to

$$B_I(u,v) = -\int_I \int_I \big(u(y,t) - u(x,t)\big)\,v(x)\,\phi_\varepsilon(x-y)\,\mathrm{d}y\,\mathrm{d}x. \tag{3.3.7}$$

Multiplying (3.3.3a) and (3.3.3b) by $u(x,t)$ and integrating shows

$$\frac{\mathrm{d}}{\mathrm{d}t}\int_0^1 u^2\,\mathrm{d}x = -\frac{2}{\lambda}B_{\mathbb{R}}(u,u) \quad \text{and} \quad \frac{\mathrm{d}}{\mathrm{d}t}\int_0^1 u^2\,\mathrm{d}x = -\frac{2}{\lambda}B_{(0,1)}(u,u),$$

respectively. In either case, the assumptions on ϕ_ε are sufficient for $\int_0^1 u^2\,\mathrm{d}x$ to be decreasing in time.

Let $V_I \subseteq L^2(I)$ denote subspaces of test and trial functions defined over $I \subseteq \mathbb{R}$, as discussed in [36]. The variational formulation for the nonlocal homogeneous Dirichlet volume-constrained problem is: Find $u \in V_{\mathbb{R}} \times (0,\infty)$, i.e., $u(x,t)$ for $x \in \mathbb{R}$ and $t > 0$, such that

$$\begin{cases} \displaystyle\int_0^1 u_t v\,\mathrm{d}x + \frac{1}{\lambda}B_{\mathbb{R}}(u,v) = 0, & \forall\, v \in V_{\mathbb{R}}, \\ u(x,t) = 0, & x \in \mathbb{R}\setminus(0,1), \quad t > 0, \\ u(x,0) = u_0(x), & x \in (0,1) \end{cases} \tag{3.3.8a}$$

and the variational formulation for the nonlocal homogeneous Neumann volume-constrained problem is: Find $u \in \bar{V}_{(0,1)} \times (0,\infty)$ such that

$$\begin{cases} \displaystyle\int_0^1 u_t v\,\mathrm{d}x + \frac{1}{\lambda}B_{(0,1)}(u,v) = 0, & \forall\, v \in \bar{V}_{(0,1)}, \\ u(x,0) = u_0(x), & x \in (0,1), \end{cases} \tag{3.3.8b}$$

[2] See also the "integration by parts" formula given in [37, Lemma 2.1].

where $\bar{V}_{(0,1)} := \{v \,|\, \int_0^1 v = \int_0^1 u_0\} \subset V_{(0,1)}$. Because $B_{(0,1)}(u,1) = 0$, the compatibility relation necessary for (3.3.8b) (or (3.3.3b)) to possess a solution is

$$\int_0^1 u(x,t)\,\mathrm{d}x = \overline{u}_0 := \int_0^1 u_0(x)\,\mathrm{d}x, \quad t \geq 0. \tag{3.3.9}$$

The compatibility relation is a statement that the integrated quantity u is conserved for all time.

The use of Green's identity (3.3.7) demonstrates that the above two variational problems imply their respective strong forms (3.3.3a)–(3.3.3b). For instance,

$$\begin{aligned} 0 &= \int_0^1 u_t v\,\mathrm{d}x + \frac{1}{\lambda} B_{(0,1)}(u,v) \\ &= \int_0^1 u_t(x,t)v(x)\,\mathrm{d}x - \frac{1}{\lambda}\int_0^1\int_0^1 \big(u(y,t) - u(x,t)\big)\, v(x)\,\phi_\varepsilon(x-y)\,\mathrm{d}y\,\mathrm{d}x \\ &= \int_0^1 \left(u_t(x,t) - \frac{1}{\lambda}\int_0^1 \big(u(y,t) - u(x,t)\big)\,\phi_\varepsilon(x-y)\,\mathrm{d}y\right) v(x)\,\mathrm{d}x \end{aligned}$$

must hold for all $v \in \bar{V}_{(0,1)}$. Therefore

$$u_t(x,t) - \frac{1}{\lambda}\int_0^1 \big(u(y,t) - u(x,t)\big)\,\phi_\varepsilon(x-y)\,\mathrm{d}y = 0, \quad x \in (0,1),$$

and so (3.3.8b) implies (3.3.3b).

The variational formulation (3.3.8a) extends the one presented in [32] for a homogeneous Dirichlet volume constraint problem[3] where only the case $1 < \alpha \leq 2$, the order of the fractional Laplacian, is considered. The formulation (3.3.8a) extends the attainable order to $0 < \alpha \leq 2$ by imposing nonlocal volume constraints over intervals of non-zero length.

3.4 Numerical Experiments

Three one-dimensional examples are presented in dimensionless form. The first example examines a nonlocal Neumann problem admitting closed-form solutions for any initial condition. Example 2, which examines numerical solutions of both nonlocal Dirichlet and nonlocal Neumann problems, and Example 3, which examines numerical solutions to the nonlocal Dirichlet problem, both use the discontinuous initial condition

$$u_0(x) = \begin{cases} 0, & 0 < x < 0.5, \\ 1, & 0.5 \leq x < 1. \end{cases} \tag{3.4.1}$$

[3] The Neumann problem (3.3.8b) is not considered.

The first two examples use the density

$$\phi(s) = \chi_{(-1,1)}(s),$$

where χ_A is the indicator function for the set A, and the third example uses Lévy stable densities $\phi = \phi^\alpha$ with stability indices $\alpha = 2, 1, 1/2$. These last choices, and their relationship to fractional diffusion where the order of the fractional Laplacian is α, are discussed in Example 3. In all cases, ϕ_ε is normalized via (3.3.4) and we investigate the effects of ε, a parameter describing the nonlocality, upon the solutions at various times.

Finite element method

Partition the interval $(0,1)$ into n subintervals Ω_i of length h, recall that χ_{Ω_i} is the indicator function for Ω_i, and let $V^h_{(0,1)}$ denote the space of piecewise constant functions on the subintervals Ω_i. Given the approximation $u_h \in V^h_{(0,1)} \times (0,\infty)$,

$$u_h(x,t) = \sum_{j=1}^{n} \gamma_j(t)\chi_{\Omega_j}(x),$$

the discrete variational problem is: Find $u_h \in V^h_{(0,1)} \times (0,\infty)$ such that

$$\begin{aligned}
\int_{\Omega_i} \dot{\gamma}_i(t)\,\mathrm{d}x &= \frac{1}{\lambda} B_I(u_h, \chi_{\Omega_i}) \\
&= \frac{1}{\lambda}\int_I\int_I \big(u_h(y,t) - u_h(x,t)\big)\phi_\varepsilon(x-y)\chi_{\Omega_i}(x)\,\mathrm{d}y\,\mathrm{d}x \\
&= \frac{1}{\lambda}\int_{\Omega_i}\int_{I\setminus\Omega_i} \big(u_h(y,t) - \gamma_i(t)\big)\phi_\varepsilon(x-y)\,\mathrm{d}y\,\mathrm{d}x \\
&= \sum_{j\neq i}\gamma_j(t)\left(\frac{1}{\lambda}\int_{\Omega_i}\int_{\Omega_j}\phi_\varepsilon(x-y)\,\mathrm{d}y\,\mathrm{d}x\right) \\
&\qquad - \gamma_i(t)\left(\frac{1}{\lambda}\int_{\Omega_i}\int_{I\setminus\Omega_i}\phi_\varepsilon(x-y)\,\mathrm{d}y\,\mathrm{d}x\right), \quad i = 1,\ldots,n,
\end{aligned} \tag{3.4.2}$$

where $I = \mathbb{R}$ and $I = (0,1)$ for the nonlocal Dirichlet (3.3.8a) and Neumann (3.3.8b) problems, respectively. A forward Euler integrator in time evolves the discrete solution.

When ϕ_ε for the nonlocal Dirichlet problem is positive over $\mathbb{R}$, the last double integral of (3.4.2) is computed as

$$\begin{aligned}
\frac{1}{\lambda}\int_{\Omega_i}\int_{\mathbb{R}\setminus\Omega_i}\phi_\varepsilon(x-y)\,\mathrm{d}y\,\mathrm{d}x &= \frac{1}{\lambda}\int_{\Omega_i}\left(1 - \int_{\Omega_i}\phi_\varepsilon(x-y)\,\mathrm{d}y\right)\mathrm{d}x \\
&= \frac{1}{\lambda}\left(1 - \int_{\Omega_i}\int_{\Omega_i}\phi_\varepsilon(x-y)\,\mathrm{d}y\,\mathrm{d}x\right).
\end{aligned}$$

In the case of the nonlocal Neumann problem, the solution $u_h \in \bar{V}^h_{(0,1)} \times (0,\infty)$ is extracted by enforcing that

$$h\sum_{j=1}^{n}\gamma_j(t) = \overline{u}_0.$$

Properties of the numerical solutions

Theorems 2-3 in [26] provide important properties for the solutions of (3.3.3a) and (3.3.3b). Namely, the numerical solution $u_h(x,t)$ given by the finite element method satisfies, for the case of the homogeneous Dirichlet problem,

$$\int_0^1 u_h^2(x,t)\,\mathrm{d}x \le e^{-c_1 t}\int_0^1 u_0^2(x)\,\mathrm{d}x, \quad c_1, t > 0 \tag{3.4.3a}$$

and, for the case of the homogeneous Neumann problem,

$$\int_0^1 u_h(x,t)\,\mathrm{d}x = \overline{u}_0, \quad t > 0, \tag{3.4.3b}$$

$$\int_0^1 \big(u_h(x,t) - \overline{u}_0\big)^2\,\mathrm{d}x \le e^{-c_2 t}\int_0^1 \big(u_0(x) - \overline{u}_0\big)^2\,\mathrm{d}x, \quad c_2, t > 0, \tag{3.4.3c}$$

where the positive constants c_1 and c_2 do not depend upon the discretization.

Examples

Example 3.4.1. Consider the nonlocal Neumann problem (3.3.3b) where $\lambda = c\varepsilon^2$,

$$\phi_\varepsilon(s) = \frac{1}{2\varepsilon}\chi_{(-\varepsilon,\varepsilon)}(s), \quad c = \frac{1}{6}, \quad \varepsilon \ge 1,$$

so that, defining $\eta := \frac{3}{\varepsilon^3}$,

$$\begin{aligned} u_t(x,t) &= \eta\int_0^1 \big(u(y,t) - u(x,t)\big)\chi_{(-\varepsilon,\varepsilon)}(x-y)\,\mathrm{d}y \\ &= \eta\bigg(\int_0^1 u(y,t)\,\mathrm{d}y - u(x,t)\bigg) \\ &= \eta\big(\overline{u}_0 - u(x,t)\big). \end{aligned}$$

The solution for this ordinary differential equation yields a convex combination of $u_0(x)$ and $\overline{u}_0$,

$$u(x,t) = u_0(x)e^{-\eta t} + \overline{u}_0\big(1 - e^{-\eta t}\big). \tag{3.4.4}$$

Thus, the solution $u(x,t)$ will lie between the initial condition $u_0(x)$ and the constant $\overline{u}_0$, for all t, and the difference $u(x,t) - \overline{u}_0$ decays exponentially in time. The rate of decay decreases with increasing nonlocality ε, and for large ε the solution is well approximated by the initial condition $u_0(x)$. Therefore, increasing nonlocality ε implies that the magnitude of the jump discontinuity present in the initial condition remains large for increasing finite time.

Increasing nonlocality is also an indication that the higher-order moments may not be small. To see this, consider the formal Taylor's expansion

$$\begin{aligned}\frac{1}{\lambda}\int_{\mathbb{R}} \big(u(y,t) - u(x,t)\big)\phi_\varepsilon(x-y)\,\mathrm{d}s &= \sum_{k=1}^{\infty} \frac{1}{\lambda}\int_{\mathbb{R}} \frac{(-1)^k}{k!}\frac{\partial^k u(x,t)}{\partial x^k}\, s^k \phi_\varepsilon(s)\,\mathrm{d}s \\ &= \sum_{k=1}^{\infty} \frac{\partial^{2k} u(x,t)}{\partial x^{2k}} \frac{1}{\lambda}\int_{\mathbb{R}} \frac{s^{2k}}{(2k)!}\phi_\varepsilon(s)\,\mathrm{d}s,\end{aligned}$$

where the odd moments disappear due to the symmetry of ϕ_ε, and then

$$\frac{1}{\lambda}\int_{\mathbb{R}} \big(u(y,t) - u(x,t)\big)\phi_\varepsilon(x-y)\,\mathrm{d}s = 6\sum_{k=1}^{\infty} \frac{\partial^{2k} u(x,t)}{\partial x^{2k}} \frac{\varepsilon^{2(k-1)}}{(2k+1)!}.$$

Truncating this expansion after one term yields the classical diffusion equation — a poor approximation when higher order moments cannot be neglected. In fact, because

$$\frac{\varepsilon^{2k}}{(2k+3)!} = \frac{\varepsilon^2}{(2k+3)(2k+2)}\frac{\varepsilon^{2(k-1)}}{(2k+1)!},$$

for any ε satisfying $\varepsilon^2 > (2K+1)(2K)$ for the smallest possible integer $K > 1$, the first K even moments form an increasing sequence since

$$\frac{\varepsilon^{2i}}{(2i+3)!} > \frac{\varepsilon^{2(i-1)}}{(2i+1)!}, \quad i = 1, \ldots, K-1.$$

Example 3.4.2. Consider the nonlocal Dirichlet (3.3.3a) and Neumann (3.3.3b) problems where $\lambda = c\varepsilon^2$,

$$\phi_\varepsilon(s) = \frac{1}{2\varepsilon}\chi_{(-\varepsilon,\varepsilon)}(s), \quad c = \frac{1}{6}, \quad \varepsilon \geq 1,$$

with $\eta = \frac{3}{\varepsilon^3}$, and the initial condition (3.4.1) is used. Because closed-form solutions are not available as in Example 3.4.1, Fig. 3.1 and Fig. 3.2 plot the approximate solutions given by the finite element method with mesh spacing $h = 5 \cdot 10^{-4}$ and $t \in [0, 0.25]$. The numerical solutions u_h computed satisfy the corresponding properties (3.4.3). The rate of decay of the magnitude of the jump discontinuity in the initial condition increases with decreasing ε.

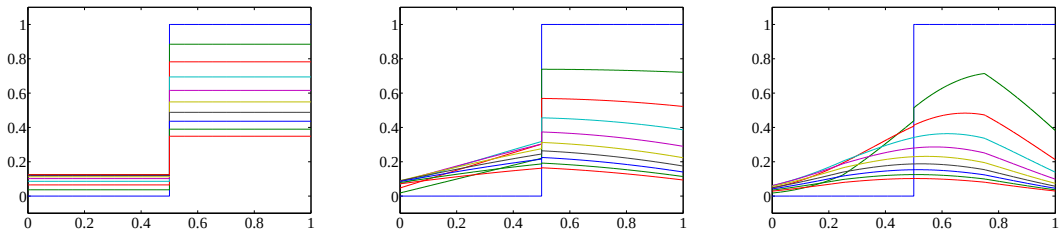

(a) $\varepsilon = 1$ (b) $\varepsilon = 0.5$ (c) $\varepsilon = 0.25$

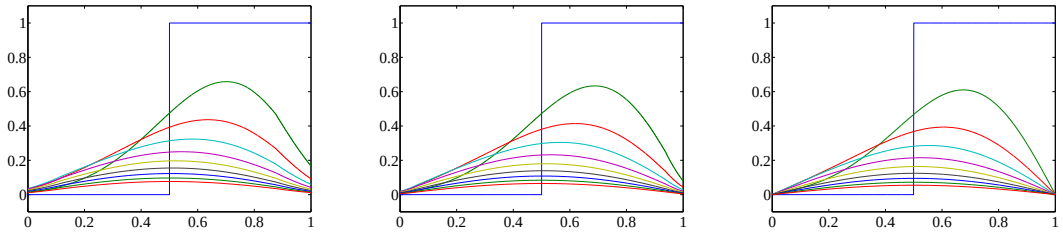

(d) $\varepsilon = 0.125$ (e) $\varepsilon = 0.0625$ (f) classical

Fig. 3.1: Panels (a)–(e) show solutions to the nonlocal homogeneous Dirichlet problem in Example 3.4.2. Panel (f) shows solutions to the corresponding classical homogeneous Dirichlet problem. The vertical axis in each panel is the value of $u_h(x,t)$ and the horizontal axis is x. The ten different solution profiles in each panel correspond to the solutions at ten different times, for $t \in [0, 0.25]$.

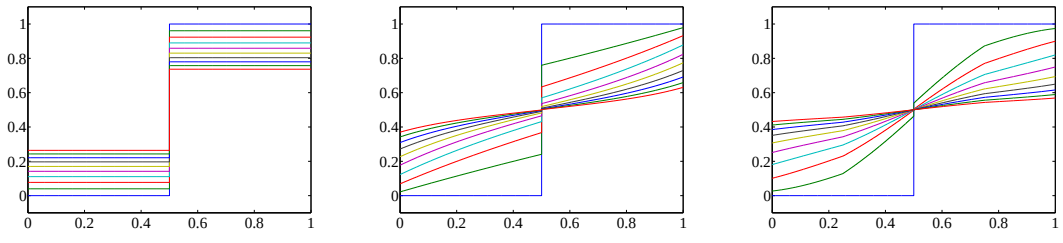

(a) $\varepsilon = 1$ (b) $\varepsilon = 0.5$ (c) $\varepsilon = 0.25$

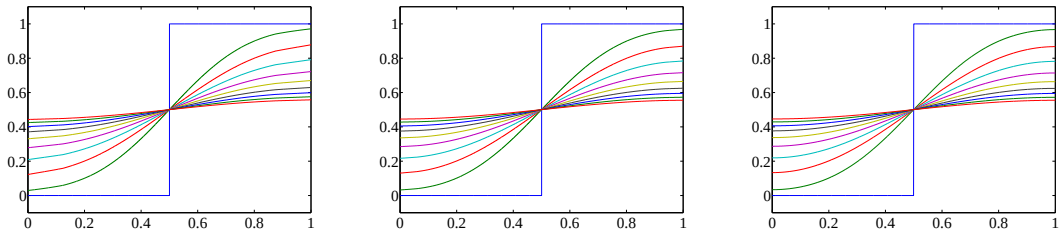

(d) $\varepsilon = 0.125$ (e) $\varepsilon = 0.0625$ (f) classical

Fig. 3.2: Panels (a)–(e) show solutions to the nonlocal homogeneous Neumann problem in Example 3.4.2. Panel (f) shows solutions to the corresponding classical homogeneous Neumann problem. The vertical axis in each panel is the value of $u_h(x,t)$ and the horizontal axis is x. The ten different solution profiles in each panel correspond to the solutions at ten different times, for $t \in [0, 0.25]$.

Fig. 3.3 plots the $L^{\infty,1,2}(0,1)$ norms of the difference, $u_h - v_h$, between numerical solutions of (3.3.3a) and (3.3.3b) and numerical solutions of (3.3.5a) and (3.3.5b), e.g.,

$$\begin{aligned}
\|u_h - v_h\|_{L^\infty(0,1)} &= \max_i \max_{x\in\Omega_i} |u_h(x,t) - v_h(x,t)|,\\
\|u_h - v_h\|_{L^1(0,1)} &= \sum_i \int_{\Omega_i} |u_h(x,t) - v_h(x,t)|\,\mathrm{d}x,\\
\|u_h - v_h\|^2_{L^2(0,1)} &= \sum_i \int_{\Omega_i} |u_h(x,t) - v_h(x,t)|^2\,\mathrm{d}x.
\end{aligned}$$

Each norm tends to zero as $t \to \infty$, reflecting agreement with steady-state solutions. However, transient solutions can differ substantially, which is witnessed by some norms increasing during small values of t. This is due to both the discontinuity in the initial condition lingering for all finite time in the solutions to the nonlocal problems and the effect of the nonlocal volume constraints, i.e., nonlocal volume constraints do not require $u_h(0^+,t) = 0$ or $(u_h)_x(0^+,t) = 0$, for instance. Further, for a fixed t, the norms tend to zero as ε decreases demonstrating agreement of solutions in the absence of nonlocality. The plots in Fig. 3.3 emphasize both the nonlocal nature of volume constraints for nonlocal diffusion and that jump discontinuities in the initial data remain for all finite time.

Fig. 3.4 plots four bar graphs for the normalized moments

$$\frac{\frac{1}{\lambda}\int_{\mathbb{R}} \frac{s^{2k}}{2k!}\phi_\varepsilon(s)\,\mathrm{d}s}{\frac{1}{\lambda}\int_{\mathbb{R}} \frac{s^2}{2!}\phi_\varepsilon(s)\,\mathrm{d}s} = 3\frac{\varepsilon^{2(k-1)}}{(2k+1)!}, \quad k = 2,3,4,5,6,7,$$

i.e., the moments are normalized so that the second moment is equal to one. The higher-order moments become negligible relative to the second moment as the nonlocality ε decreases leading to better agreement between the solutions to the nonlocal and classical diffusion equations. A side-by-side comparison of Fig. 3.4 to Fig. 3.1 and Fig. 3.2 illustrates this point.

Example 3.4.3. The fractional diffusion behavior of (3.3.3a) is examined by choosing $\phi = \phi^\alpha$ to be a centered and symmetric stable density with stability index $\alpha = 2, 1, 1/2$. As explained in Section 3.2, α represents the fraction of the Laplacian in the equation (3.2.7). Such centered and symmetric stable densities are characterized through their Fourier transforms, i.e.,

$$\phi^\alpha(s) = \mathcal{F}^{-1}\left(\exp\left(-|\xi|^\alpha\right)\right)(s),$$

see [4, §§ 1.2.5] for relevant definitions and theorems. We use the normalization (3.3.4) to define

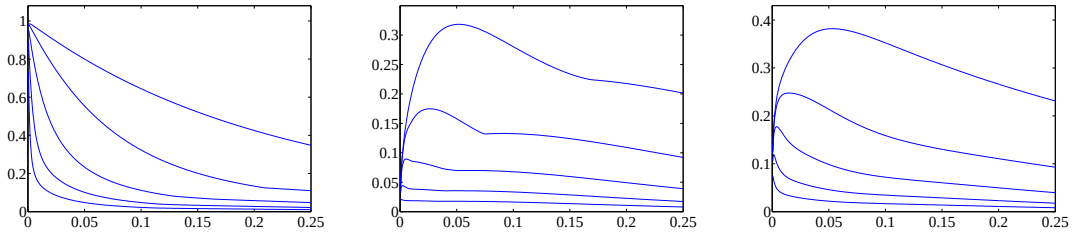

(a) $\|u_h - v_h\|_{L^\infty(0,1)}$ (b) $\|u_h - v_h\|_{L^1(0,1)}$ (c) $\|u_h - v_h\|_{L^2(0,1)}$

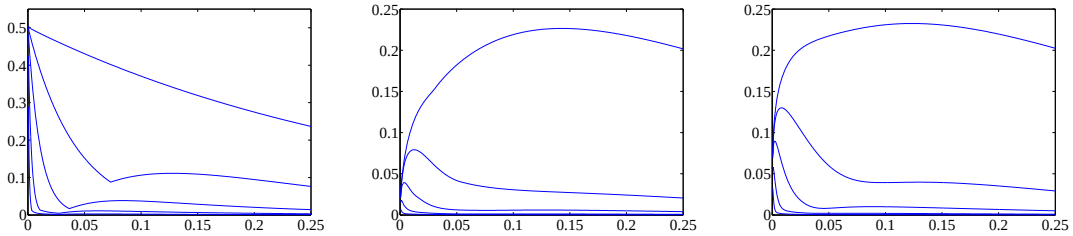

(d) $\|u_h - v_h\|_{L^\infty(0,1)}$ (e) $\|u_h - v_h\|_{L^1(0,1)}$ (f) $\|u_h - v_h\|_{L^2(0,1)}$

Fig. 3.3: Panels (a)–(c) show $L^{\infty,1,2}(0,1)$ norms of $u_h - v_h$, where u and v solve (3.3.3a) and (3.3.5a), respectively. Panels (d)–(f) show $L^{\infty,1,2}(0,1)$ norms of $u_h - v_h$, where u and v solve (3.3.3b) and (3.3.5b), respectively. The vertical axis in each panel is the value of the given norm and the horizontal axis is $t \in [0, 0.25]$. The five different curves correspond to the five different values of ε in ϕ_ε considered.

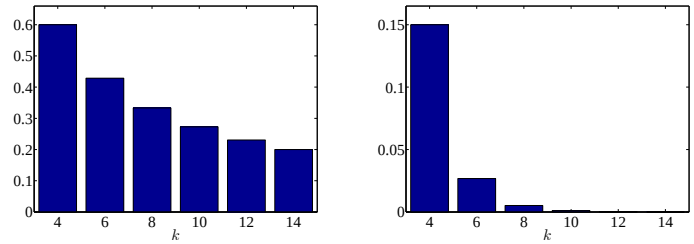

(a) $\varepsilon = 1$ (b) $\varepsilon = 0.5$

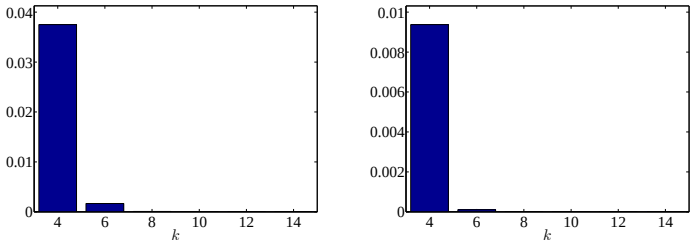

(c) $\varepsilon = 0.25$ (d) $\varepsilon = 0.125$

Fig. 3.4: The normalized moments described in Example 3.4.2.

ϕ_ε^α and for the special cases $\alpha = 2, 1$ we have closed-form expressions for ϕ_ε^α:

$$\phi_\varepsilon^\alpha(s) = \begin{cases} \left(\dfrac{1}{4\pi\varepsilon^6}\right)^{\frac{1}{2}} \exp\left(-\dfrac{s^2}{4\varepsilon^2}\right), & \alpha = 2, \\ \dfrac{1}{\pi(s^2+\varepsilon^2)}, & \alpha = 1, \end{cases}$$

which are scaled Gaussian and Cauchy densities, respectively. The case $\alpha = 1/2$, however, does not admit a closed-form for $\phi_\varepsilon^\alpha(s)$. These three densities have similarities, e.g., they are symmetric and unimodal, but differ significantly in other aspects. For instance, the second moment of ϕ_ε^2 is finite, whereas the two second moments associated with $\phi_\varepsilon^{1,1/2}$ are infinite. Moreover, the two first moments of $\phi_\varepsilon^{1,1/2}$ are undefined and infinite, respectively.

Fig. 3.5 plots the time-evolutions of the approximate solutions to (3.3.3a) for $\alpha = 2, 1, 1/2$, respectively, and various ε given by the finite element method with mesh spacing $h = 5 \cdot 10^{-4}$ and $t \in [0, 0.25]$. The numerical solutions u_h computed satisfy the corresponding properties (3.4.3). The solutions of (3.3.3a) with ϕ_ε^2 behave asymptotically, with respect to ε, as solutions to the classical diffusion equation. However, the asymptotic behavior of solutions of (3.3.3a) with $\phi_\varepsilon^{1,1/2}$ is given by a fractional Laplace parabolic equation. Consequently, the magnitude of the jump discontinuity in the initial data decays more slowly in these latter two cases.

3.5 Summary

The contribution of this paper was to present volume-constrained problems for nonlocal diffusion on bounded domains. This included a variational formulation that lead to a conforming finite element method using piecewise discontinuous shape functions. Nonlocal diffusion was demonstrated to be a model for anomalous diffusion applicable when Fick's first law represents an inaccurate model. A generalization of Fick's first law in terms of a nonlocal flux was demonstrated to hold, and a relationship between nonlocal and fractional diffusion was also reviewed, where the order of the fractional Laplacian can lie in the interval $(0, 2]$. The nonlocal Dirichlet and Neumann volume constraints used represent generalizations of the classical boundary conditions. Several examples are given where the effect of nonlocality is studied. The relationship between nonlocal and fractional diffusion explained that the numerical solution of volume-constrained problems, where the order of the fractional Laplacian can lie in the interval $(0, 2]$, is possible.

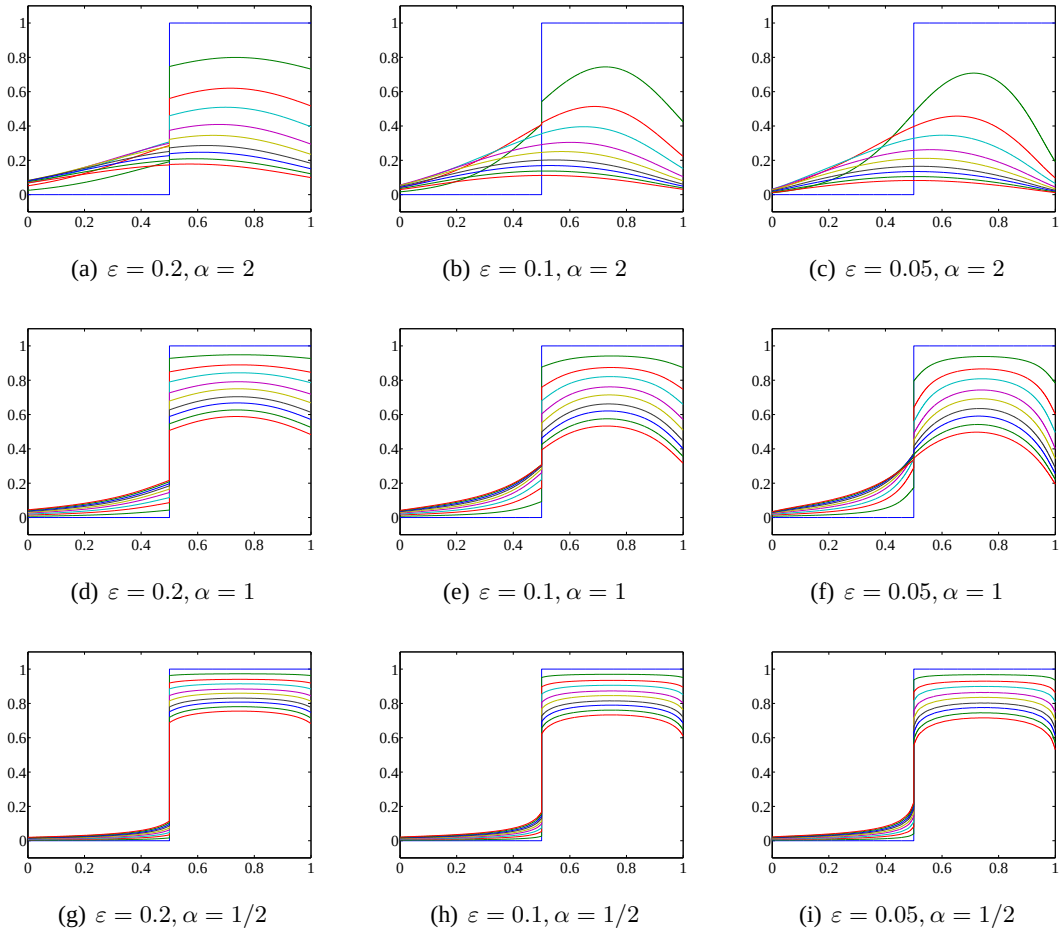

(a) $\varepsilon = 0.2, \alpha = 2$ (b) $\varepsilon = 0.1, \alpha = 2$ (c) $\varepsilon = 0.05, \alpha = 2$

(d) $\varepsilon = 0.2, \alpha = 1$ (e) $\varepsilon = 0.1, \alpha = 1$ (f) $\varepsilon = 0.05, \alpha = 1$

(g) $\varepsilon = 0.2, \alpha = 1/2$ (h) $\varepsilon = 0.1, \alpha = 1/2$ (i) $\varepsilon = 0.05, \alpha = 1/2$

Fig. 3.5: Solutions to the nonlocal homogeneous Dirichlet problem with ϕ_ε^α in Example 3.4.3. The vertical axis in each panel is the value of $u_h(x,t)$ and the horizontal axis is x. The ten different solution profiles in each panel correspond to the solutions at ten different times, for $t \in [0, 0.25]$.

4. THE NONLOCAL CATTANEO-VERNOTTE EQUATION ON BOUNDED DOMAINS

This chapter is concerned with studying the nonlocal Cattaneo-Vernotte equation on bounded domains. The work in this chapter is currently in preparation for journal submission by the author. We demonstrate that the nonlocal Cattaneo-Vernotte equation is obtained by including a relaxation effect in the nonlocal diffusion equation and, in fact, arises from a generalization of Fick's first law in terms of a nonlocal flux. In a certain limit of vanishing nonlocality and relaxation time, we find a relationship between the nonlocal Cattaneo-Vernotte equation and the classical and fractional diffusion equations. The contribution of this paper is to introduce volume constraints for the nonlocal Cattaneo-Vernotte equation, which induce boundary conditions for the underlying CTRWs. Further, the variational and finite element formulations for these nonlocal volume-constrained problems are reviewed and demonstrated to be powerful tools. We review well-posedness of these nonlocal boundary value problems and provide properties of their solutions. We investigate the effect of relaxation time, i.e., non-Markovian effects, and nonlocality.

4.1 Introduction

This chapter focuses on the nonlocal Cattaneo-Vernotte equation

$$u_t(x,t) + \frac{\tau}{2} u_{tt}(x,t) = \frac{1}{\beta} \int_{\mathbb{R}} \big(u(y,t) - u(x,t)\big)\, \phi(x-y)\, \mathrm{d}y, \tag{4.1.1}$$

where u is some field, e.g., temperature or probability, ϕ is a symmetric function, i.e., $\phi(x-y) = \phi(y-x)$, and $\tau, \beta > 0$. The integral operator in (4.1.1) is nonlocal because the change at time t of the field u at x depends on u at $y \neq x$ via the convolution of u and ϕ. The equation (4.1.1) is the generalized master equation for a non-Markovian CTRW, namely a renewal-reward process

$$Y_t = \sum_{k=1}^{N_t} R_k, \tag{4.1.2}$$

where the wait-times are *not* exponentially distributed and $R_k \overset{iid}{\sim} \phi$. In this setting, ϕ is a probability density function so that $\phi(x-y)$ represents the step density from x to y of the random walker.

Moreover, β is the mean wait-time between steps and $\tau/2 > 0$ is a relaxation time. We note the nonlocal Cattaneo-Vernotte equation (4.1.1) is also a model for nonlocal hyperbolic heat conduction.

It is revealing to contrast (4.1.1) to the classical Cattaneo-Vernotte equation

$$w_t + \frac{\tau}{2} w_{tt} = a w_{xx}, \tag{4.1.3}$$

where $\tau/2 > 0$ is again a relaxation time and $a > 0$ is the diffusion coefficient. The equation (4.1.3) is a model for diffusion that admits finite speeds of propagation, specifically $\sqrt{2a/\tau}$. When w is a temperature field, (4.1.3) is a model of hyperbolic heat conduction [45]. Further, (4.1.3) arises from the classical balance law, $w_t = -q_x$, and a generalization of Fick's first law in which the flux is given by a convolution of the gradient of the field w and a relaxation kernel [39],

$$q(x,t) = -a \int_0^t \frac{2}{\tau} \exp\left(-\frac{t-t'}{\tau/2}\right) w_x(x,t') \, \mathrm{d}t'. \tag{4.1.4}$$

The assumption (4.1.4) also takes the more familiar form of Cattaneo's equation [25],

$$q + \frac{\tau}{2} q_t = -a w_x. \tag{4.1.5}$$

Equation (4.1.3) overcomes limitations of the classical diffusion equation

$$w_t = a w_{xx}, \tag{4.1.6}$$

which arises from the classical balance law, $w_t = -q_x$, and Fick's first law

$$q = -a w_x. \tag{4.1.7}$$

One such limitation is that (4.1.6) implies an infinite speed of propagation since its fundamental solution is given by

$$w(x,t) = \frac{1}{\sqrt{4\pi a t}} \exp\left(-\frac{x^2}{4at}\right), \tag{4.1.8}$$

which is positive for all x, for any arbitrarily small t. This is referred to in the literature as "unphysical" since disturbances are instantaneously propagated. Moreover, (4.1.6) is incapable of capturing transient dynamics of the field in situations involving short times, high frequencies, and short wave lengths [45]. One approach to remedy these issues is to introduce a relaxation time [39] and a special case of this is the classical Cattaneo-Vernotte equation (4.1.3). A criticism of the classical

Cattaneo-Vernotte equation as a model for heat conduction, however, is that it can violate the second law of thermodynamics.

It is also revealing to contrast (4.1.1) with the nonlocal diffusion equation

$$u_t(x,t) = \frac{1}{\lambda}\int_{\mathbb{R}} \big(u(y,t) - u(x,t)\big)\phi(x-y)\,\mathrm{d}y, \tag{4.1.9}$$

which has been used in various applications, see [5, 17, 24, 35], and is well-understood as the generalized master equation for a Markovian CTRW, namely a compound Poisson process

$$Y_t = \sum_{k=1}^{N_t} R_k, \tag{4.1.10}$$

where, again, $R_k \overset{iid}{\sim} \phi$, but the wait-times *are* exponentially distributed. As in (4.1.1), the second-order spatial derivative in (4.1.9) has been replaced with the nonlocal integral operator and, consequently, is a model for anomalous diffusion. Models for anomalous diffusion include (4.1.1), (4.1.9), and the fractional diffusion equation

$$v_t = -c\,(-\Delta)^{\alpha/2}\,v, \quad 0 < \alpha \leq 2, \tag{4.1.11}$$

which includes (4.1.6) as the special case $\alpha = 2$ and $c = a$. The fundamental solution to the fractional diffusion equation (4.1.11) satisfies

$$\widehat{v}(\xi,t) = \exp\left(-c|\xi|^{\alpha}t\right),$$

which is the density of a centered and symmetric stable process, S_t^{α}, with index of stability α. Again, the case $\alpha = 2$ and $c = a$ yields (4.1.8), the probability density function of Brownian motion.

Volume constraints on the solution play the role of boundary conditions and have been studied for the integral operator in (4.1.1) and (4.1.9), see [36], and specifically for the nonlocal diffusion equation, see [21, 26]. As expected, the resulting nonlocal volume-constrained value problems for (4.1.1) and (4.1.9) were demonstrated in [22] to be the generalized master equations for non-Markovian and Markovian CTRW, respectively, on bounded domains. Thus, the variational formulations of such nonlocal volume-constrained problems and ensuing finite element method provide a powerful tool for studying CTRW on bounded domains. The contribution of this chapter is to investigate the effect of a nonzero relaxation time, i.e., differences between Markovian and

non-Markovian random walks, by comparing solutions of the nonlocal boundary value problems corresponding to (4.1.9) to those corresponding to (4.1.1).

The rest of this chapter is organized as follows. Section 4.2 demonstrates how (4.1.1) arises from a generalization of Fick's first law in which the flux is given by a convolution of a memory kernel and a nonlocal spatial operator acting as the gradient of the field, in contrast to (4.1.4). The relationships between (4.1.1), (4.1.11), and (4.1.9) are also reviewed. Further, we show that the nonlocal Cattaneo-Vernotte equation is the master equation for a renewal-reward process and that it admits infinite speeds of propagation. Volume constraints for (4.1.1) are reviewed in Section 4.3 as are the variational formulation and ensuing finite element method. Section 4.4 provides numerical examples to illustrate the effects of nonzero relaxation time and nonlocality. In these examples, we investigate the effect of relaxation time and study the effect of nonlocality and the relationship to fractional diffusion.

4.2 The Nonlocal Cattaneo-Vernotte Equation in Free Space

In this section, we study the nonlocal Cattaneo-Vernotte equation in free space. Namely, we demonstrate how (4.1.1) arises from a generalization of Fick's first law in which the flux is given by a convolution of a memory kernel and a nonlocal spatial operator acting as the gradient of the field, in contrast to (4.1.4). The relationships between (4.1.1), (4.1.11), and (4.1.9) are also reviewed. Further, we show that the nonlocal Cattaneo-Vernotte equation is the master equation for a renewal-reward process and that it admits infinite speeds of propagation.

Generalization of Fick's first law and a nonlocal flux

We demonstrate that (4.1.1) arises via the classical balance law, $u_t = -\varrho_x$, and a generalization of Fick's first law,

$$\varrho(x,t) = \int_0^t \frac{2}{\tau} \exp\left(-\frac{t-t'}{\tau/2}\right)\left(\frac{1}{\beta}p(x,t')\right) \mathrm{d}t', \tag{4.2.1}$$

where

$$p(x,t) := -\frac{1}{2}\int_{\mathbb{R}}\int_{\Omega} \big(u(x+(1-\mu)z,t) - u(x-\mu z,t)\big) z\phi(z)\,\mathrm{d}\mu\,\mathrm{d}z.$$

Differentiating (4.2.1) with respect to t and rearranging reveals

$$\varrho + \frac{\tau}{2}\varrho_t = \frac{1}{\beta}p, \tag{4.2.2}$$

and so

$$u_t = -\frac{1}{\beta}p_x + \frac{\tau}{2}\varrho_{xt} = -\frac{1}{\beta}p_x - \frac{\tau}{2}u_{tt}.$$

Noll's Lemma I [46, 54] implies that

$$-\frac{1}{\beta}p_x(x,t') = \frac{1}{\beta}\int_{\mathbb{R}} \big(u(x+z,t') - u(x,t')\big)\phi(z)\,\mathrm{d}z, \tag{4.2.3}$$

and so (4.1.1) is established.

A relationship to fractional and classical diffusion equations

A formal relationship between (4.1.1) and (4.1.3) in the presence of vanishing nonlocality is now established. Fix $\tau > 0$, let $\beta = \varepsilon^2$, where $\varepsilon > 0$, and define the symmetric probability density

$$\phi_\varepsilon(s) := \frac{1}{\varepsilon}\phi(s/\varepsilon), \tag{4.2.4}$$

where the given symmetric density ϕ satisfies

$$\int_{\mathbb{R}} s^{2k}\phi(s)\,\mathrm{d}s < \infty, \quad k = 0, 1, 2\ldots.$$

As $\varepsilon \to 0$, $\phi_\varepsilon(x-y)$ weights points nearby x more heavily, relative to points further away. Specifying the second moment appropriately, the Fourier transform of ϕ has an expansion of the form

$$\widehat{\phi}(\xi) = 1 - a|\xi|^2 + \mathrm{o}(|\xi|^2), \quad a > 0.$$

With ϕ_ε in place of ϕ and assuming a formal Taylor expansion is valid for sufficiently small ε,

$$\begin{aligned}
\frac{1}{\beta}p(x,t) &= -\frac{1}{2}\int_{\mathbb{R}}\int_{\Omega}\frac{1}{\varepsilon^2}\left(u_x(x,t)z^2 + \sum_{k=2}^{\infty}\frac{1}{k!}z^{k+1}\frac{\partial^k u(x,t)}{\partial x^k}\right)\phi_\varepsilon(z)\,\mathrm{d}\mu\,\mathrm{d}z \\
&= -au_x(x,t) + \frac{1}{\varepsilon^2}\sum_{k=2}^{\infty}\frac{\partial^{2k-1}u(x,t)}{\partial x^{2k-1}}\frac{1}{(2k-1)!}\int_{\mathbb{R}} z^{2k}\phi_\varepsilon(z)\,\mathrm{d}z \\
&= -au_x(x,t) + \sum_{k=2}^{\infty}\frac{\partial^{2k-1}u(x,t)}{\partial x^{2k-1}}\frac{\varepsilon^{2(k-1)}}{(2k-1)!}\int_{\mathbb{R}} z^{2k}\phi(z)\,\mathrm{d}z
\end{aligned}$$

and, utilizing (4.2.2), we obtain an approximation of (4.1.5),

$$\varrho + \frac{\tau}{2}\varrho_t = -au_x + \mathrm{O}(\varepsilon^2). \tag{4.2.5}$$

Thus, in the absence of nonlocality, the nonlocal Cattaneo-Vernotte equation (4.1.1) reduces to the classical Cattaneo-Vernotte equation (4.1.3). The effect of the density ϕ_ε with $\beta = \varepsilon^2$ as ε decreases

is to "localize" the diffusion of (4.1.1). Indeed, taking $\phi(x-y) = \delta(x-y) + a\delta''(x-y)$ in (4.1.1) recovers (4.1.3). Moreover, if $\tau = \mathrm{O}(\varepsilon^2)$, (4.2.5) reduces to

$$\varrho = -au_x + \mathrm{O}(\varepsilon^2), \tag{4.2.6}$$

approximating (4.1.7). Thus, in the absence of both relaxation time and nonlocality, the nonlocal Cattaneo-Vernotte equation (4.1.1) reduces to the classical diffusion equation (4.1.6).

Finally, we establish a relationship to the fractional diffusion equation (4.1.11). Suppose ϕ is a symmetric probability density function with the expansion

$$\widehat{\phi}(\xi) = 1 - c|\xi|^\alpha + \mathrm{o}(|\xi|^\alpha), \quad 0 < \alpha \leq 2, \tag{4.2.7}$$

for $c > 0$, so that, defining ϕ_ε via (4.2.4),

$$\widehat{\phi}_\varepsilon(\xi) = 1 - c\varepsilon^\alpha|\xi|^\alpha + \mathrm{o}(\varepsilon^\alpha|\xi|^\alpha).$$

Assuming $\beta = \varepsilon^\alpha$, the Fourier transform of (4.1.1) gives

$$\begin{aligned}
\widehat{u}_t(\xi,t) + \frac{\tau}{2}\widehat{u}_{tt}(\xi,t) &= \frac{1}{\varepsilon^\alpha}\left(\widehat{\phi}_\varepsilon(\xi) - 1\right)\widehat{u}(\xi,t) \\
&= \frac{1}{\varepsilon^\alpha}(-c\varepsilon^\alpha|\xi|^\alpha + \mathrm{o}(\varepsilon^\alpha|\xi|^\alpha))\widehat{u}(\xi,t) \\
&= -c|\xi|^\alpha\widehat{u}(\xi,t) + \mathrm{O}(\varepsilon^\alpha|\xi|^\alpha),
\end{aligned}$$

implying that u, formally, is approximately given by the fractional Cattaneo-Vernotte equation

$$v_t(x,t) + \frac{\tau}{2}v_{tt}(x,t) = -c(-\Delta)^{\alpha/2}v(x,t). \tag{4.2.8}$$

Further, if $\tau = \mathrm{O}(\varepsilon^\alpha)$, u is approximately given by the fractional diffusion equation (4.1.11).

Master equation for a renewal-reward process

We now show that (4.1.2) is the master equation for a renewal reward process. First, recall the master equation for an arbitrary CTRW,

$$u_t(x,t) = \int_0^t \Lambda(t-t') \int_{\mathbb{R}} \big(u(y,t') - u(x,t')\big)\phi(x-y)\,\mathrm{d}y\,\mathrm{d}t'. \tag{4.2.9}$$

Choosing

$$\Lambda(t-t') = \frac{1}{\beta}\frac{2}{\tau}\exp\left(-\frac{t-t'}{\tau/2}\right), \tag{4.2.10}$$

where ϕ is a symmetric function, i.e., $\phi(x-y)=\phi(y-x)$, and $\beta \geq 2\tau > 0$, gives the nonlocal Cattaneo-Vernotte equation. The assumption (4.2.10) is tantamount to

$$\omega(t) = \begin{cases} \dfrac{t}{\tau^2}\exp\left(-\dfrac{1}{\tau}t\right), & \beta = 2\tau, \\ \dfrac{2}{\sqrt{\beta(\beta-2\tau)}}\exp\left(-\dfrac{t}{\tau}\right)\sinh\left(\dfrac{\sqrt{\beta(\beta-2\tau)}}{\beta\tau}t\right), & \beta > 2\tau. \end{cases} \tag{4.2.11}$$

The special case $\beta = 2\tau$ implies $W \sim \text{Gamma}(2,\tau)$, where W is the wait-time random variable. The restriction $\beta \geq 2\tau$ has appealing consequences as well, e.g., positivity of solutions and conservation of mass. We note

$$\widehat{\omega}(s) = \frac{2}{\beta\tau s^2 + 2\beta s + 2} = \sum_{k=0}^{\infty}\frac{(-1)^k}{k!}\mathbb{E}(W^k)s^k = 1 - \beta s + \mathrm{o}(s),$$

which shows that the mean wait-time is indeed β.

We focus on the special case $\beta = 2\tau$. By independence,

$$\sum_{k=1}^{n} W_k \sim \text{Gamma}\left(2n,\tau\right),$$

so that

$$f_n(t) = \frac{t^{2n-1}}{\tau^{2n}(2n-1)!}\exp\left(-\frac{t}{\tau}\right),$$

where $f_n(t)$ denotes the density of $\sum_{k=1}^{n} W_k$. Notice

$$P(N_t \geq n) = P\left(\sum_{k=1}^{n} W_k \leq t\right) = \int_0^t f_n(s)\,\mathrm{d}s$$

and thus

$$P(N_t = n) = \int_0^t f_n(s)\,\mathrm{d}s - \int_0^t f_{n+1}(s)\,\mathrm{d}s = \exp\left(-\frac{t}{\tau}\right)\left[\frac{(t/\tau)^{2n}}{(2n)!} + \frac{(t/\tau)^{2n+1}}{(2n+1)!}\right].$$

The characteristic function is then found directly,

$$\begin{aligned}
\varphi_{Y_t}(\xi) &= \mathbb{E}(e^{i\xi Y_t}) \\
&= \mathbb{E}\left(\exp\left(i\xi\sum_{k=1}^{N_t} R_k\right)\right) \\
&= \sum_{n=0}^{\infty} \mathbb{E}\left(\exp\left(i\xi\sum_{k=1}^{n} R_k\right)\right) P(N_t = n) \\
&= \sum_{n=0}^{\infty} \left[\mathbb{E}\left(\exp\left(i\xi R_1\right)\right)\right]^n P(N_t = n) \\
&= \exp\left(-\frac{t}{\tau}\right) \sum_{n=0}^{\infty} \left[\varphi_{R_1}(\xi)\right]^n \left[\frac{(t/\tau)^{2n}}{(2n)!} + \frac{(t/\tau)^{2n+1}}{(2n+1)!}\right] \\
&= \exp\left(-\frac{t}{\tau}\right) \left[\sum_{n=0}^{\infty}\left(\frac{(t(\varphi_{R_1}(\xi))^{1/2}/\tau)^{2n}}{(2n)!}\right) + (\varphi_{R_1}(\xi))^{-1/2}\sum_{n=0}^{\infty}\left(\frac{(t(\varphi_{R_1}(\xi))^{1/2}/\tau)^{2n+1}}{(2n+1)!}\right)\right] \\
&= \exp\left(-\frac{t}{\tau}\right) \left[\cosh\left(\frac{t}{\tau}(\varphi_{R_1}(\xi))^{1/2}\right) + (\varphi_{R_1}(\xi))^{-1/2}\sinh\left(\frac{t}{\tau}(\varphi_{R_1}(\xi))^{1/2}\right)\right]. \qquad (4.2.12)
\end{aligned}$$

Speed of propagation

From (4.2.12), we note that the Fourier transform of the solution to (4.1.1) for the case $\beta = 2\tau = \varepsilon^2$ with $u(x,0) = \delta(x)$ and $u_t(x,0) = 0$ is

$$\widehat{u}(\xi,t) = \exp\left(-\frac{t}{\tau}\right)\left[\cosh\left(\frac{t}{\tau}(\widehat{\phi}_\varepsilon(\xi))^{1/2}\right) + \frac{1}{\tau}\left(\tau(\widehat{\phi}_\varepsilon(\xi))^{-1/2}\right)\sinh\left(\frac{t}{\tau}(\widehat{\phi}_\varepsilon(\xi))^{1/2}\right)\right].$$

The Fourier transform of the solution to (4.1.3) with $w(x,0) = \delta(x)$ and $w_t(x,0) = 0$ is

$$\widehat{w}(\xi,t) = \exp\left(-\frac{t}{\tau}\right)\left[\cosh(\eta t) + \frac{1}{\tau\eta}\sinh(\eta t)\right], \qquad (4.2.13)$$

where

$$\eta = \sqrt{\frac{1}{\tau^2} - \frac{2a\varepsilon^2}{\tau}\xi^2},$$

see [40]. As we know, (4.1.3) admits a finite speed of propagation, namely $\sqrt{2a/\tau}$. As expected, if $\widehat{\phi}_\varepsilon(\xi) = 1 - 2a\tau\varepsilon^2\xi^2$, i.e., $\phi_\varepsilon(x-y) = \delta(x-y) + 2a\tau\varepsilon^2\delta''(x-y)$, then (4.2.12) reduces to (4.2.13). An effect of replacing the Laplacian with the nonlocal operator in (4.1.1) is that disturbances propagate with an infinite speed.

Theorem 4.2.1. *For the equation* (4.1.1)*, disturbances propagate with an infinite speed.*

Proof. A disturbance at x and time t will propagate at least to $(x-\delta, x+\delta)$, where $\text{supp}(\phi) \supseteq (-\delta, \delta)$, at time $t+\widetilde{t}$ for any $\widetilde{t} > 0$. An inductive argument demonstrates that a disturbance at x and time t will be felt at least within $(x-k\delta, x+k\delta)$ at time $t+\widetilde{t}$ for $\widetilde{t} = \sum_{i=1}^{k} \widetilde{t}_i$, where $\widetilde{t}_i > 0$. Taking $k \to \infty$ such that $\widetilde{t}$ remains finite demonstrates an infinite speed of propagation. □

4.3 The Nonlocal Cattaneo-Vernotte Equation with Volume Constraints

The results in [36] provide a variational formulation for volume-constrained problems for (4.1.1). This follows closely to that presented for the nonlocal diffusion equation (4.1.9) in [21].

Volume constraints and variational formulation

We consider the bounded domain Ω and the bilinear form

$$B_I(u,v) := \frac{1}{2}\int_I \int_I \big(u(y,t)-u(x,t)\big)\big(v(y)-v(x)\big)\,\phi_\varepsilon(x-y)\,\mathrm{d}y\,\mathrm{d}x, \tag{4.3.1}$$

where $I \in \{\mathbb{R}, \Omega\}$. Let $\bar{V}_I$ denote the possible choices for the subspaces of test and trial functions,

$$\bar{V}_{\mathbb{R}} := \left\{ v \in V_{\mathbb{R}} \;\middle|\; v\,|_{\mathbb{R}\setminus\Omega} = 0 \right\} \text{ and } \bar{V}_{\Omega} := \left\{ v \in V_{\Omega} \;\middle|\; \int_\Omega v\,\mathrm{d}x = \int_\Omega u_0\,\mathrm{d}x \right\},$$

where $u(x,0) = u_0(x)$ is a given initial density satisfying $u_0 \geq 0$ and $\int_\Omega u_0(x)\,\mathrm{d}x = 1$ and

$$V_I := \left\{ v \;\middle|\; \int_I |v|^2\,\mathrm{d}x < \infty \right\}.$$

The nonlocal homogeneous Dirichlet ($I = \mathbb{R}$) and Neumann ($I = \Omega$) volume-constrained problems for (4.1.1) are presented together: find $u \in \bar{V}_I \times (0,\infty)$ such that

$$\begin{cases} u_t(x,t) + \dfrac{\tau}{2}u_{tt}(x,t) = \dfrac{1}{\beta}\displaystyle\int_I \big(u(y,t)-u(x,t)\big)\phi_\varepsilon(x-y)\,\mathrm{d}y, & x \in \Omega, \\ u(x,0) = u_0(x), & x \in \Omega, \\ u_t(x,0) = 0, & x \in \Omega. \end{cases} \tag{4.3.2}$$

We recall the nonlocal homogeneous Dirichlet and Neumann volume-constrained problems for (4.1.9),

$$\begin{cases} u_t(x,t) = \dfrac{1}{\lambda}\displaystyle\int_I \big(u(y,t)-u(x,t)\big)\phi_\varepsilon(x-y)\,\mathrm{d}y, & x \in \Omega, \\ u(x,0) = u_0(x), & x \in \Omega, \end{cases} \tag{4.3.3}$$

studied in [21, 26, 36]. Both (4.3.2) and (4.3.3) were studied in [22] in the context of CTRW. Well-posedness of (4.3.3) has been treated in [26] and we now present a useful result from [31] on the well-posedness of (4.3.2).

Theorem 4.3.1 (Emmrich and Weckner (2006))**.** *Suppose*

$$\kappa_0 := \operatorname{esssup}_{x\in I} |K_0(x)| < \infty \quad \textit{and} \quad \kappa := \int_\Omega \int_\Omega |K(x,y)|^2 \,\mathrm{d}y\,\mathrm{d}x < \infty.$$

Then, for a given $u_0 \in \bar{V}_I$, there is a unique mild solution $u \in C^2([0,T];\bar{V}_I)$ to

$$\frac{2}{\tau}u_t(x,t) + u_{tt}(x,t) = \int_\Omega K(x,y)u(y,t)\,\mathrm{d}y - K_0(x)u(x,t).$$

Existence and uniqueness of solutions to (4.3.2) follow from Theorem 4.3.1 with

$$K(x,y) := \frac{2}{\tau\beta}\phi_\varepsilon(x-y) \quad \text{and} \quad K_0(x) = \int_I \frac{2}{\tau\beta}\phi_\varepsilon(x-y)\,\mathrm{d}y.$$

The variational formulations to (4.3.2) and (4.3.3) are: find $u \in \bar{V}_I \times (0,\infty)$ such that

$$\begin{cases} \displaystyle\int_\Omega u_t v\,\mathrm{d}x + \frac{\tau}{2}\int_\Omega u_{tt} v\,\mathrm{d}x + \frac{1}{\beta}B_I(u,v) = 0, & \forall\, v \in V_I, \\ u(x,0) = u_0(x), & x \in \Omega, \\ u_t(x,0) = 0, & x \in \Omega \end{cases} \tag{4.3.4}$$

and find $u \in \bar{V}_I \times (0,\infty)$ such that

$$\begin{cases} \displaystyle\int_\Omega u_t v\,\mathrm{d}x + \frac{1}{\lambda}B_I(u,v) = 0, & \forall\, v \in V_I, \\ u(x,0) = u_0(x), & x \in \Omega. \end{cases} \tag{4.3.5}$$

We refer the reader to [21, 36] for more details concerning the variational formulations.

The nonlocal Dirichlet volume constraint constrains the field u on the volume $\mathbb{R} \setminus \Omega$, whereas the nonlocal Neumann volume constraint restricts diffusion to occur only inside Ω, i.e., density neither enters nor exits Ω. Further, since $B_\Omega(u,1) = 0$, the compatibility condition necessary for the Neumann problems in both (4.3.2) and (4.3.3) to possess solutions is

$$\overline{u}_0 := \int_\Omega u_0(x)\,\mathrm{d}x = \int_\Omega u(x,t)\,\mathrm{d}x, \quad \forall t \geq 0, \tag{4.3.6}$$

which is a statement that the integrated quantity u is conserved for all time.

Properties of solutions

The following theorem and its corollary demonstrate that solutions of (4.3.2) necessarily converge to a stationary solution as $t \to \infty$.

Theorem 4.3.2. *Let $u \in C^2([0,T];\bar{V}_I)$ be the unique solution to* (4.3.2)*. Then, $u_t(x,t) \to 0$, as $t \to \infty$, for almost every $x \in I$.*

Proof. Multiply (4.3.2) by $u_t(x,t)$, integrate over $x \in I$, and then integrate in t to obtain

$$\frac{\tau}{4}\int_I u_t^2(x,t)\,\mathrm{d}x = \frac{1}{2\beta}\left(B_I(u_0,u_0) - B_I(u,u)\right) - \int_0^t \int_I u_t^2(x,s)\,\mathrm{d}x\,\mathrm{d}s$$

and thus

$$B_I(u_0,u_0) \geq B_I(u,u) + 2\beta\int_0^t\int_I u_t^2(x,s)\,\mathrm{d}x\,\mathrm{d}s \geq 2\beta\int_0^t\int_I u_t^2(x,s)\,\mathrm{d}x\,\mathrm{d}s.$$

Since $B_I(u_0,u_0) < \infty$, $u_t(x,t) \in L^2(I)$ for all t and

$$\|u_t(x,t)\|^2_{L^2(I)} = \int_I u_t^2(x,t)\,\mathrm{d}x \to 0.$$

The completeness of $L^2(I)$ implies that $u_t \to g$ with $\|g\|_{L^2(I)} = 0$, i.e., $g = 0$ almost everywhere and, thus, $u_t \to 0$ for almost every $x \in I$. □

A stationary solution to (4.3.2), $u_s \in \bar{V}_I$, solves

$$\int_I \big(u_s(y) - u_s(x)\big)\phi(x-y)\,\mathrm{d}y = 0, \quad \forall x \in \Omega.$$

The results in [26, 36] demonstrate that the unique stationary solution, $x \in I$, of the homogeneous Dirichlet problem is $u_s = 0$ and that of the homogeneous Neumann problem is $u_s = \overline{u}_0$. Consequently, a simple corollary to Theorem 4.3.2 exists.

Corollary 4.3.3. *For almost every $x \in \Omega$, $u(x,t) \to u_s(x)$ as $t \to \infty$.*

We have thus supplied the following properties for the solutions of (4.3.2): for the case of the homogeneous Dirichlet problem,

$$\int_\Omega u(x,t)\,\mathrm{d}x \to 0, \quad \text{as } t \to \infty, \tag{4.3.7a}$$

$$\int_\Omega u^2(x,t)\,\mathrm{d}x \to 0, \quad \text{as } t \to \infty, \tag{4.3.7b}$$

and, for the case of the homogeneous Neumann problem,

$$\int_\Omega u(x,t)\,\mathrm{d}x = 1, \quad t > 0, \tag{4.3.7c}$$

$$\int_\Omega \big(u(x,t) - \overline{u}_0\big)^2\,\mathrm{d}x \to 0, \quad \text{as } t \to \infty. \tag{4.3.7d}$$

The results of [26] provide properties for the solutions of (4.3.3): for the homogeneous Dirichlet problem,

$$\int_\Omega u(x,t)\,\mathrm{d}x \le e^{-\frac{c_1}{2}t}\sqrt{\int_\Omega u_0^2(x)\,\mathrm{d}x}, \quad c_1, t > 0 \tag{4.3.8a}$$

$$\int_\Omega u^2(x,t)\,\mathrm{d}x \le e^{-c_1 t}\int_\Omega u_0^2(x)\,\mathrm{d}x, \quad c_1, t > 0 \tag{4.3.8b}$$

and, for the homogeneous Neumann problem,

$$\int_\Omega u(x,t)\,\mathrm{d}x = 1, \quad t > 0, \tag{4.3.8c}$$

$$\int_\Omega \big(u(x,t) - \overline{u}_0\big)^2\,\mathrm{d}x \le e^{-c_2 t}\int_\Omega \big(u_0(x) - \overline{u}_0\big)^2\,\mathrm{d}x, \quad c_2, t > 0. \tag{4.3.8d}$$

A semi-discrete finite element formulation

To formulate the finite element method, we partition Ω into n subintervals Ω_i and let $\chi_{\Omega_i}(x)$ be the indicator function for Ω_i. We denote the space of piecewise constant functions on the subintervals Ω_i by V_Ω^h. Note any $u_h \in V_\Omega^h \times (0,\infty)$ can be written

$$u_h(x,t) = \sum_{j=1}^{n} \gamma_j(t)\chi_{\Omega_j}(x).$$

The discrete variational problems to (4.3.4) and (4.3.5) are then: find $u_h \in V_\Omega^h \times (0,\infty)$ such that

$$\mathbf{M}\dot{\boldsymbol{\gamma}} + \frac{\tau}{2}\mathbf{M}\ddot{\boldsymbol{\gamma}} = -\frac{1}{\beta}\mathbf{A}\boldsymbol{\gamma} \quad \text{and} \quad \mathbf{M}\dot{\boldsymbol{\gamma}} = -\frac{1}{\lambda}\mathbf{A}\boldsymbol{\gamma},$$

respectively, where $\mathbf{M}$ and $\mathbf{A}$ are the mass and stiffness matrices defined by

$$M_{ii} = |\Omega_i| \quad \text{and} \quad A_{ij} = \begin{cases} -\displaystyle\int_{\Omega_i}\int_{\Omega_j} \phi_\varepsilon(x-y)\,\mathrm{d}y\,\mathrm{d}x, & i \ne j, \\ \displaystyle\int_{\Omega_i}\int_{I\setminus\Omega_i} \phi_\varepsilon(x-y)\,\mathrm{d}y\,\mathrm{d}x, & i = j. \end{cases}$$

For the Neumann problems, in light of (4.3.6), $u_h \in V_\Omega^h \times (0,\infty)$ is extracted by enforcing that

$$\sum_{j=1}^{n} \gamma_j(t)|\Omega_j| = \overline{u}_0.$$

The numerical solutions satisfy the appropriate properties in (4.3.7) and (4.3.8).

4.4 Numerical Experiments

In this section, we present examples demonstrating various properties of numerical solutions of the nonlocal Cattaneo-Vernotte equation on bounded domains. In each example, ϕ_ε is defined in (4.2.4) and we use the scaling

$$\beta = 2\tau = c\varepsilon^\alpha, \tag{4.4.1}$$

where α and c are given in (4.2.7). In Example 4.4.1, we take $\lambda = \beta$ and investigate the effect of relaxation time by comparing solutions of the nonlocal Cattaneo-Vernotte equation (4.1.1) to the nonlocal diffusion equation (4.1.9). Example 4.4.2 investigates the relationship of solutions of the nonlocal Cattaneo-Vernotte equation to those of fractional diffusion in the limit of vanishing nonlocality and relaxation time. The analysis in Example 4.4.3 studies the effect of relaxation time and nonlocality on solutions by comparing solutions of the classical Cattaneo-Vernotte, nonlocal Cattaneo-Vernotte, classical diffusion, and nonlocal diffusion equations.

Example 4.4.1. This example examines a nonlocal Cattaneo-Vernotte equation with homogeneous Neumann volume constraints that admits an analytic solution for any initial condition. We demonstrate that solutions can be viewed as perturbations of solutions to the corresponding nonlocal diffusion equation (4.1.9) and we investigate the effects of a nonzero relaxation time.

Consider the nonlocal homogeneous Neumann Cattaneo-Vernotte equation

$$\begin{cases} u_t(x,t) + \dfrac{\varepsilon^2}{24}u_{tt}(x,t) = \dfrac{6}{\varepsilon^2}\displaystyle\int_\Omega \big(u(y,t) - u(x,t)\big)\phi_\varepsilon(x-y)\,\mathrm{d}y, & x \in \Omega, \\ u(x,0) = u_0(x), & x \in \Omega, \\ u_t(x,0) = 0, & x \in \Omega, \end{cases} \tag{4.4.2}$$

where

$$\phi_\varepsilon(s) = \frac{1}{2\varepsilon}\chi_{(-\varepsilon,\varepsilon)}(s), \quad \varepsilon \geq 1,$$

so that $\alpha = 2$, $c = 1/6$, and, consequently, $\beta = \varepsilon^2/6$ and $\tau = \varepsilon^2/12$.

In this example, since $\varepsilon \geq 1$ and supp$(\phi(x-y))$ contains Ω for all $x \in \Omega$, (4.4.2) reduces to an ordinary differential equation

$$\begin{cases} u_t(x,t) + \dfrac{\varepsilon^2}{24}u_{tt}(x,t) = \dfrac{3}{\varepsilon^3}\left(\overline{u}_0 - u(x,t)\right), & x \in \Omega, \\ u(x,0) = u_0(x), & x \in \Omega, \\ u_t(x,0) = 0, & x \in \Omega, \end{cases}$$

whose solution can be given as a convex combination of the initial condition $u_0(x)$ and $\overline{u}_0$,

$$u_c(x,t) = \overline{u}_0(1-\zeta_c(t)) + \zeta_c(t)u_0(x), \tag{4.4.3}$$

where

$$\zeta_c(t) = \exp\left(-\frac{12}{\varepsilon^2}t\right)\left(\sqrt{\frac{1}{1-\frac{1}{2\varepsilon}}}\sinh\left(\frac{12}{\varepsilon^2}\sqrt{1-\frac{1}{2\varepsilon}}t\right) + \cosh\left(\frac{12}{\varepsilon^2}\sqrt{1-\frac{1}{2\varepsilon}}t\right)\right).$$

The function $\zeta_c(t) \in (0,1]$ is a strictly decreasing function that tends to zero as $t \to \infty$. If $u_0(x) = \overline{u}_0$ for some $x \in \Omega$, then x is a fixed point, i.e., $u(x,t) = u_0(x)$, for all $t \geq 0$. Also, the monotonicity of ζ_c implies $u(x,t) \nearrow \overline{u}_0$ if $u_0(x) < \overline{u}_0$ and, likewise, $u(x,t) \searrow \overline{u}_0$ if $u_0(x) > \overline{u}_0$ as $t \to \infty$. As $\varepsilon \to \infty$, $\zeta_c(t) \to 1$ for any fixed $t < \infty$. Thus, $u_c(x,t)$ can be well-approximated by $u_0(x)$ for arbitrarily large finite time by choosing ε sufficiently large.

To investigate the effects of a relaxation time, we consider (4.1.9) with homogeneous Neumann volume constraints as well,

$$\begin{cases} u_t(x,t) = \dfrac{6}{\varepsilon^2}\displaystyle\int_\Omega \big(u(y,t) - u(x,t)\big)\phi_\varepsilon(x-y)\,\mathrm{d}y, & x \in \Omega, \\ u(x,0) = u_0(x), & x \in \Omega, \end{cases} \tag{4.4.4}$$

for the same ϕ_ε as in (4.4.2). As shown in [21], (4.4.4) also reduces to an ordinary differential equation whose solution is given by a convex combination of $u_0(x)$ and $\overline{u}_0$,

$$u_d(x,t) = \overline{u}_0(1-\zeta_d(t)) + \zeta_d(t)u_0(x), \tag{4.4.5}$$

where

$$\zeta_d(t) = \exp\left(-\frac{3}{\varepsilon^3}t\right).$$

Thus, solutions of (4.4.2) may be written

$$u_c(x,t) = u_d(x,t) + (\zeta_c(t) - \zeta_d(t))(u_0(x) - \overline{u}_0),$$

the sum of the solution to (4.4.4) and a perturbation $(\zeta_c(t) - \zeta_d(t))(u_0(x) - \overline{u}_0)$ due to a nonzero relaxation time. Since $u_0(x)$ and $\overline{u}_0$ are fixed for a given initial condition, we study the difference $u_c(x,t) - u_d(x,t)$ simply by investigating $\zeta_c(t) - \zeta_d(t)$.

In Fig. 4.1, we plot $\zeta_c(t) - \zeta_d(t)$ for $t \in [0,3]$ and $\varepsilon \in [1,3]$. As $t \to \infty$, $\zeta_c(t) - \zeta_d(t) \to 0$, but more slowly for increasing ε. This reflects agreement of stationary solutions for the two problems.

For small values of t, $\zeta_c(t) > \zeta_d(t)$, which is an effect of the nonzero relaxation time. After this short time frame, $\zeta_c(t) - \zeta_d(t) = 0$, i.e., the solutions agree exactly at some point in time $t > 0$, and then $\zeta_c(t) < \zeta_d(t)$ for the duration of time. These observations hold for all ε, but are less dramatic as ε increases.

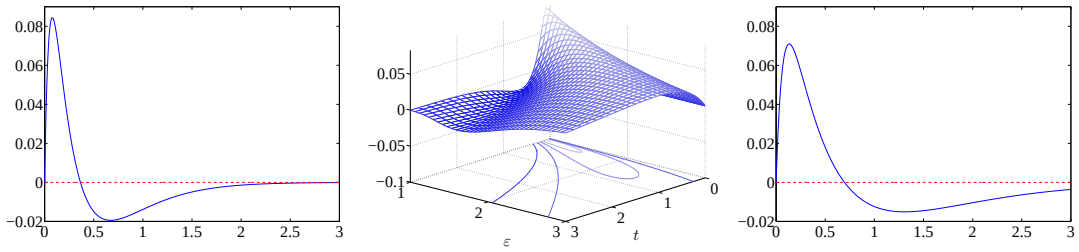

(a) $\varepsilon = 1$ and $t \in [0, 3]$ (b) $\varepsilon \in [1, 3]$ and $t \in [0, 3]$ (c) $\varepsilon = 5/4$ and $t \in [0, 3]$

Fig. 4.1: The vertical axes are $\zeta_c(t) - \zeta_d(t)$ and in panels (a) and (c) the horizontal axis is $t \in [0, 3]$.

Example 4.4.2. The fractional diffusion behavior of the boundary value problems for (4.1.1) is examined by choosing $\phi = \phi^\alpha$ to be a centered and symmetric stable density with stability index $\alpha \in \{2, 3/2, 1, 1/2\}$. As explained in Section 2, α represents the fraction of the Laplacian in the equations (4.1.11) and (4.2.8). Such centered and symmetric stable densities, normalized so that $c = 1$, are characterized through their Fourier transforms via the Lévy-Khintchine representation, i.e.,

$$\phi^\alpha(s) = \mathcal{F}^{-1}\left(\exp\left(-|\xi|^\alpha\right)\right)(s), \tag{4.4.6}$$

see [4, §§ 1.2.5]. We use (4.2.4) to define ϕ^α_ε and the cases $\alpha = 2, 1$ yield closed-form expressions for ϕ^α_ε:

$$\phi^\alpha_\varepsilon(s) = \begin{cases} \left(\dfrac{1}{4\pi\varepsilon^2}\right)^{\frac{1}{2}} \exp\left(-\dfrac{s^2}{4\varepsilon^2}\right), & \alpha = 2, \\ \dfrac{\varepsilon}{\pi(s^2 + \varepsilon^2)}, & \alpha = 1, \end{cases} \tag{4.4.7}$$

which are Gaussian and Cauchy densities, respectively. For other values of α, ϕ^α_ε is symmetric and unimodal though closed-forms for ϕ^α_ε typically do not exist. For $\alpha < 2$, the second moment is infinite and for $\alpha < 1$, all moments are infinite. We consider the discontinuous initial condition

$$u_0(x) = \begin{cases} 0, & 0 < x < 0.5, \\ 1, & 0.5 \le x < 1 \end{cases} \tag{4.4.8}$$

and investigate the effects of vanishing relaxation time and nonlocality, i.e., letting $\varepsilon \to 0$, on the solutions to a nonlocal Dirichlet boundary value problem.

Fig. 4.2 plots the time-evolutions of the approximate solutions to the nonlocal homogeneous Dirichlet boundary value problem in (4.3.2) given by the finite element method with mesh spacing $h = 5 \cdot 10^{-4}$ and $t \in [0, 0.25]$. We consider $\alpha \in \{2, 3/2, 1, 1/2\}$ and various ε. The solutions of (4.3.2) with ϕ_ε^2 behave asymptotically, with respect to ε, as solutions to the classical diffusion equation (4.1.6). However, the asymptotic behavior of solutions of (4.3.2) with $\phi_\varepsilon^{\alpha \neq 2}$ is given by a fractional Laplace parabolic equation (4.1.11). Consequently, the magnitude of the jump discontinuity in the initial data decays more slowly in these latter cases.

Example 4.4.3. In this example, we study the effect of relaxation time for a homogeneous nonlocal Dirichlet boundary value problem with an initial condition

$$u_0(x) = \frac{1}{\sqrt{4\pi(0.02)^2}} \exp\left(-\frac{(x-0.5)^2}{4(0.02)^2}\right), \quad x \in \Omega,$$

which, to numerical precision, integrates to one. We use both of the densities ϕ_ε^α in (4.4.7) in this example.

In Fig. 4.3, we plot the approximate solutions for the nonlocal diffusion, nonlocal Cattaneo-Vernotte, classical diffusion, and classical Cattaneo-Vernotte equations. The relatively large nonlocality, i.e., $\varepsilon = 0.10$, explains the differences between the solutions of the nonlocal and classical equations. The effect of the relaxation time in the nonlocal equations is slight in the transient time and the asymptotic behavior of the two solutions is the same. In the classical equations, though the asymptotic behavior of the solutions are the same, the effect of relaxation time is dramatic in transient time. In fact, the solution of the classical Cattaneo-Vernotte equation becomes bimodal, a characteristic not shared by the other solutions. For the nonlocal equations, $\int_\Omega u_h(x,t)\,\mathrm{d}x$ decreases faster initially than for the classical equations. The asymptotic behavior of both $\int_\Omega u_h(x,t)\,\mathrm{d}x$ and $\int_\Omega u_h^2(x,t)\,\mathrm{d}x$, however, are the same for the nonlocal and classical equations.

In Fig. 4.4, the nonlocality is small so that little difference between the nonlocal and classical equations is present. Moreover, the relaxation time is also small and there is little effect due to the relaxation time. This corroborates the notion that the solutions to the four equations all behave like the classical diffusion equation in the limit of vanishing nonlocality and relaxation time.

The results in Fig. 4.5 show that even in the limit vanishing nonlocality and relaxation time the solutions to the nonlocal equations with $\alpha \neq 2$ behave very differently than those to the classical

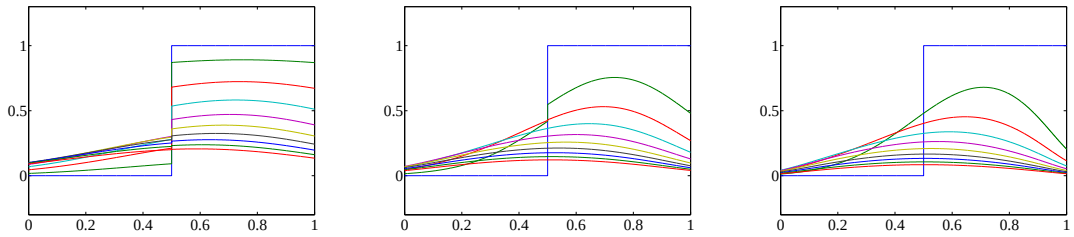

(a) $\alpha = 2, \varepsilon = 1/4$ (b) $\alpha = 2, \varepsilon = 1/8$ (c) $\alpha = 2, \varepsilon = 1/16$

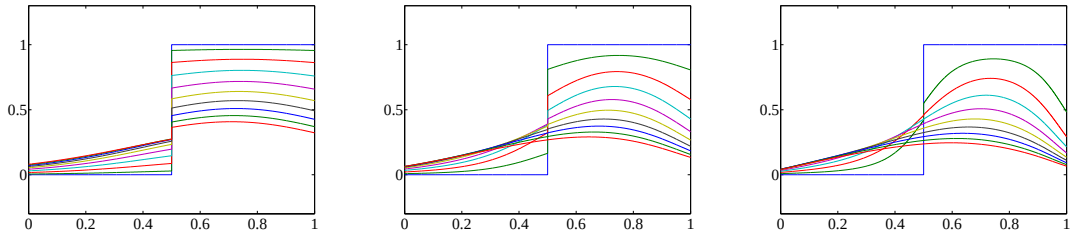

(d) $\alpha = 3/2, \varepsilon = 1/4$ (e) $\alpha = 3/2, \varepsilon = 1/8$ (f) $\alpha = 3/2, \varepsilon = 1/16$

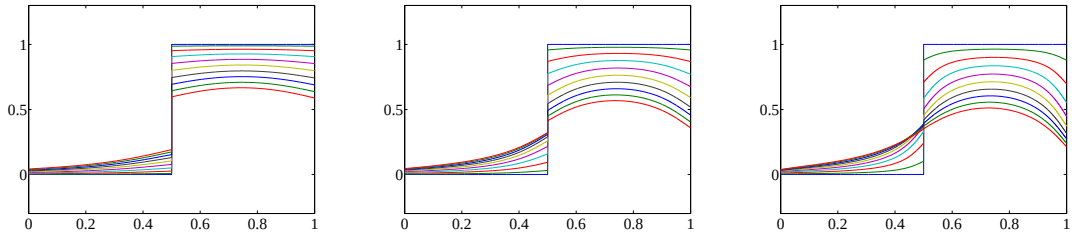

(g) $\alpha = 1, \varepsilon = 1/4$ (h) $\alpha = 1, \varepsilon = 1/8$ (i) $\alpha = 1, \varepsilon = 1/16$

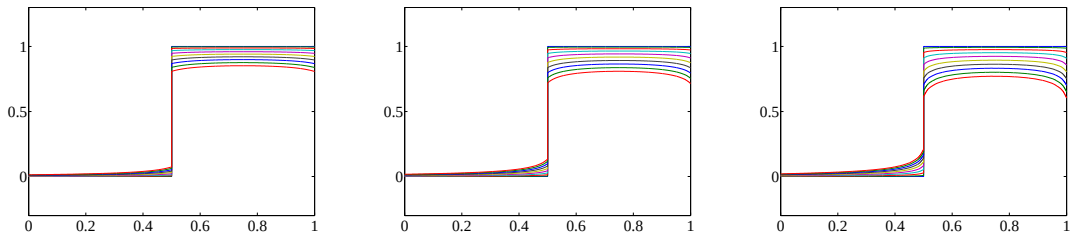

(j) $\alpha = 1/2, \varepsilon = 1/4$ (k) $\alpha = 1/2, \varepsilon = 1/8$ (l) $\alpha = 1/2, \varepsilon = 1/16$

Fig. 4.2: Each panel shows solutions to the nonlocal homogeneous Dirichlet problem for different α and ε. The density ϕ_ε^α is used, where ϕ^α is a Lévy stable density with index of stability α. Since $c = 1$, we take $2\tau = \varepsilon^\alpha$. The vertical axis in each panel is the value of $u_h(x,t)$ and the horizontal axis is x. The ten different solution profiles in each panel correspond to the solutions at ten different times, $t \in [0, 0.25]$.

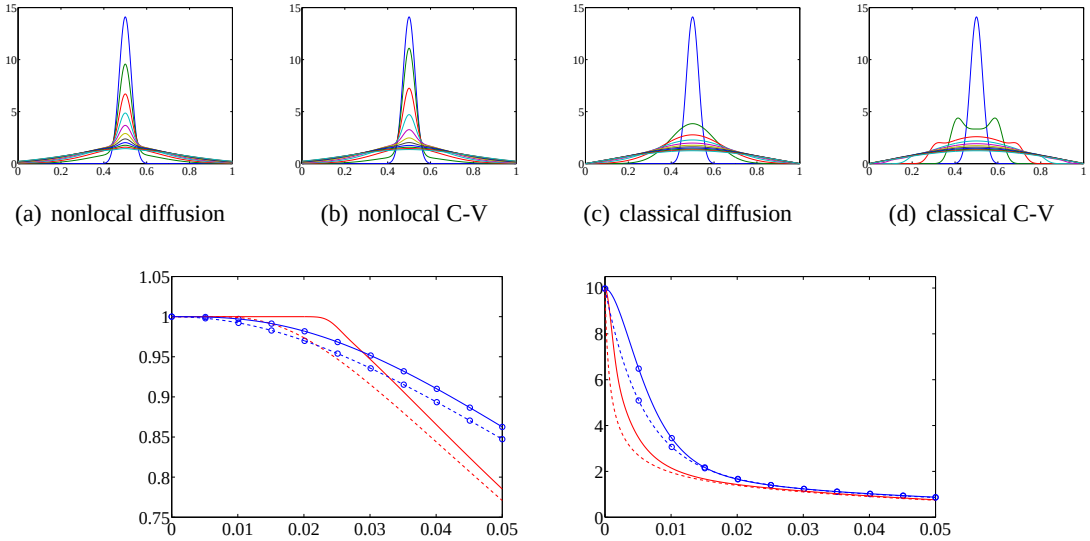

(a) nonlocal diffusion (b) nonlocal C-V (c) classical diffusion (d) classical C-V

(e) $\int_\Omega u_h(x,t)\,\mathrm{d}x$ vs. t (f) $\int_\Omega u_h^2(x,t)\,\mathrm{d}x$ vs. t

Fig. 4.3: Top: Panels (a)–(d) show approximate solutions, $u_h(x,t)$, for $t \in [0, 0.05]$ to the nonlocal and classical diffusion and Cattaneo-Vernotte (C-V) equations, respectively. The vertical axis in each panel is $u_h(x,t)$ and the horizontal axis is $x \in \Omega$. Bottom: Panels (e) and (f) show solutions of the nonlocal (marked) and classical (unmarked) diffusion (dashed) and C-V (solid) equations. In this experiment, $\alpha = 2$ and $\varepsilon = 0.10$.

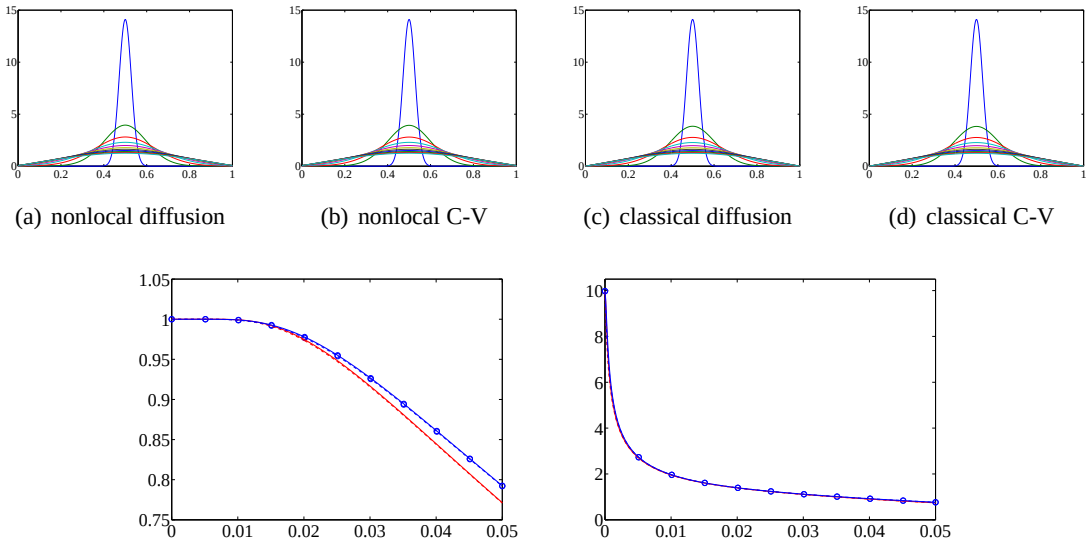

(a) nonlocal diffusion (b) nonlocal C-V (c) classical diffusion (d) classical C-V

(e) $\int_\Omega u_h(x,t)\,\mathrm{d}x$ vs. t (f) $\int_\Omega u_h^2(x,t)\,\mathrm{d}x$ vs. t

Fig. 4.4: Top: Panels (a)–(d) show approximate solutions, $u_h(x,t)$, for $t \in [0, 0.05]$ to the nonlocal and classical diffusion and Cattaneo-Vernotte (C-V) equations, respectively. The vertical axis in each panel is $u_h(x,t)$ and the horizontal axis is $x \in \Omega$. Bottom: Panels (e) and (f) show solutions of the nonlocal (marked) and classical (unmarked) diffusion (dashed) and C-V (solid) equations. In this experiment, $\alpha = 2$ and $\varepsilon = 0.02$.

equations. This is because the asymptotic behavior of the nonlocal equations is given by a fractional diffusion equation.

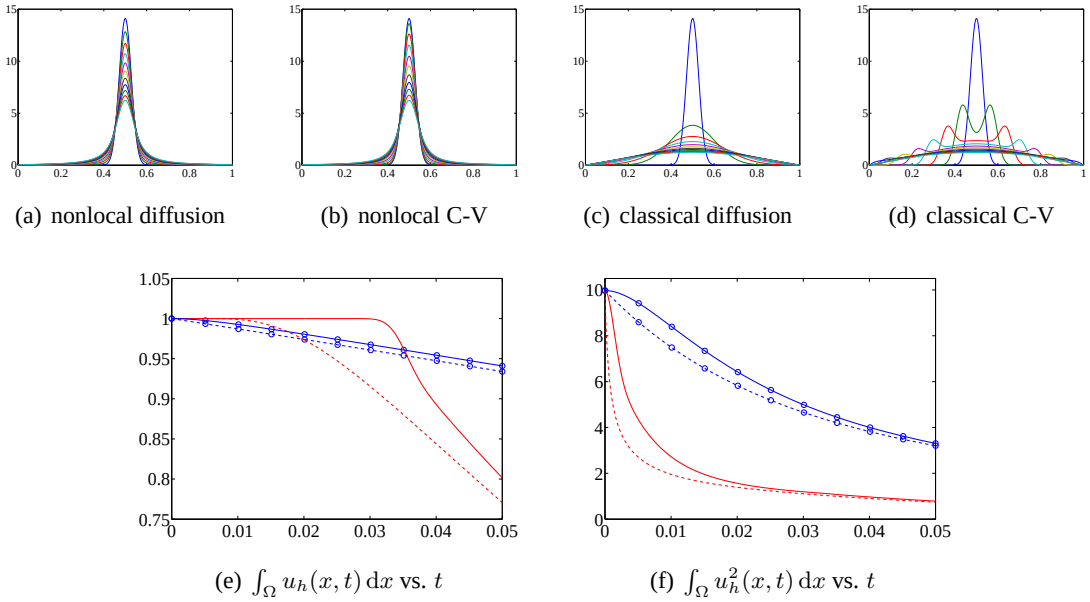

(a) nonlocal diffusion (b) nonlocal C-V (c) classical diffusion (d) classical C-V

(e) $\int_\Omega u_h(x,t)\,\mathrm{d}x$ vs. t (f) $\int_\Omega u_h^2(x,t)\,\mathrm{d}x$ vs. t

Fig. 4.5: Top: Panels (a)–(d) show approximate solutions, $u_h(x,t)$, for $t \in [0, 0.05]$ to the nonlocal and classical diffusion and Cattaneo-Vernotte (C-V) equations, respectively. The vertical axis in each panel is $u_h(x,t)$ and the horizontal axis is $x \in \Omega$. Bottom: Panels (e) and (f) show solutions of the nonlocal (marked) and classical (unmarked) diffusion (dashed) and C-V (solid) equations. In this experiment, $\alpha = 1$ and $\varepsilon = 0.02$.

4.5 Summary

We demonstrate that the nonlocal Cattaneo-Vernotte equation is obtained by including a relaxation effect in the nonlocal diffusion equation and, in fact, arises from a generalization of Fick's first law in terms of a nonlocal flux. In a certain limit of vanishing nonlocality and relaxation time, we find a relationship between the nonlocal Cattaneo-Vernotte equation and the classical and fractional diffusion equations. The contribution of this paper is to introduce volume constraints, in the form of volume constraints, for the nonlocal Cattaneo-Vernotte equation, which induce volume constraints for the underlying CTRWs. Further, the variational and finite element formulations for these nonlocal boundary value problems are reviewed and demonstrated to be powerful tools. We review well-posedness of these nonlocal boundary value problems and provide properties of their solutions. We investigate the effect of relaxation time, i.e., non-Markovian effects, and nonlocality.

5. CONTINUOUS TIME RANDOM WALKS ON BOUNDED DOMAINS

A useful perspective when studying anomalous diffusion processes is that of a continuous time random walk and its associated master equation. In particular, for $\phi \in L^1(\mathbb{R})$, the nonlocal diffusion equation,

$$u_t(x,t) = \frac{1}{\lambda}\int_{\mathbb{R}} \big(u(y,t) - u(x,t)\big)\phi(x-y)\,\mathrm{d}y, \tag{5.0.1}$$

and the nonlocal Cattaneo-Vernotte equation,

$$u_t(x,t) + \frac{\tau}{2}u_{tt}(x,t) = \frac{1}{\beta}\int_{\mathbb{R}} \big(u(y,t) - u(x,t)\big)\phi(x-y)\,\mathrm{d}y, \tag{5.0.2}$$

are the master equations for Markovian and non-Markovian CTRWs, respectively. We restrict the random walker to a bounded domain where two types of interactions between the random walker and the boundary are considered. We derive the master equations for CTRWs that are restricted to a bounded domain and compare numerical solutions to density estimates of the probability density function computed from simulations. The numerical solution of the master equation represents a powerful tool in the study of CTRWs on bounded domains. Much of this chapter has been taken directly from published work of the author in [22].

5.1 Introduction

Anomalous diffusion processes have been observed in many applications, for example, contaminant flow in groundwater [28], dynamic motions in proteins [51], turbulence in fluids [43], and dynamics of financial markets [47] have all been verified experimentally to exhibit characteristics of anomalous diffusion; see [42] for a review of such applications. A diffusion process is termed anomalous when the mean square displacement has a nonlinear dependence on time, i.e.,

$$\langle X_t^2\rangle = \int_{\mathbb{R}} x^2 v(x,t)\,\mathrm{d}x \sim t^{\gamma}, \quad \gamma \neq 1, \tag{5.1.1}$$

unlike normal diffusion, where $\gamma = 1$. In (5.1.1), v is the probability density function of the random variable $X(t)$, which is the displacement of a diffusing particle at time t. When $0 < \gamma < 1$ such

a process is subdiffusive, while $\gamma > 1$ indicates a superdiffusive process. A thorough survey of theoretical considerations for anomalous diffusion processes can be found in [49].

One common perspective to take when studying anomalous diffusion processes is that of a CTRW and its associated master equation [49, 52]. As is discussed in [49, 50, 64], this perspective is especially useful when the diffusion process lacks finite characteristic scales, e.g., mean square displacement of a particle or the mean wait-time between collisions. Though the relationship between CTRWs in free space and anomalous diffusion processes has been well-studied, the same cannot be said for the subsequent relationship on bounded domains. Of the existing research, much is concerned with graphs and lattices and there exists comparatively little work into the master equations for CTRWs on general bounded domains. Recent efforts, namely [50], however, have made advances to remedy this by investigating certain Markovian CTRWs with absorbing and reflecting boundary conditions. The analysis in [50] is limited in relying on special cases so that explicit, closed-form, solutions to the master equations can be found for simple one-dimensional domains. This analysis becomes difficult when the Markovian assumption is removed, the domains in two and three dimensions are not simple, and the step density is not suitably chosen, e.g., it is approximated from data.

There is a well-known relationship between the master equations for CTRWs in free space and fractional diffusion equations. Considerably more research exists for fractional diffusion than for integro-differential equations, such as the aforementioned master equations, on bounded domains. For instance, the paper [71] gives a probabilistic interpretation of the Lévy-Feller fractional diffusion equation with absorbing boundaries, where the fraction of the Laplacian is restricted to $\alpha \in (1, 2)$, i.e., the cases $\gamma \geq 2$ in equation (5.1.1) are not considered. Other work, e.g., [44], considers fractional diffusion equations on bounded domains with reflecting boundaries. However, even for fractional diffusion, there is little notion of general boundary conditions outside of specialized domains, e.g., rectangles and parallelepipeds in two and three dimensions, respectively.

In this paper, we derive the master equations for both Markovian and non-Markovian CTRWs on bounded domains with either absorbing or insulated boundaries. An insulated boundary restricts the random walker from taking a step past the boundary, e.g., a special case of insulated boundaries is the reflective behavior described in [50]. Boundary conditions such as these appear naturally when a diffusion process is restricted to a bounded domain, e.g., contaminant flow in an underground

aquifer. The boundary conditions for a random walker induce volume constraints on the solution of the master equation and the resulting equations are then studied via a variational formulation and conforming finite element method described in [21, 36]. This computational approach allows for the study of a wide-class of problems on nontrivial bounded domains in two and three dimensions, a capability currently unavailable.

We demonstrate the numerical solutions to the master equations agree with density estimates of the solution from CTRW simulations. This renders the aforementioned finite element formulation a powerful tool in studying CTRW as models of anomalous diffusion because computationally intensive simulations may be avoided.

5.2 Continuous Time Random Walks in Free Space

We consider separable CTRWs, i.e., wait-times are independent of the choice of step. The wait-time density is denoted with ω and the step density with $J(y,x)$. That is, $J(y,x)$ is the probability density of taking a step from y to x and, consequently, $\int_{\mathbb{R}} J(y,x)\,\mathrm{d}x = 1$. Note, however, that $\int_{\mathbb{R}} J(y,x)\,\mathrm{d}y \neq 1$ in general. It is well-known, see for instance [14, 47, 49], that the probability density function of the CTRWs, $u(x,t)$, satisfies the master equation

$$u_t(x,t) = \int_0^t \Lambda(t-t')L^J_{\mathbb{R}}u(x,t')\,\mathrm{d}t', \tag{5.2.1}$$

where the Laplace transform of the memory kernel Λ is

$$\widehat{\Lambda}(\zeta) = \frac{\zeta\widehat{\omega}(\zeta)}{1-\widehat{\omega}(\zeta)}$$

and we have introduced the operator

$$L^f_I u(x,t) := \int_I \Big(u(y,t)f(y,x) - u(x,t)f(x,y)\Big)\,\mathrm{d}y.$$

The analogous operator to $L^f_I u(x,t)$ for a CTRW on a lattice has been studied previously [41].

We consider two choices of Λ in (5.2.1):

$$\Lambda(t-t') = \frac{1}{2\tau}\delta(t-t') \tag{5.2.2a}$$

$$\Lambda(t-t') = \frac{1}{\tau^2}\exp\left(-\frac{t-t'}{\tau/2}\right), \tag{5.2.2b}$$

which are tantamount to specifying that wait-times are distributed as

$$\text{Exp}(2\tau), \text{ i.e., } \omega(t) = \frac{1}{2\tau}\exp\left(-\frac{t}{2\tau}\right) \tag{5.2.3a}$$

$$\text{Gamma}(2,\tau), \text{ i.e., } \omega(t) = \frac{t}{\tau^2}\exp\left(-\frac{t}{\tau}\right), \tag{5.2.3b}$$

respectively, both of which imply finite mean wait-times. In fact, (5.2.3a) and (5.2.3b) imply the underlying CTRWs are compound Poisson and renewal reward processes, respectively. With (5.2.2), (5.2.1) reduces to

$$u_t(x,t) = \frac{1}{2\tau}L^J_{\mathbb{R}}u(x,t) \tag{5.2.4a}$$

$$u_t(x,t) + \frac{\tau}{2}u_{tt}(x,t) = \frac{1}{2\tau}L^J_{\mathbb{R}}u(x,t). \tag{5.2.4b}$$

Since the mean wait-time is finite, (5.2.4a) and (5.2.4b) are models for either normal diffusion or anomalous superdiffusion, depending on whether $\int_{\mathbb{R}}(x-y)^2J(y,x)\,\mathrm{d}x$ is finite or infinite, respectively. By selecting a heavy-tailed wait-time density, we may obtain models for subdiffusion, normal diffusion, or superdiffusion, depending now upon the interplay between the characteristic step-length variance and characteristic mean wait-time. For the discussion in this section, we assume J is a radial step density, i.e., $J(y,x) = J(y-x) = J(x-y)$. Moreover, we assume J is a Lévy stable density with stability index α. Such densities are characterized via their Lévy-Khintchine representation [4, §§ 1.2.5], i.e.,

$$J(s) = \mathcal{F}^{-1}\left\{\exp\left(-\varepsilon^\alpha|\xi|^\alpha\right)\right\}(s).$$

Relationship to fractional diffusion

We now establish a relationship between the nonlocal operator $(2\tau)^{-1}L^J_{\mathbb{R}}$ and the fractional Laplacian $-(-\Delta)^{\alpha/2}$. The fractional Laplacian may be defined in Fourier space, i.e.,

$$\mathcal{F}\left\{-(-\Delta)^{\alpha/2}u(x,t)\right\}(\xi) = -|\xi|^\alpha\widehat{u}(\xi,t),$$

and we refer the reader to [4, 60, 73] for more details. Setting $2\tau = \varepsilon^\alpha$,

$$\begin{aligned}
&\mathcal{F}\left\{(2\tau)^{-1}L^J_{\mathbb{R}}u(x,t)\right\}(\xi,t)\\
&\quad= \mathcal{F}\left\{\varepsilon^{-\alpha}\int_{\mathbb{R}}\big(u(y,t)-u(x,t)\big)J(x-y)\,\mathrm{d}y\right\}(\xi,t)\\
&\quad= \varepsilon^{-\alpha}(\widehat{J}(\xi)-1)\widehat{u}(\xi,t)\\
&\quad= -|\xi|^\alpha\widehat{u}(\xi,t) + \mathrm{O}(\varepsilon^\alpha),
\end{aligned}$$

demonstrating the nonlocal operator is well-approximated by the fractional Laplacian for small ε. A distinction between the two operators is that the nonlocal operator encapsulates the fractional derivative within the step density J. The cases $\alpha = 2, 1$ yield closed-form expressions for J:

$$J(s) = \begin{cases} \left(\dfrac{1}{4\pi\varepsilon^2}\right)^{\frac{1}{2}} \exp\left(-\dfrac{s^2}{4\varepsilon^2}\right), & \alpha = 2, \\ \dfrac{\varepsilon}{\pi(s^2+\varepsilon^2)}, & \alpha = 1, \end{cases}$$

which are Gaussian and Cauchy densities, respectively.

Anomalous diffusion

For $\alpha \in (0, 2)$, the mean square displacement diverges for the CTRWs described in (5.2.4a) and (5.2.4b), i.e.,

$$\langle X_t^2 \rangle = \int_{\mathbb{R}} x^2 u(x,t)\,\mathrm{d}x = \infty, \quad \forall t > 0.$$

We instead consider a pseudo mean square displacement,

$$\langle X_t^2 \rangle_B = \int_{B_1 t^{1/\alpha}}^{B_2 t^{1/\alpha}} x^2 u(x,t)\,\mathrm{d}x, \tag{5.2.5}$$

for appropriately chosen B_1 and B_2. This so-called pseudo mean square displacement was introduced in [38], see also [49], and we find

$$\langle X_t^2 \rangle_B \sim t^{2/\alpha}. \tag{5.2.6}$$

We now demonstrate numerically that both (5.2.4a) and (5.2.4b) are models for anomalous diffusion, in the sense of (5.2.6). As an example, we consider $\alpha = 1.2$, $\varepsilon = 0.25$, $B_1 = 10$, $B_2 = 20$, and start 100,000 random walkers at the origin. We compute the pseudo mean square displacement of the random walkers on the time interval $t \in [1, 10]$. A log-log plot of the simulations and least-squares fit to the data is shown in Fig. 5.1. The slopes of the least-squares fits are 1.6658 and 1.6722, respectively, which approximate the slope 1.6667 predicted from (5.2.6). This confirms that the diffusion processes underlying the equations in (5.2.4) are indeed anomalous. We refer the reader to [49] for further information.

To understand this analytically, we recall (5.2.1) for symmetric J,

$$u_t(x,t) = \int_0^t \Lambda(t-t') \int_{\mathbb{R}} \big(u(y,t') - u(x,t')\big) J(x-y)\,\mathrm{d}y\,\mathrm{d}t'$$

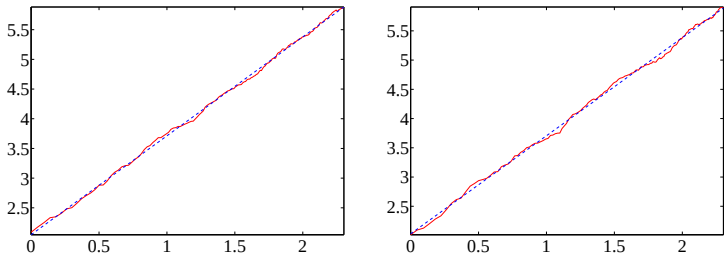

Fig. 5.1: Left: $\langle X_t^2 \rangle_B$ for the CTRW of (5.2.4a). Right: $\langle X_t^2 \rangle_B$ for the CTRW of (5.2.4b). The horizontal axis is time and the vertical axis is $\langle X_t^2 \rangle_B$, in log scales. The solid line denotes the pseudo mean square displacement from the simulations and the dashed line is the least-squares fit.

and apply both Fourier and Laplace transforms to obtain:

$$s\widehat{\widehat{u}}(\xi,s) - \widehat{u}(\xi,0) = \widehat{\Lambda}(s)\left(\widehat{\phi}(\xi)-1\right)\widehat{\widehat{u}}(\xi,s) = \frac{s\widehat{\omega}(s)\left(\widehat{\phi}(\xi)-1\right)}{1-\widehat{\omega}(s)}\widehat{\widehat{u}}(\xi,s).$$

Rearranging,

$$\widehat{u}(\xi,0) = \frac{s\left(1-\widehat{\omega}(s)\widehat{\phi}(\xi)\right)}{1-\widehat{\omega}(s)}\widehat{\widehat{u}}(\xi,s),$$

so that

$$\widehat{\widehat{u}}(\xi,s) = \frac{1-\widehat{\omega}(s)}{s\left(1-\widehat{\omega}(s)\widehat{\phi}(\xi)\right)},$$

where, for convenience, we have taken $u_0(x) = \delta(x)$, i.e., $\widehat{u}(\xi,0) = 1$.

We assume $\widehat{\omega}$ and $\widehat{\phi}$ have expansions of the form

$$\begin{aligned} \widehat{\omega}(s) &= 1 - c_\gamma s^\gamma + \mathrm{o}(s^\gamma), \quad \gamma \in (0,1], \\ \widehat{\phi}(\xi) &= 1 - c_\alpha \xi^\alpha + \mathrm{o}(\xi^\alpha), \quad \alpha \in (0,2]. \end{aligned} \tag{5.2.7}$$

Then, see [38, 49], we find (5.2.6). There are then three cases to consider. First, when $2\gamma < \alpha$, long wait-times dominate the behavior, resulting in subdiffusion. On the other hand, when $2\gamma > \alpha$, long step-lengths dominate the behavior, resulting in superdiffusion. When $2\gamma = \alpha$, wait-times and step-lengths appropriately balance each other, resulting in (normal) diffusion, which is not to be confused with classical diffusion.

5.3 Continuous Time Random Walks with Volume Constraints

Boundary conditions for CTRWs, which manifest themselves in the definition of the step density $J(y,x)$, are now formulated. We let ϕ be a symmetric probability density that should be interpreted as the step density in the absence of boundary conditions.

We first describe the behavior of fully absorbing boundaries. Once a random walker reaches, or steps beyond, the boundary $\partial\Omega$, it is banned from Ω for all future time. This description gives the step density

$$J(y,x) = \begin{cases} \phi(x-y), & y \in \Omega, \\ \delta(x-y), & y \notin \Omega. \end{cases} \tag{5.3.1}$$

It is convenient then to set $u(x,t) = 0$ for $x \notin \Omega$ and insertion of (5.3.1) into (5.2.1) yields

$$\begin{cases} u_t(x,t) = \displaystyle\int_0^t \Lambda(t-t') L_{\mathbb{R}}^{\phi} u(x,t') \, \mathrm{d}t', & x \in \Omega, \\ u(x,t) = 0, & x \notin \Omega \end{cases}$$

and, thus,

$$u_t(x,t) = \frac{1}{2\tau} L_{\mathbb{R}}^{\phi} u(x,t), \quad x \in \Omega, \tag{5.3.2a}$$

$$u_t(x,t) + \frac{\tau}{2} u_{tt}(x,t) = \frac{1}{2\tau} L_{\mathbb{R}}^{\phi} u(x,t), \quad x \in \Omega. \tag{5.3.2b}$$

The equation (5.3.2a) was studied in the context of Markovian CTRWs in [50], while (5.3.2b) belongs to a non-Markovian CTRW.

Next, in the case of fully insulated boundaries, a random walker is restricted from reaching, or stepping beyond, $\partial\Omega$ and this description gives rise to

$$J(y,x) = \chi_{\Omega}(x)\phi(x-y) + \delta(x-y) \int_{\mathbb{R}\setminus\Omega} \phi(z-y) \, \mathrm{d}z, \quad y \in \Omega, \tag{5.3.3}$$

The step density (5.3.3) states that a random walker may step from $y \in \Omega$ to $x \in \Omega$ via the radial density $\phi(x-y)$. Further, there is a nonzero probability, $\int_{\mathbb{R}\setminus\Omega} \phi(z-y) \, \mathrm{d}z$, of the walker at $y \in \Omega$ not taking a step. Together, these guarantee that the random walker remains in Ω for all time and, consequently, defining $J(y,x)$ for $y \notin \Omega$ in (5.3.3) is not required. Insertion of (5.3.3) into (5.2.1) gives

$$u_t(x,t) = \int_0^t \Lambda(t-t') L_{\Omega}^{\phi} u(x,t') \, \mathrm{d}t', \quad x \in \Omega$$

and, thus,

$$u_t(x,t) = \frac{1}{2\tau} L_{\Omega}^{\phi} u(x,t), \quad x \in \Omega, \tag{5.3.4a}$$

$$u_t(x,t) + \frac{\tau}{2} u_{tt}(x,t) = \frac{1}{2\tau} L_{\Omega}^{\phi} u(x,t), \quad x \in \Omega. \tag{5.3.4b}$$

Now, we relate the equations (5.3.2) and (5.3.4) to nonlocal volume-constrained problems that have been postulated and studied in various different settings, see [3, 21, 26, 36, 50]. A nonlocal

volume-constrained problem augments (5.2.4) by constraining the solution on a nonzero volume, generalizing the notion of classical boundary conditions to that of a volume constraint. Such volume constraints need not be relegated to the exterior of Ω. We specify an initial density $u_0(x)$ on Ω, satisfying $u_0 \geq 0$ and $\int_\Omega u_0(x)\,\mathrm{d}x = 1$.

The nonlocal Dirichlet boundary value problems are

$$\begin{cases} u_t(x,t) = \dfrac{1}{2\tau} L^{\phi}_{\mathbb{R}} u(x,t), & x \in \Omega, \\ u(x,t) = 0, & x \notin \Omega, \\ u(x,0) = u_0(x), & x \in \Omega \end{cases} \tag{5.3.5a}$$

and

$$\begin{cases} u_t(x,t) + \dfrac{\tau}{2} u_{tt}(x,t) = \dfrac{1}{2\tau} L^{\phi}_{\mathbb{R}} u(x,t), & x \in \Omega, \\ u(x,t) = 0, & x \notin \Omega, \\ u(x,0) = u_0(x), & x \in \Omega, \\ u_t(x,0) = 0, & x \in \Omega. \end{cases} \tag{5.3.5b}$$

The nonlocal Dirichlet boundary condition constrains u for $x \notin \Omega$, analogous to the classical Dirichlet boundary condition that does so at the points on the boundary.

The nonlocal Neumann boundary value problems are

$$\begin{cases} u_t(x,t) = \dfrac{1}{2\tau} L^{\phi}_{\Omega} u(x,t), & x \in \Omega, \\ u(x,0) = u_0(x), & x \in \Omega \end{cases} \tag{5.3.6a}$$

and

$$\begin{cases} u_t(x,t) + \dfrac{\tau}{2} u_{tt}(x,t) = \dfrac{1}{2\tau} L^{\phi}_{\Omega} u(x,t), & x \in \Omega, \\ u(x,0) = u_0(x), & x \in \Omega, \\ u_t(x,0) = 0, & x \in \Omega. \end{cases} \tag{5.3.6b}$$

The integrals in (5.3.6), in contrast to those in (5.3.5), are over Ω rather than all of $\mathbb{R}$. This implies a constraint on diffusion so that it occurs strictly inside Ω, i.e., density neither enters nor exits Ω, which is analogous to the classical Neumann boundary condition.

In summary, the descriptions of the boundary conditions for the CTRWs determine J in (5.2.1) so that (5.2.1) reduces to an appropriate nonlocal volume-constrained problem in (5.3.5) or (5.3.6). Evidently, these nonlocal volume-constrained problems describe the time-evolution of the probability density of the state of the corresponding CTRWs. The analysis in [21, 36] allows us to analyze (5.3.5) and (5.3.6) via a variational formulation and conforming finite element method so extending the class of problems computationally tractable.

5.4 Finite Element Method and Density Estimation from Simulations

Data from the CTRW simulations are used to estimate the density $u(x,t)$. Let $p_i(t)$ denote the i-th random walker's position at time t and partition $\Omega = (0,1)$ into n subintervals Ω_i. Then, define the density estimate

$$\mu_N(x,t) = \sum_{k=1}^{n} \chi_{\Omega_k}(x) \left(\frac{1}{Nh} \sum_{i=1}^{N} \chi_{\Omega_k}(p_i(t)) \right). \tag{5.4.1}$$

Though results exist that give the "optimal" bandwidth, i.e., h, so not to over-smooth or under-smooth the data, it is convenient in this case to pick h to be the mesh size induced by the finite element discretization. We denote the numerical solutions to (5.3.5) and (5.3.6) with u_h.

For each of the homogeneous Dirichlet problems,

$$\int_0^1 u(x,t)\,\mathrm{d}x \to 0, \quad \text{as } t \to \infty, \tag{5.4.2a}$$

$$\int_0^1 u^2(x,t)\,\mathrm{d}x \to 0, \quad \text{as } t \to \infty, \tag{5.4.2b}$$

and, for each of the homogeneous Neumann problems,

$$\int_0^1 u(x,t)\,\mathrm{d}x = 1, \quad t > 0, \tag{5.4.2c}$$

$$\int_0^1 \left(u(x,t) - \overline{u}_0\right)^2 \mathrm{d}x \to 0, \quad \text{as } t \to \infty. \tag{5.4.2d}$$

With (5.4.1), we compute density estimate analogs to (5.4.2). For absorbing boundaries,

$$\int_\Omega \mu_N(x,t)\,\mathrm{d}x = \frac{1}{N} \sum_{i=1}^{N} \chi_\Omega(p_i(t)), \tag{5.4.3a}$$

$$\int_\Omega \mu_N^2(x,t)\,\mathrm{d}x = \frac{1}{N^2 h} \sum_{k=1}^{n} \left(\sum_{i=1}^{N} \chi_{\Omega_k}(p_i(t)) \right)^2, \tag{5.4.3b}$$

and, for the case of insulated boundaries,

$$\int_\Omega \mu_N(x,t)\,\mathrm{d}x = \frac{1}{N} \sum_{i=1}^{N} \chi_\Omega(p_i(t)), \tag{5.4.3c}$$

$$\int_\Omega \left(\mu_N(x,t) - \overline{u}_0\right)^2 \mathrm{d}x = \frac{1}{N^2 h} \sum_{k=1}^{n} \left(\sum_{i=1}^{N} \chi_{\Omega_k}(p_i(t)) \right)^2 - \frac{1}{|\Omega|}. \tag{5.4.3d}$$

We simulate N random walkers and a density estimate of u at various points in time is computed. This density estimate is compared to the finite element solution of the associated nonlocal boundary value problem.

A walker begins at a random location $x_0 \in (0,1)$ according to the initial density $u_0(x)$. For each k, a wait-time t_k is generated from ω and the arrival-time $a_k = a_{k-1} + t_k$ is recorded. A step s_k is generated from ϕ, the new location $x_k = x_{k-1} + s_k$ is recorded, and then boundary conditions are imposed. For instance, if $x_k \notin (0,1)$ for the case of absorbing boundary conditions, the random walk is stopped. In the case of insulated boundary conditions, if $x_k \notin (0,1)$, we set $x_k = x_{k-1}$, i.e., the walker waits at the current position. Again, this treatment of an insulated boundary differs from the reflective behavior in [50] and is merely one approach for treating insulated boundaries. Deciding on the appropriate treatment is application specific and depends largely on the mechanism driving the CTRWs. This algorithm is summarized in Algorithm 5.1. Note that the position of the random walker is known for all time, e.g., the walker is at position x_k for the time interval $[a_k, a_{k+1})$.

Algorithm 5.1: Pseudo code for simulating a CTRW on a bounded domain

```
a_0 = 0
simulate x_0 ~ u_0(x)
for k from 1 to T do
    simulate t_k ~ ω(t)
    a_k = a_{k-1} + t_k
    simulate s_k ~ φ(s)
    x_k = x_{k-1} + s_k
    if x_k ∉ (0,1) then
        apply appropriate BC
    end
end
```

We now demonstrate that the nonlocal volume-constrained problems govern the joint probability densities of the corresponding CTRWs on bounded domains with appropriate boundary conditions. We select ϕ to be a Lévy stable density with $\alpha = 3/2$ and $\varepsilon = 0.25$. The results we present simulate N random walkers with $\varepsilon = 0.25$, $\alpha = 3/2$, $h = 0.01$, and $t \in [0, 0.5]$. Unless stated otherwise, assume $N = 8 \cdot 10^4$. To compare the difference between u_h and μ_N, we compute the L^2-norm, denoted simply with $\|\cdot\|$, of their difference,

$$\begin{aligned} \|u_h - \mu_N\|^2 &= \sum_{k=1}^{n} \int_{\Omega_k} \big(u_h(x,t) - \mu_N(x,t)\big)^2 \,\mathrm{d}x \\ &= h \sum_{k=1}^{n} \left(\gamma_k(t) - \frac{1}{Nh} \sum_{i=1}^{N} \chi_{\Omega_k}(p_i(t)) \right)^2 . \end{aligned} \tag{5.4.4}$$

The density estimate is plotted as a piecewise linear function by plotting the height of μ_N at the midpoint of the subinterval Ω_i and then connecting the points. This gives a more pleasing visual comparison of u_h and μ_N.

Fig. 5.2 shows results of the CTRW simulations on $(0,1)$ with absorbing boundaries and the solutions of the appropriate Dirichlet volume-constrained problems with $u_0(x) = 2x$. The L^2-norm decays of u_h and μ_N, corresponding to (5.4.2b) and (5.4.3b), are shown in panel (c).

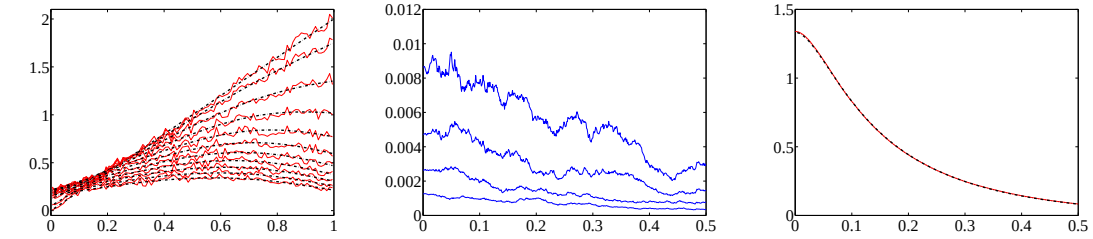

(a) $u_h(x,t)$ and $\mu_N(x,t)$, $t \in [0, 0.5]$ (b) $\|u_h - \mu_N\|^2$, varying N (c) $\|u_h\|^2$ and $\|\mu_N\|^2$

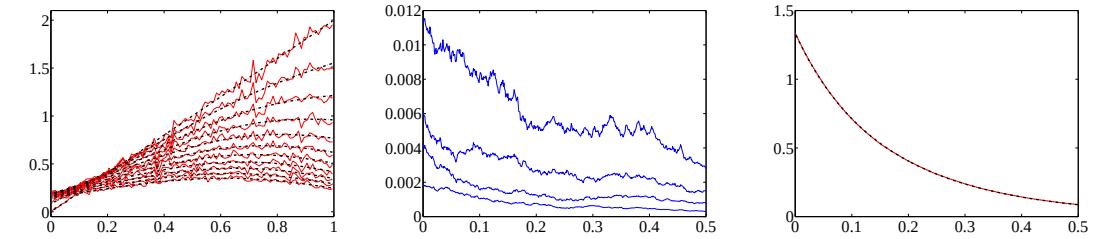

(d) $u_h(x,t)$ and $\mu_N(x,t)$, $t \in [0, 0.5]$ (e) $\|u_h - \mu_N\|^2$, varying N (f) $\|u_h\|^2$ and $\|\mu_N\|^2$

Fig. 5.2: Results of CTRW simulations on $(0,1)$ with absorbing boundaries and solution of the nonlocal Dirichlet problem. The horizontal axis is t and the vertical axis is the value of the norm.

Fig. 5.3 shows results of the CTRW simulations on $(0,1)$ with insulated boundaries and the solution of the appropriate Neumann volume-constrained problems with $u_0(x) = \frac{\pi}{2}\sin(\pi x)$. The L^2-norm decays of $u_h - \overline{u}_0$ and $\mu_N - \overline{u}_0$, corresponding to (5.4.2b) and (5.4.3b), are shown in panel (c).

5.5 Summary

The results in Section 5.2 corroborate that the nonlocal boundary value problems in (5.3.5) and (5.3.6) are indeed the master equations for CTRWs with appropriate boundary conditions. The recently developed variational formulation and numerical methods employed in obtaining these results are thus a powerful tool in studying CTRWs restricted to bounded domains. Consequently, a rapid means of investigating statistics of the CTRWs, e.g., exit-times, exists via approximating solutions to master equations. Without this capability, estimating such statistics requires simulations of the CTRW, a computationally demanding task.

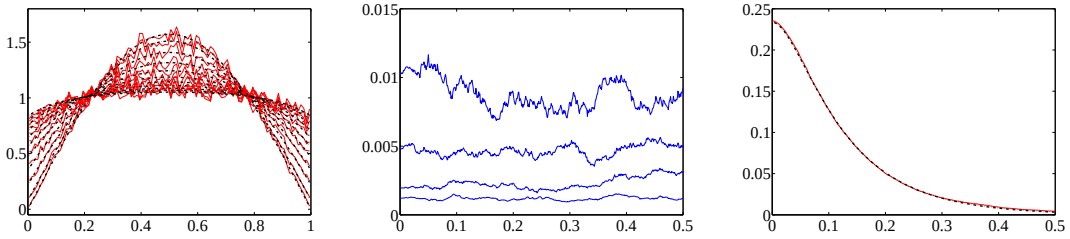

(a) $u_h(x,t)$ and $\mu_N(x,t)$, $t \in [0, 0.5]$ (b) $\|u_h - \mu_N\|^2$, varying N (c) $\|u_h - 1\|^2$ and $\|\mu_N - 1\|^2$

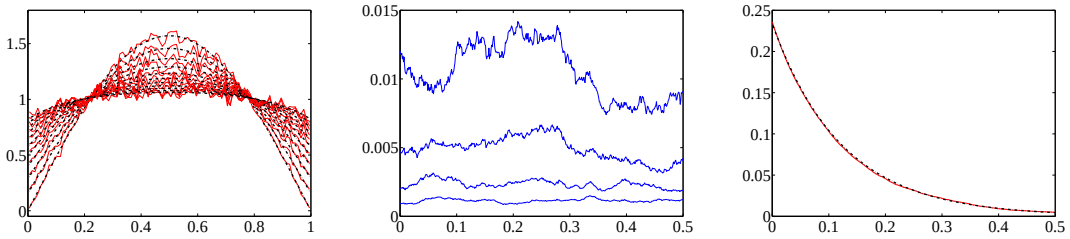

(d) $u_h(x,t)$ and $\mu_N(x,t)$, $t \in [0, 0.5]$ (e) $\|u_h - \mu_N\|^2$, varying N (f) $\|u_h - 1\|^2$ and $\|\mu_N - 1\|^2$

Fig. 5.3: Results of CTRW simulations on $(0, 1)$ with insulated boundaries and solution of the nonlocal Neumann problem. The horizontal axis is t and the vertical axis is the value of the norm.

6. VOLUME CONSTRAINTS AND EXIT-TIMES FOR LÉVY PROCESSES

This chapter studies pure jump Lévy processes on bounded domains via the corresponding master equation, i.e., a nonlocal diffusion equation with volume constraints. Volume constraints allow for the study of exit-times of the process from a bounded domain via solution of the master equation. We describe how the activity of the process, variation of the sample paths, exit-time distribution of the process, and smoothing of the nonlocal operator are all related. In particular, the type of diffusion can be identified from these statistics. General volume constraints allow for the study of exit-times from nontrivial domains as well. The contribution of this chapter is to present the master equations for pure jump Lévy processes restricted to a bounded domain and then numerical techniques to approximate probability densities of the stochastic process. With this, an efficient means for computing important statistics of the process is available.

6.1 Introduction

Lévy processes, see [4], are a general class of stochastic processes that arise in several applications, e.g., see [14, 38, 43, 42, 49, 58, 62, 64], and include Brownian motion, compound Poisson processes, interlacing processes, and stable processes. Applications involving Brownian motion and compound Poisson processes are abundant in many fields, as are stable processes and more general Lévy processes. The increments of a Lévy process have infinitely divisible distributions, which include Gaussian, Cauchy, exponential, Poisson, and gamma distributions as special cases.

Several statistics of a Lévy process, e.g., moments, the median, or exit-times, that characterize the process are necessary in any given application. Though such statistics are easily computed given the density of the process, $u(x,t)$, often the density is unavailable. Instead, it is common in practice to simulate the random process multiple times and produce an estimate of the density which can then be used to estimate such desired statistics. The master equation for a Lévy process, i.e., the deterministic equation that governs the time evolution of the density $u(x,t)$, provides a powerful alternative to simulation-based approaches.

The contribution of this chapter is to present the master equations for pure jump Lévy processes restricted to a bounded domain. The resulting master equations are so-called nonlocal diffusion equations with general volume constraints. We present numerical techniques for finding approximate densities and compare to density estimates computed from simulations of the process. With this, an efficient means for computing exit-times of the process is available. Exit-times are not traditionally studied via the master equation because many cases do not lead to a well-posed problem, e.g., fractional diffusion with the order of the Laplacian $\alpha \in (0, 1)$ on a bounded domain. The emerging work in [3, 29] have presented well-posed master equations for a large class of Lévy processes restricted to a bounded domain. An equivalence between the smoothing of the nonlocal operator and the activity of the stochastic process and variation of the sample paths is established. Numerically solving the master equation also provides a means for dealing with processes of infinite activity, where simulation is impossible and difficult to even approximate such processes. Also, the general volume constraints allow for consideration of non-simple domains, e.g., not connected, which appear naturally in many applications but traditionally are not easily handled.

A Lévy processes is characterized by a so-called Lévy triple (b, c, ν), where b is the drift, c is the diffusion coefficient, and ν is a measure. This characterization is a consequence of the celebrated Lévy-Khintchine decomposition and is reviewed in Section 6.2. Depending on the triple, the master equation takes very different forms, e.g.,

1. the transport equation,
$$u_t(x,t) = -bu_x(x,t), \tag{6.1.1}$$
arises from the triplet $(b, 0, 0)$ and is the master equation for a deterministic drift process

2. the classical diffusion equation,
$$u_t(x,t) = \frac{c}{2}u_{xx}(x,t), \tag{6.1.2}$$
arises from the triplet $(0, c, 0)$ and is the master equation for Brownian motion

3. the nonlocal diffusion equation,
$$u_t(x,t) = \int_{\mathbb{R}} \big(u(y,t) - u(x,t)\big)\nu(y-x)\,\mathrm{d}y, \tag{6.1.3}$$
arises from the triplet $(0, 0, \nu)$ and is the master equation for a jump process.

As many of the applications mentioned in [14, 38, 43, 42, 49, 58, 62, 64] are posed on bounded domains, a restriction of the stochastic process to a bounded domain is in order and we study statistics that are specific to this restriction, e.g., exit-times out of the bounded domain. Simulating stochastic processes on bounded domains has been studied in various settings, but often little attention is given to the corresponding master equations. The master equations for triples of the form $(b, c, 0)$, e.g., (6.1.1) and (6.1.2), restricted to a bounded domain have been well-studied in classical PDE literature. However, master equations for processes with $\nu \neq 0$ restricted to a bounded domain have received far less attention. In the papers [3, 36, 29, 29], nonlocal diffusion equations with general volume constraints are formulated and we demonstrate that they are the master equations for such processes. For $\nu \in L^1(\mathbb{R})$, [50] presents analytic solution techniques for such master equations, whereas a variational and finite element formulation is given in [21, 22] and used to compute numerical solutions.

The case $\nu \notin L^1(\mathbb{R})$ has been studied in [29, 72] in terms of the smoothing of the nonlocal operator. The underlying stochastic process in this case is not a compound Poisson process and, instead, is a square integrable pure jump martingale. The distinction between $\nu \in L^1(\mathbb{R})$ and $\nu \notin L^1(\mathbb{R})$ is tantamount to distinguishing the cases when the stochastic process has finite activity and infinite activity, respectively. Evidently, the activity of the process implies the smoothing of the operator in the corresponding master equation.

The rest of the chapter is organized as follows. In Section 6.2, we review the Lévy-Khintchine formula and describe how a Lévy process can be split into drift, diffusion, and jump components. We then discuss in detail the jump component of the process and distinguish between cases of finite and infinite activity. Volume-constrained problems are then introduced as the master equations for a Lévy process restricted to a bounded domain. Variational formulations, a conforming finite element method, and simulation procedures are reviewed in Section 6.3. Several numerical experiments are given in Section 6.4 and we summarized our findings in Section 6.5.

6.2 Understanding Particle Motion via the Lévy-Khintchine Formula

We now give a brief introduction to Lévy processes. A Lévy process L_t is a stochastic process beginning at the origin, i.e., $L_0 = 0$, that has independent and stationary increments and whose sample paths are almost surely right continuous with left limits. A Lévy process can be decomposed

into four independent processes (constant drift bt, Brownian motion $\sqrt{c}W_t$, compound Poisson process Y_t, and square integrable martingale Z_t), i.e.,

$$L_t = bt + \sqrt{c}W_t + Y_t + Z_t. \tag{6.2.1}$$

We note that Y_t and Z_t comprise the jump components of the process. The decomposition (6.2.1) is a consequence of the Lévy-Khintchine decomposition, which characterizes an arbitrary Lévy process by its characteristic function

$$\varphi_{L_t}(\xi) = \exp\left(\left(ib\xi - \frac{c\xi^2}{2} + \int_{\mathbb{R}} \left(e^{i\xi x} - 1 - i\xi x I_{\{|x|<\delta\}}\right) \nu(\mathrm{d}x)\right) t\right), \tag{6.2.2}$$

where $b \in \mathbb{R}$, $c \in \mathbb{R}_{\geq 0}$, and the so-called Lévy measure ν satisfies

$$\nu(\{0\}) = 0 \quad \text{and} \quad \int_{\mathbb{R}} \left(1 \wedge |x|^2\right) \nu(\mathrm{d}x) < \infty. \tag{6.2.3}$$

Consequently, a Lévy process is associated with a Lévy triplet (b, c, ν). The parameter δ distinguishes between small jumps, i.e., $|L_t - L_{t-}| < \delta$, and large jumps, i.e., $|L_t - L_{t-}| \geq \delta$ and is an arbitrary positive number.

We assume that the Lévy measure $\nu(\mathrm{d}x)$ can be written $\nu(x)\mathrm{d}x$, where ν is a function. In this chapter, we focus only on triplets of the form $(0, 0, \nu)$, where ν is symmetric, i.e.,

$$\nu(-x) = \nu(x), \quad \forall x \neq 0, \tag{6.2.4}$$

since the case $(b, c, 0)$ has been well-studied. The symmetry of ν removes the need for the compensator $i\xi x I_{\{|x|<\delta\}}$ so that (6.2.2) reduces to

$$\varphi_{L_t}(\xi) = \exp\left(\left(\int_{\mathbb{R}} \left(e^{i\xi x} - 1\right) \nu(x)\, \mathrm{d}x\right) t\right). \tag{6.2.5}$$

We introduce the Fourier transform of the density, $\widehat{u}(\xi, t)$, which, by definition, is the characteristic function $\varphi_{L_t}(\xi)$. Then, differentiating (6.2.5) with respect to t gives

$$\widehat{u}_t(\xi, t) = \left(\int_{\mathbb{R}} \left(e^{i\xi x} - 1\right) \nu(x)\, \mathrm{d}x\right) \widehat{u}(\xi, t).$$

Inverse Fourier transforming yields the master equation for $L_t = Y_t + Z_t$,

$$u_t(x, t) = \int_{\mathbb{R}} \big(u(y, t) - u(x, t)\big) \nu(y - x)\, \mathrm{d}y. \tag{6.2.6}$$

Processes with finite activity

We first consider the case $\nu \in L^1(\mathbb{R})$ so that the stochastic process has finite activity, i.e., almost surely the particle motion exhibits a finite number of jumps on every compact time interval. In this case, the Lévy process is a compound Poisson process, i.e.,

$$L_t = \sum_{k=1}^{N_t} R_k. \tag{6.2.7}$$

In (6.2.7), N_t is a Poisson process with intensity λ^{-1} that is independent of $R_k \overset{iid}{\sim} \phi$, where we have defined the probability density function ϕ and mean wait-time λ so that

$$\phi(z) = \frac{1}{\lambda}\nu(z). \tag{6.2.8}$$

Consequently, the master equation for L_t in this case reduces to

$$u_t(x,t) = \frac{1}{\lambda}\int_{\mathbb{R}} \big(u(y,t) - u(x,t)\big)\phi(y-x)\,\mathrm{d}y. \tag{6.2.9}$$

To understand the smoothing effect of the nonlocal operator in (6.1.3), we introduce the fractional diffusion equation

$$u_t(x,t) = -c(-\Delta)^{\alpha/2}u(x,t), \quad 0 < \alpha \leq 2, \tag{6.2.10}$$

which arises from the triplet $(0,0,\nu)$, with $\nu(x) = \frac{c}{|x|^{1+\alpha}}$, and is the master equation for a centered and symmetric stable process S_t^α. The analysis in [3, 26, 29, 72] demonstrates that the nonlocal operator in (6.2.9) does not smooth the data, i.e, the solution is no smoother than the initial condition. In particular, a discontinuity in the initial data will remain for all finite time. This result is given in Theorem 6.2.1.

Theorem 6.2.1 (Chasseigne et al. [26])**.** *If $\phi \in L^1(\mathbb{R})$ and $\widehat{\phi} \in L^1(\mathbb{R})$, then the fundamental solution, i.e., the solution with $u(x,0) = \delta(x)$, where $\delta(x)$ is the Dirac measure, of* (6.2.9) *is given by*

$$g_u(x,t) = \exp(-\lambda^{-1}t)\delta(x) + w(x,t), \tag{6.2.11}$$

where w is smooth.

Relationships between fractional and nonlocal diffusion have been studied in several fashions, e.g., the asymptotic behaviors were shown to converge in [26] and an equivalence between the appropriate solution spaces was demonstrated in [29, 72]. As nonlocality vanishes, per the interpretation in [21], the nonlocal diffusion well-approximates fractional diffusion for special choices of $\nu \in L^1(\mathbb{R})$. We now show under suitable conditions that the processes underlying the fractional diffusion equation (6.2.10) can be well-approximated by a sequence of processes underlying the nonlocal diffusion equation, which is summarized in Theorem 6.2.2.

Theorem 6.2.2. *Assume $\widehat{\phi}(\xi) = \exp(-c\varepsilon^\alpha|\xi|^\alpha)$, $\alpha \in (0, 2]$, and $\lambda = \varepsilon^\alpha$, where ϕ and λ are defined in* (6.2.8)*. Let $u^\varepsilon \in C([0,\infty), L^1(\mathbb{R}))$ denote the solution to*

$$\begin{cases} u_t^\varepsilon(x,t) = \dfrac{1}{\lambda}\displaystyle\int_{\mathbb{R}} \big(u^\varepsilon(y,t) - u^\varepsilon(x,t)\big)\phi(y-x)\,\mathrm{d}y, \\ u^\varepsilon(x,0) = \delta(x) \end{cases} \tag{6.2.12}$$

and $v \in C([0,\infty), H^{\alpha/2}(\mathbb{R}))$ denote the solution to

$$\begin{cases} v_t(x,t) = -c(-\Delta)^{\alpha/2}v(x,t), \\ v(x,0) = \delta(x). \end{cases} \tag{6.2.13}$$

Denote the compound Poisson process corresponding to u^ε with Y_t^ε and the stable process corresponding to v with S_t^α. Then, for all $t > 0$, as $\varepsilon \to 0$,

$$Y_t^\varepsilon \xrightarrow{d} S_t^\alpha,$$

i.e., Y_t^ε converges in distribution to S_t^α.

Proof. The characteristic function for Y_t^ε is

$$\widehat{u}^\varepsilon(\xi,t) = \widehat{u}_0(\xi)\exp\left(\frac{1}{\lambda}\left(\widehat{\phi}(\xi) - 1\right)t\right) = \widehat{u}_0(\xi)\exp\left(\frac{1}{\varepsilon^\alpha}\left(\exp(-c\varepsilon^\alpha|\xi|^\alpha) - 1\right)t\right).$$

Clearly,

$$\lim_{\varepsilon\to 0}\widehat{u}^\varepsilon(\xi,t) = \widehat{u}_0(\xi)\exp\left(-c|\xi|^\alpha t\right),$$

which is continuous at $\xi = 0$, so that the Lévy Continuity Theorem gives the result. □

Corollary 6.2.3. *Let $F_{Y_t^\varepsilon}$ and $F_{S_t^\alpha}$ denote the distribution functions of Y_t^ε and S_t^α. Then, since $F_{S_t^\alpha}$ is continuous,*

$$\int_{-\infty}^{x} u^\varepsilon(z,t)\,\mathrm{d}z \to \int_{-\infty}^{x} v(z,t)\,\mathrm{d}z,$$

for all $x \in \mathbb{R}$.

We remark that $\lambda = \varepsilon^\alpha$ specifies a scaling of time and space as ϕ becomes localized. In the case of $\alpha = 2$, the scaling $\lambda = \varepsilon^2$ is is typical of classical diffusion processes. Formally, Theorem 6.2.2 can be interpreted as stating that the distinction between the compound Poisson and centered and symmetric stable processes is negligible as $\varepsilon \to 0$ because the size of the jumps becomes so small that the error made in approximating the former with the latter is small.

Processes with infinite activity

In the case $\nu \notin L^1(\mathbb{R})$, the stochastic process has infinite activity, i.e., almost surely the particle motion exhibits an infinite number of jumps on every compact time interval. To condense the presentation, we only consider choices for ν of the form $\nu(x) = \frac{C}{|x|^{1+\alpha}}$, $\alpha \in (0,2)$, $C > 0$. In this case, the Lévy process is comprised of a compound Poisson process Y_t of the large jumps and a square integrable martingale Z_t of the small jumps, i.e., $L_t = Y_t + Z_t$ and

$$\begin{aligned}\varphi_{L_t}(\xi) &= \varphi_{Y_t}(\xi) \cdot \varphi_{Z_t}(\xi) \\ &= \exp\left(\left(\int_{|x|\geq\delta} \left(e^{i\xi x} - 1\right) \nu(x)\,\mathrm{d}x\right) t\right) \cdot \exp\left(\left(\int_{|x|<\delta} \left(e^{i\xi x} - 1\right) \nu(x)\,\mathrm{d}x\right) t\right).\end{aligned}$$

The compound Poisson process Y_t can be understood readily by defining $\lambda = \left(\int_{|x|\geq\delta} \nu(x)\,\mathrm{d}x\right)^{-1}$ and $\phi(x) = \lambda\nu(x)$ so that

$$\varphi_{Y_t}(\xi) = \exp\left(\frac{1}{\lambda}\left(\int_{|x|\geq\delta} \left(e^{i\xi x} - 1\right) \phi(x)\,\mathrm{d}x\right) t\right).$$

The master equation for Z_t is then

$$u_t(x,t) = \int_{\mathbb{R}} \big(u(y,t) - u(x,t)\big)\nu(y-x)\,\mathrm{d}y, \tag{6.2.14}$$

where $\nu(x) = \frac{C}{|x|^{1+\alpha}}\chi_{(-\delta,\delta)}(x)$.

For the choice $\nu(x) = \frac{(2-\alpha)\delta^{\alpha-2}}{|x|^{1+\alpha}}\chi_{(-\delta,\delta)}(x)$, $\alpha \in (0,2)$, the analysis in [29, 72] gives that solutions to (6.2.14) converge to the solution of the classical diffusion (6.1.2) as $\delta \to 0$. The following theorem corroborates this result from the viewpoint of the underlying stochastic processes.

Theorem 6.2.4. *Let Z_t^δ denote the jump process to* (6.2.14) *with $\nu(x) = \frac{(2-\alpha)\delta^{\alpha-2}}{|x|^{1+\alpha}}\chi_{(-\delta,\delta)}(x)$, $\alpha \in (0,2)$. Then,*

$$Z_t^\delta \xrightarrow{d} \sqrt{2}W_t,$$

as $\delta \to 0$.

Proof. The characteristic function of Z_t^δ is given by

$$\varphi_{Z_t^\delta}(\xi) = \exp\left(t\int_{-\delta}^{\delta}\left(e^{i\xi x}-1\right)\frac{(2-\alpha)\delta^{\alpha-2}}{|x|^{1+\alpha}}\,\mathrm{d}x\right).$$

Expanding $e^{i\xi x}$ in a Taylor series about the origin and noticing the odd terms vanish, we have

$$\begin{aligned}\varphi_{Z_t^\delta}(\xi) &= \prod_{k=1}^{\infty}\exp\left(t\int_{-\delta}^{\delta}\frac{(i\xi x)^{2k}}{(2k)!}\frac{(2-\alpha)\delta^{\alpha-2}}{|x|^{1+\alpha}}\,\mathrm{d}x\right)\\ &= \exp\left(t\int_{-\delta}^{\delta}\frac{(i\xi x)^{2}}{2}\frac{(2-\alpha)\delta^{\alpha-2}}{|x|^{1+\alpha}}\,\mathrm{d}x\right)\cdot\exp\left(\mathrm{O}(\delta)\right)\\ &= \exp\left(-t\xi^2\right)\cdot\exp\left(\mathrm{O}(\delta)\right),\end{aligned}$$

which, taking $\delta\to 0$ and an application of the Lévy Continuity Theorem, completes the proof. □

The analysis of [29, 72] demonstrates that the nonlocal operator in (6.2.14) has a fractional smoothing effect, i.e., the nonlocal operator maps into $H^{\alpha/2}(\mathbb{R})$, $\alpha\in(0,2)$. We contrast this with the lack of smoothing in the case $\nu\in L^1(\mathbb{R})$. Specifically, the Lévy process has finite activity ($\nu\in L^1(\mathbb{R})$) if and only if the spatial operator in the corresponding master equation has no smoothing. That is, the Lévy process has infinite activity ($\nu\notin L^1(\mathbb{R})$) if and only if the spatial operator in the corresponding master equation has smoothing. Further, the amount of smoothing is related to the variation of the sample paths. For instance, in the case $\alpha\in(0,1)$, the sample paths have finite variation (less smoothing). On the other hand, if $\alpha\in[1,2)$, the sample paths have infinite variation (more smoothing).

Volume constraints

In this section we present volume constraints for (6.1.3), which have been studied in [3, 21, 22, 29, 36]. We consider the bounded domain Ω and assume the initial density $u(x,0)=u_0(x)$ satisfies $u_0\geq 0$ and $\int_\Omega u_0(x)\,\mathrm{d}x=1$. We impose homogeneous Dirichlet volume constraints on u over the nonzero volume $\Gamma=\mathbb{R}\setminus\Omega$. Let

$$V=\left\{v\in L^1(\mathbb{R})\;\middle|\; v\,\big|_\Gamma=0\right\}$$

be the subspaces of test and trial functions.

Thus, the Dirichlet problem reads: find $u\in V\times(0,\infty)$ such that

$$\begin{cases} u_t(x,t)=\dfrac{1}{\lambda}\displaystyle\int_{\mathbb{R}}\big(u(y,t)-u(x,t)\big)\phi(y-x)\,\mathrm{d}y, & x\in\Omega,\\ u(x,0)=u_0(x), & x\in\Omega.\end{cases}\tag{6.2.15}$$

Well-posedness of (6.2.15) has been treated in [29]. Such problems when Ω is a connected domain have been studied in [3, 21, 22, 26, 36]. Such a volume constraint arises by imposing absorbing behaviors of the stochastic process on the volumes; see [22] for an example.

In the paper [29], the smoothing of the nonlocal diffusion equation with volume constraints was considered. The smoothing of the operator with volume constraints corresponds again to the activity and variation of sample paths of the Lévy process on a bounded domain.

6.3 Finite Element Method and Density Estimation from Simulations

We present the variational and finite element formulations. Then we discuss simulations and density estimation. Properties of the analytic solutions are also presented.

Variational and finite element method

Define the bilinear form $B : V \times V \to \mathbb{R}$

$$B(u,v) = \frac{1}{2}\int_{\mathbb{R}}\int_{\mathbb{R}} \big(u(y,t) - u(x,t)\big)\big(v(y) - v(x)\big)\,\phi(y-x)\,\mathrm{d}y\,\mathrm{d}x. \tag{6.3.1}$$

The variational formulation to (6.2.15) is: find $u \in V \times (0,\infty)$ such that

$$\begin{cases} \displaystyle\int_\Omega u_t v\,\mathrm{d}x + \frac{1}{\lambda}B(u,v) = 0, \quad \forall\, v \in L^1(\Omega), \\ \qquad\qquad u = u_0, \quad x \in \Omega. \end{cases} \tag{6.3.2}$$

To formulate the finite element method, we partition Ω into n subintervals Ω_k of width h_k and let $\chi_{\Omega_k}(x)$ be the indicator function for Ω_k. We denote the space of piecewise constant functions on the subintervals Ω_k by V_Ω^h. Note any $u_h \in V_\Omega^h \times (0,\infty)$ can be written

$$u_h(x,t) = \sum_{k=1}^{n} \gamma_k(t)\chi_{\Omega_k}(x). \tag{6.3.3}$$

The discrete variational problem to (6.3.2) is then: find $u_h \in V_\Omega^h \times (0,\infty)$ such that

$$\mathbf{M}\dot{\boldsymbol{\gamma}} = -\frac{1}{\lambda}\mathbf{A}\boldsymbol{\gamma},$$

respectively, where $\mathbf{M}$ and $\mathbf{A}$ are the mass and stiffness matrices defined by

$$M_{kk} = |\Omega_k| \quad \text{and} \quad A_{kj} = \begin{cases} -\displaystyle\int_{\Omega_k}\int_{\Omega_j} \phi(y-x)\,\mathrm{d}y\,\mathrm{d}x, & k \neq j, \\ \displaystyle\int_{\Omega_k}\int_{\mathbb{R}\setminus\Omega_k} \phi(y-x)\,\mathrm{d}y\,\mathrm{d}x, & k = j. \end{cases}$$

We note that this is a conforming finite element method and convergence studies and error analysis has been studied [27].

We consider N realizations of the stochastic process, which might represent data from an experiment. Let $p_i(t)$ denote the i-th particle's position at time t. We construct the density estimate

$$\mu_N(x,t) = \sum_{k=1}^{n} \chi_{\Omega_k}(x) \left(\frac{1}{Nh_k} \sum_{i=1}^{N} \chi_{\Omega_k}(p_i(t)) \right) \tag{6.3.4}$$

and note that the bins are defined precisely by the finite element discretization. In general, one seeks an optimal h_k so not to over-smooth or under-smooth the data. This choice of density estimate allows for discontinuous solutions and an easy specification of the support of the density estimate, which is known from the volume constraints. Standard kernel density estimation techniques, e.g.,

$$D_N(x,t) = \frac{1}{dN} \sum_{i=1}^{N} K\left(\frac{x - p_i(t)}{d} \right),$$

where K is a Gaussian kernel and d is the bandwidth, do not share these properties. Also, the choice of kernel has a dramatic impact on the resulting estimate and requires a priori knowledge of the density u, which is unavailable.

There are several nice consequences of the choice (6.3.4), summarized in the following theorem. For conciseness of the presentation, we assume $h_k = h$ throughout the duration of the chapter.

Theorem 6.3.1. *The density estimate $\mu_N(x,t)$ is*

(a) unbiased in the sense that

$$\lim_{n\to\infty} \mathbb{E}(\mu_N(x,t)) = u(x,t)$$

(b) the variance is given by

$$\begin{aligned} \mathrm{Var}(\mu_N(x,t)) &= \mathbb{E}\left((\mu_N(x,t) - \mathbb{E}(\mu_N(x,t)))^2 \right) \\ &= \frac{1}{Nh^2} \sum_{k=1}^{n} \chi_{\Omega_k}(x) \left(\int_{\Omega_k} u(z,t)\,\mathrm{d}z - \left(\int_{\Omega_k} u(z,t)\,\mathrm{d}z \right)^2 \right), \end{aligned}$$

which tends to zero as $N \to \infty$

(c) almost surely,

$$\lim_{N\to\infty} \|\mu_N - u\|^2_{L^2(\Omega)} = \sum_{k=1}^{n} \int_{\Omega_k} \left(\frac{1}{h} \int_{\Omega_k} u(z,t)\,\mathrm{d}z - u(x,t) \right)^2 \mathrm{d}x,$$

which then tends to zero as $n \to \infty$.

Proof. To prove (a), we first note

$$\mathbb{E}(\mu_N(x,t)) = \sum_{k=1}^{n} \chi_{\Omega_k}(x) \frac{1}{h} \int_{\Omega_k} u(z,t)\,\mathrm{d}z.$$

Then,

$$\lim_{n\to\infty} \mathbb{E}(\mu_N(x,t)) = \lim_{n\to\infty} \frac{1}{h} \int_{\Omega_{k(n)}} u(z,t)\,\mathrm{d}z,$$

where $\Omega_{k(n)}$ is the subdomain that contains x for a given n. Taking $n \to \infty$ shows (a). Showing (b) is a straightforward computation. Now, to show (c), first note

$$\|\mu_N - u\|^2_{L^2(\Omega)} = \sum_{k=1}^{n} \int_{\Omega_k} \left(\frac{1}{hN} \sum_{i=1}^{N} \chi_{\Omega_k}(p_i(t)) - u(x,t) \right)^2 \mathrm{d}x.$$

Then, by the Strong Law of Large Numbers, almost surely,

$$\lim_{N\to\infty} \|\mu_N - u\|^2_{L^2(\Omega)} = \sum_{k=1}^{n} \int_{\Omega_k} \left(\frac{1}{h} \int_{\Omega_k} u(z,t)\,\mathrm{d}z - u(x,t) \right)^2 \mathrm{d}x.$$

The mean value theorem for integrals gives

$$\sum_{k=1}^{n} \int_{\Omega_k} \left(\frac{1}{h} \int_{\Omega_k} u(z,t)\,\mathrm{d}z - u(x,t) \right)^2 \mathrm{d}x = \sum_{k=1}^{n} \left(u(c_k,t) - u(d_k,t) \right)^2 h,$$

where $c_k, d_k \in \Omega_k$. Taking $n \to \infty$ shows (c). □

Properties of solutions

The results of [26] provide properties for the solutions of (6.2.15), namely

$$\|u\|_{L^1(\Omega)} \le e^{-\frac{c_1}{2}t} \|u_0\|_{L^2(\Omega)}, \quad c_1, t > 0, \tag{6.3.5a}$$

$$\|u\|^2_{L^2(\Omega)} \le e^{-c_1 t} \|u_0\|^2_{L^2(\Omega)}, \quad c_1, t > 0, \tag{6.3.5b}$$

where

$$\|u\|_{L^p(\Omega)} = \left(\int_\Omega u^p\,\mathrm{d}x \right)^{1/p}$$

and

$$c_1 = \inf_{u \in L^2(\Omega)} \frac{B(u,u)}{\|u\|^2_{L^2(\Omega)}}. \tag{6.3.6}$$

We note that (6.3.5a) follows from an application of the Cauchy-Schwarz inequality to (6.3.5b). The equation (6.3.5a) implies the probability of the particle remaining in Ω decreases. We compute estimates of (6.3.5) using the density estimate from simulations, namely

$$\int_\Omega \mu_N(x,t)\,\mathrm{d}x = \frac{1}{N}\sum_{i=1}^{N} \chi_\Omega(p_i(t)), \quad t>0, \tag{6.3.7a}$$

$$\int_\Omega \mu_N^2(x,t)\,\mathrm{d}x = \frac{1}{N^2 h}\sum_{k=1}^{n}\left(\sum_{i=1}^{N}\chi_{\Omega_k}(p_i(t))\right)^2, \quad t>0. \tag{6.3.7b}$$

We now consider the exit-time T of the process from the bounded domain Ω. Notice the distribution function of T is given by

$$F(t) = 1 - \int_\Omega u(x,t)\,\mathrm{d}x. \tag{6.3.8}$$

Since $T \geq 0$, the expected exit-time can be computed via

$$\mathbb{E}(T) = \int_0^\infty (1-F(t))\,\mathrm{d}t = \int_0^\infty \int_\Omega u(x,t)\,\mathrm{d}x\,\mathrm{d}t \tag{6.3.9}$$

and is always finite since, by (6.3.5a),

$$\int_0^\infty \int_\Omega u(x,t)\,\mathrm{d}x\,\mathrm{d}t \leq \frac{2}{c_1}\sqrt{\int_\Omega u_0^2(x)\,\mathrm{d}x}.$$

The bound on the mean exit-time is inversely proportional to c_1, e.g., decreases as the eigenvalue c_1 increases. All of the moments,

$$\mathbb{E}(X^k) = \int_\Omega x^k u(x,t)\,\mathrm{d}x,$$

also decay to zero.

The exit-time distribution is approximated from the numerical solutions via

$$F_h(t) = 1 - \int_\Omega u_h(x,t)\,\mathrm{d}x = 1 - h\sum_{k=1}^{n}\gamma_k(t) \tag{6.3.10}$$

and from the density estimates via

$$F_N(t) = 1 - \int_\Omega \mu_N(x,t)\,\mathrm{d}x = 1 - \frac{1}{N}\sum_{i=1}^{N}\chi_\Omega(p_i(t)). \tag{6.3.11}$$

Notice that $F_N(t)$ is an unbiased estimator of $F(t)$ and also

$$\mathrm{Var}(F_N(t)) = \frac{1}{N}\left(\int_\Omega u(x,t)\,\mathrm{d}x\right)\left(1 - \int_\Omega u(x,t)\,\mathrm{d}x\right),$$

which tends to zero as $N \to \infty$.

For $\nu \in L^1(\mathbb{R})$, L_t is a compound Poisson process. Simulating such a process on a bounded domain is simple and is presented in Algorithm 1; see [22] also. If $\nu \notin L^1(\mathbb{R})$, we recall

$$\begin{aligned}\varphi_{L_t}(\xi) &= \varphi_{Y_t}(\xi) \cdot \varphi_{Z_t}(\xi) \\ &= \exp\left(\frac{1}{\lambda}\left(\int_{|x|\geq\delta}\left(e^{i\xi x}-1\right)\phi(x)\,\mathrm{d}x\right)t\right)\cdot\exp\left(\left(\int_{|x|<\delta}\left(e^{i\xi x}-1\right)\nu(x)\,\mathrm{d}x\right)t\right),\end{aligned}$$

where $\lambda = \left(\int_{|x|\geq\delta}\nu(x)\,\mathrm{d}x\right)^{-1}$ and $\phi(x) = \lambda\nu(x)$. The process of large jumps, Y_t, is a compound Poisson process, which is easily treated and thus removed from this discussion. The process of small jumps, Z_t, however, is not a compound process. Unfortunately, such processes are impossible to simulate since, for example, an infinite number of jumps are present on every arbitrarily small compact time interval. Thus, we instead approximate Z_t with a compound Poisson process Z_t^τ with characteristic function given by

$$\varphi_{Z_t^\tau}(\xi) = \exp\left(\left(\int_{\tau\leq|x|<\delta}\left(e^{i\xi x}-1\right)\nu(x)\,\mathrm{d}x\right)t\right).$$

Again, in the more familiar notation,

$$\varphi_{Z_t^\tau}(\xi) = \exp\left(\frac{1}{\lambda^\tau}\left(\int_{\tau\leq|x|<\delta}\left(e^{i\xi x}-1\right)\phi^\tau(x)\,\mathrm{d}x\right)t\right),$$

where $\lambda^\tau = \left(\int_{\tau\leq|x|<\delta}\nu(x)\,\mathrm{d}x\right)^{-1}$ and $\phi^\tau(x) = \lambda^\tau\nu(x)$. The process Z_t^τ approximates Z_t in the sense that as $\tau \to 0$, $Z_t^\tau \xrightarrow{d} Z_t$, which can be shown with an application of Lévy Continuity Theorem. This approximation is the so-called Poisson approximation.

Algorithm 6.1: Simulating a compound Poisson process

```
a_0 = 0
simulate L_0 ~ u_0(x)
for k from 1 to T do
    simulate t_k ~ Exp(λ)
    a_k = a_{k-1} + t_k
    simulate s_k ~ φ(s)
    L_{t_k} = L_{t_{k-1}} + s_k
    if L_{t_k} ∉ Ω then
        break
    end
end
```

Algorithm 6.2: Simulating a pure jump martingale

```
choose τ sufficiently small
define λ^τ and φ^τ
follow Algorithm 6.1 to simulate
Z_t^τ
```

Example 6.4.1 (Comparison of numerical solutions to density estimates from simulations)**.** We now demonstrate the capability of simulating processes for both $\nu \in L^1(\mathbb{R})$ and $\nu \notin L^1(\mathbb{R})$, with the latter being the Poisson approximation, obtaining density estimates from the simulations, and numerically solving the corresponding master equations via the finite element method. In both, we let $\Omega = (0,1)$, $u_0(x) = 6x\chi_{(0,1/2)}(x)$, and $h = 0.005$

We first consider $\nu \in L^1(\mathbb{R})$ with

$$\phi(x) = \frac{1}{\sqrt{4\pi\varepsilon^2}} \exp\left(-\frac{x^2}{4\varepsilon^2}\right), \tag{6.4.1}$$

$\varepsilon = 0.25$, $\lambda = \varepsilon^2$. We plot the numerical solutions and density estimates at the times $t = 0, 0.05, 0.1$ in Fig. 6.1. Two different numbers of realizations are considered, $N = 1 \cdot 10^4$ and $N = 5 \cdot 10^4$, and three different bin widths are considered, h, $5h$, and $10h$. Fig. 6.1 demonstrates the capability of

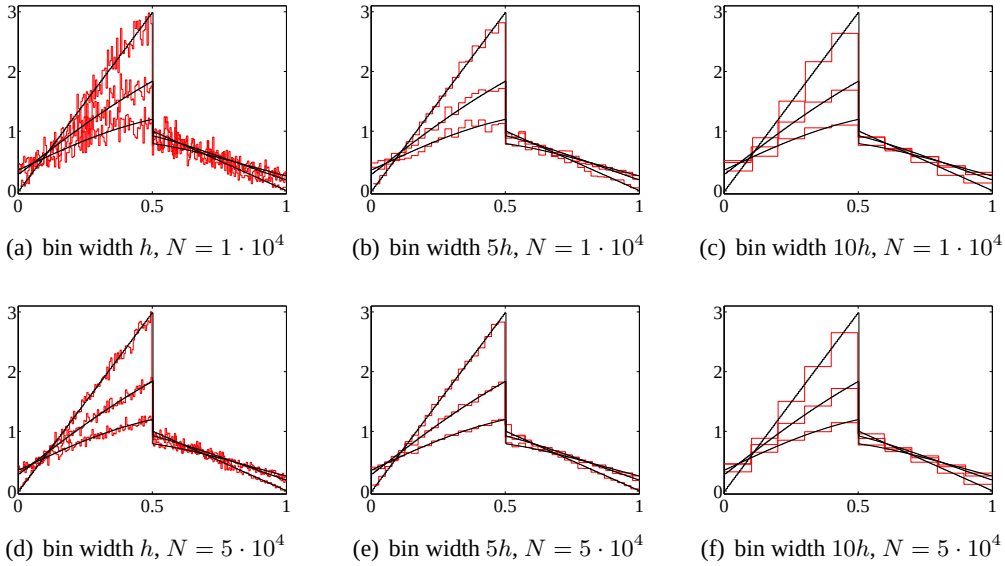

(a) bin width h, $N = 1 \cdot 10^4$ (b) bin width $5h$, $N = 1 \cdot 10^4$ (c) bin width $10h$, $N = 1 \cdot 10^4$

(d) bin width h, $N = 5 \cdot 10^4$ (e) bin width $5h$, $N = 5 \cdot 10^4$ (f) bin width $10h$, $N = 5 \cdot 10^4$

Fig. 6.1: Numerical solutions $u_h(x,t)$ and density estimates $\mu_N(x,t)$ from simulations. For computing μ_N, we consider two different values of N and three different bin widths. The three profiles in each panel correspond to times $t = 0, 0.05, 0.1$.

approximating the density $u(x,t)$ by solving the master equation rather than relying on simulations. The effect the bin width has on smoothing the data is evident, e.g., a bin width of h seems to under-smooth the data, whereas a bin width of $10h$ seems to over-smooth the data.

We next consider $\nu \notin L^1(\mathbb{R})$,

$$\nu(x) = \frac{1}{x^{3/2}}. \tag{6.4.2}$$

We plot the numerical solutions and density estimates at the times $t = 0, 0.025, 0.05$ in Fig. 6.2. We simulate $N = 5 \cdot 10^4$ realizations and we select h as the bin width. The Poisson approximation of Z_t is used with three different values of τ. Notice the disagreement between the density estimate

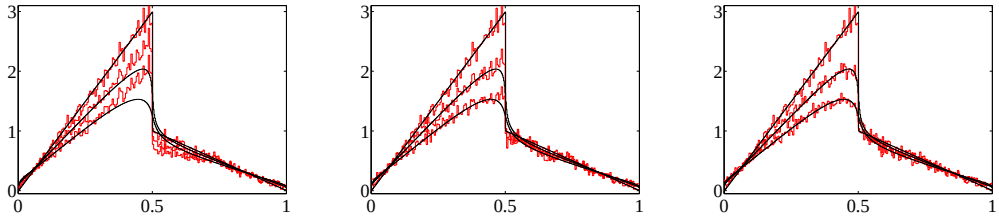

(a) bin width h, $\tau = 0.25$ (b) bin width h, $\tau = 0.05$ (c) bin width h, $\tau = 0.01$

Fig. 6.2: Numerical solutions $u_h(x,t)$ and density estimates $\mu_N(x,t)$ from the Poisson approximation of simulations for three different values of τ.

from the simulations and the numerical solution for large τ. This is corrected by decreasing τ, i.e., improving the approximation of Z_t Also notice the lack of smoothing for $\nu \in L^1$ compared to the smoothing effect in the other case.

We finally compare the exit-times distributions for the two choices (6.4.1) and (6.4.2), shown in Fig. 6.3. Moreover, the mean exit-times are approximately 0.2484 and 0.1527, respectively. The time required for 90% (95%, 99%) of the density to leave Ω are approximately 0.5610 (0.7250, 1.1060) and 0.3460 (0.4490, 0.6850), respectively.

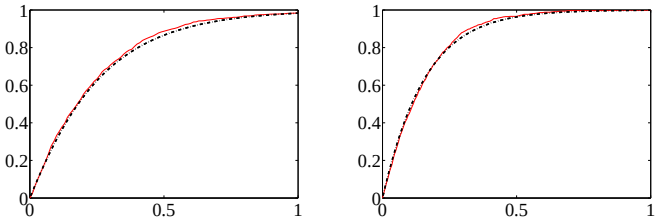

(a) $\nu \in L^1(\mathbb{R})$ (b) $\nu \notin L^1(\mathbb{R})$

Fig. 6.3: Approximate exit-time distributions $F_h(t)$ (solid) and $F_N(t)$ (dashed) for $t \in [0,1]$ and $N = 1000$.

Example 6.4.2 (Identifying different types of diffusion)**.** We present density estimates and numerical solutions of the master equation for $\nu \in L^1(\mathbb{R})$ with $\lambda = \frac{1}{\varepsilon^\alpha}$ and

$$\widehat{\phi}(\xi) = \exp\left(-\varepsilon^\alpha |\xi|^\alpha\right).$$

We plot the time-evolutions of the approximate solutions for $\alpha = 2$ and $\alpha = 1/2$ and various ε given by the finite element method with mesh spacing $h = 0.0005$ and $t \in [0, 0.25]$ in Fig. 6.4. For $\alpha = 2$, the solutions behave asymptotically, with respect to ε, as solutions to the classical diffusion equation. For $\alpha = 1/2$, however, the asymptotic behavior of solutions is given by a fractional Laplace parabolic equation.

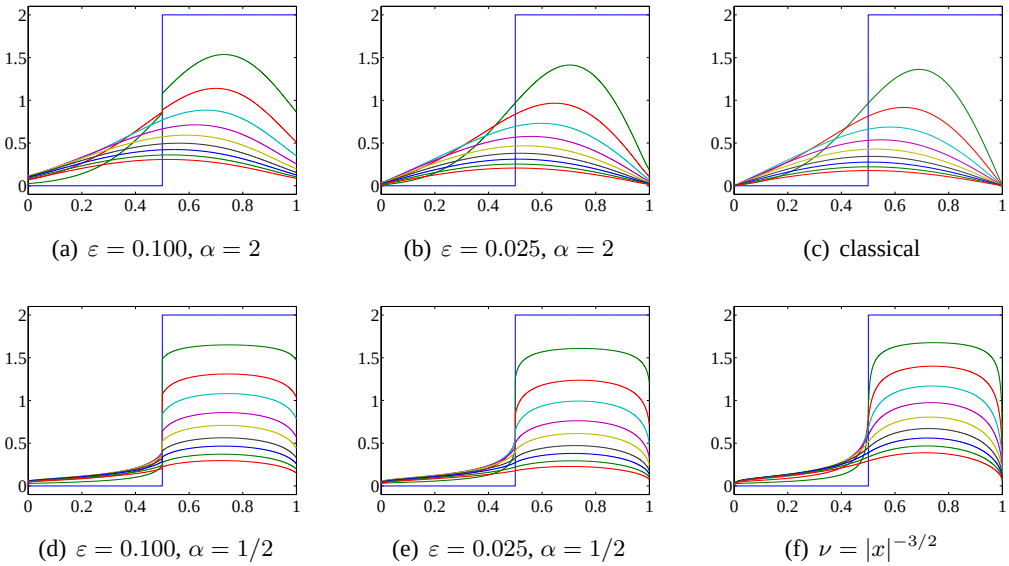

(a) $\varepsilon = 0.100$, $\alpha = 2$ (b) $\varepsilon = 0.025$, $\alpha = 2$ (c) classical

(d) $\varepsilon = 0.100$, $\alpha = 1/2$ (e) $\varepsilon = 0.025$, $\alpha = 1/2$ (f) $\nu = |x|^{-3/2}$

Fig. 6.4: Solutions to the nonlocal homogeneous Dirichlet problem with ϕ_ε^α in Example 6.4.2. The vertical axis in each panel is the value of $u_h(x,t)$ and the horizontal axis is x. The ten different solution profiles in each panel correspond to the solutions at ten different times, for $t \in [0, 0.25]$. In panels (c) and (f), the solutions to (6.1.2) and (6.2.10) are given, respectively.

Example 6.4.3. This example demonstrates one advantage of considering general volume constraints. In particular, we show exit-times from non-simple, e.g., not connected, domains can be studied via the appropriate master equation. Moreover, the nonlocal nature of the equation allows for the process to jump between non-connected parts of the domain. For this discussion, we assume $\nu(x) = \frac{1}{\sqrt{4\pi\varepsilon^2}} \exp\left(-\frac{x^2}{4\varepsilon^2}\right)$.

In general, we consider a bounded domain Ω that is given by

$$\Omega = \bigcup_{k=1}^{D} \Omega_k \quad \text{and} \quad \Gamma = \bigcup_{k=1}^{D+1} \Gamma_k.$$

We are interested in the density exchanges between volumes. More specifically, define

$$M_{\Omega_j}^{\Gamma_k}(t) = \frac{1}{\lambda} \int_0^t \int_{\Gamma_k} \int_{\Omega_j} u(x,s)\phi(y-x)\,\mathrm{d}x\,\mathrm{d}y\,\mathrm{d}s,$$

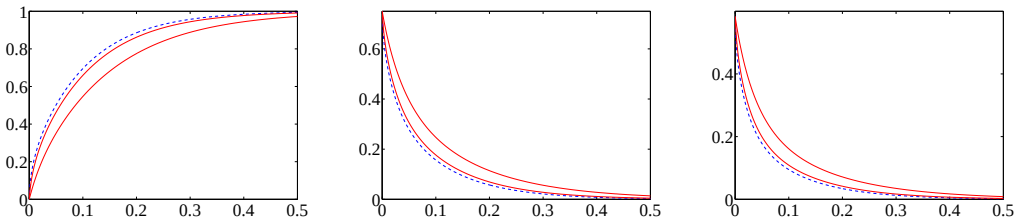

(a) $F_h(t)$, $\alpha = 2$ (b) first moment, $\alpha = 2$ (c) second moment, $\alpha = 2$

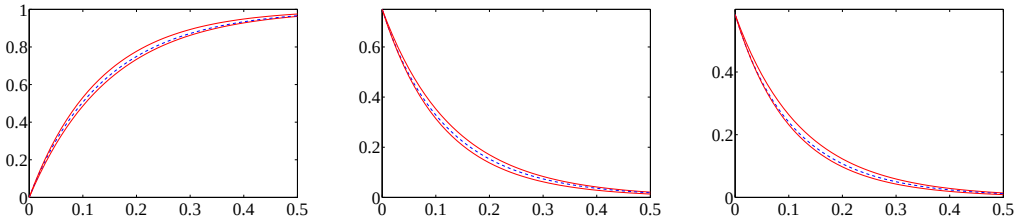

(d) $F_h(t)$, $\alpha = 1/2$ (e) first moment, $\alpha = 1/2$ (f) second moment, $\alpha = 1/2$

Fig. 6.5: In each panel, we plot the appropriate statistic computed from the numerical solution with $\varepsilon = 0.100$, $\varepsilon = 0.025$, and the classical (top) and fractional (bottom) diffusion.

which represents the density that has moved from Ω_j to Γ_k by time t. Integrating (6.2.9),

$$\frac{\mathrm{d}}{\mathrm{d}t}\left(\int_\Omega u(x,t)\,\mathrm{d}x\right) = -\frac{1}{\lambda}\int_\Gamma\int_\Omega u(x,t)\phi(y-x)\,\mathrm{d}x\,\mathrm{d}y$$

so that

$$\int_\Omega u(x,t)\,\mathrm{d}x - \int_\Omega u_0(x)\,\mathrm{d}x = -\frac{1}{\lambda}\int_0^t\int_\Gamma\int_\Omega u(x,s)\phi(y-x)\,\mathrm{d}x\,\mathrm{d}y\,\mathrm{d}s.$$

The quantity on the left is the negative of the density that has exited Ω and we thus have

$$\int_\Omega u_0(x)\,\mathrm{d}x - \int_\Omega u(x,t)\,\mathrm{d}x = \sum_k\sum_j M_{\Omega_j}^{\Gamma_k}(t).$$

To illustrate this, we consider a specific example. Let $\Omega = (0,1/2)\cup(3/5,1)$ and $\Gamma = \mathbb{R}\setminus\Omega$. We impose Dirichlet volume constraints on Γ. We compute the density that exits the constrained regions $\Gamma_1 = (-\infty,0)$, $\Gamma_2 = (0.5,0.6)$, and $\Gamma_3 = (1,\infty)$. The results are plotted in Fig. 6.6.

We study the effect of varying ε on these quantities. As $\varepsilon \to 0$, half of the density leaves Ω to Γ_1 and the other half to Γ_2. For nonzero ε, however, the nonlocal nature allows density that starts in Ω_1 to leave Ω to Γ_3. The results are plotted in Fig. 6.7.

6.5 Summary

This chapter studies pure jump Lévy processes on bounded domains via the master equation, i.e., a nonlocal diffusion equation with volume constraints. Volume constraints allows for the study of

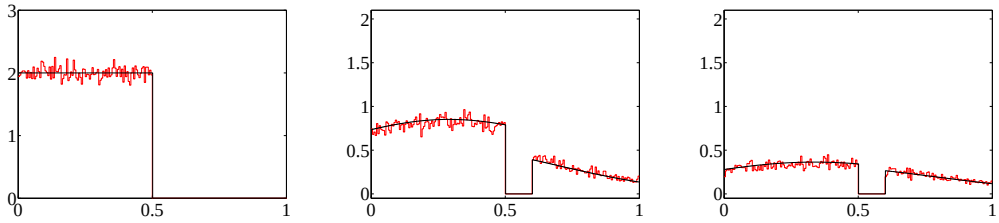

(a) $\varepsilon = 0.25$, $t = 0$ (b) $\varepsilon = 0.25$, $t = 0.1$ (c) $\varepsilon = 0.25$, $t = 0.2$

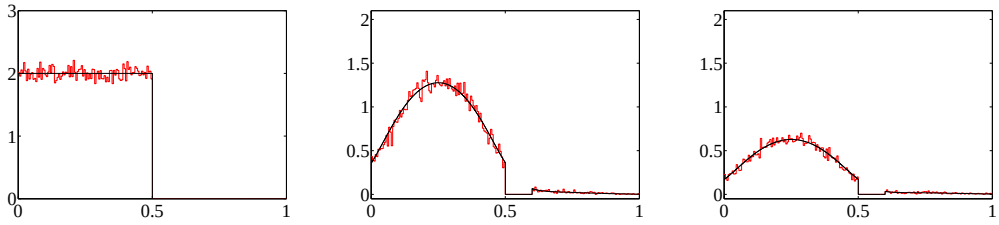

(d) $\varepsilon = 0.05$, $t = 0$ (e) $\varepsilon = 0.05$, $t = 0.025$ (f) $\varepsilon = 0.05$, $t = 0.05$

Fig. 6.6: The numerical solution u_h and density estimate μ_N with $h = 0.005$, $N = 5 \cdot 10^4$, and bin width h. Three different times and two different values of ε are considered.

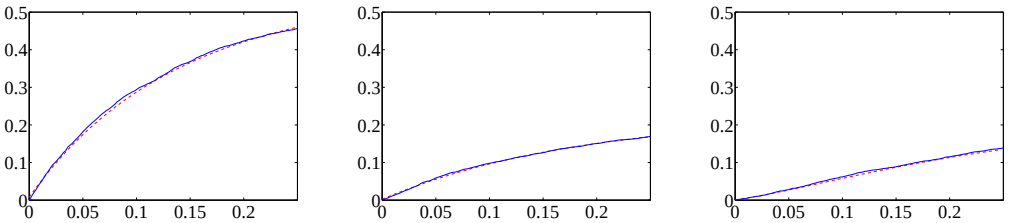

(a) $\varepsilon = 0.25$, $M_\Omega^{\Gamma_1}(t)$ (b) $\varepsilon = 0.25$, $M_\Omega^{\Gamma_2}(t)$ (c) $\varepsilon = 0.25$, $M_\Omega^{\Gamma_3}(t)$

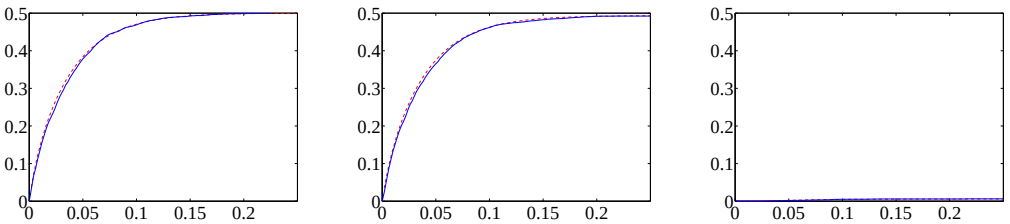

(d) $\varepsilon = 0.05$, $M_\Omega^{\Gamma_1}(t)$ (e) $\varepsilon = 0.05$, $M_\Omega^{\Gamma_2}(t)$ (f) $\varepsilon = 0.05$, $M_\Omega^{\Gamma_3}(t)$

Fig. 6.7: The quantities $M_\Omega^{\Gamma_i}$ for $t \in [0, 0.25]$ and two different values of ε.

exit-times of the process from a bounded domain. Such nonlocal diffusion equations with volume constraints have received much attention lately and we describe how the activity of the process, variation of the sample paths, exit-time distribution of the process, and smoothing of the nonlocal operator are all related. We show how the exit-times vary with respect to the type of diffusion. Moreover, the general volume constraints allow for the study of exit-times from nontrivial domains.

Part II

Formulation and Analysis for Elliptic Problems on Uncertain Domains

7. A SURVEY OF COMPUTATIONS FOR ELLIPTIC PROBLEMS WITH STOCHASTIC COEFFICIENTS AND DATA

Many natural phenomena are modeled by boundary value problems for PDEs. Given a fixed set of input data into the model, e.g., boundary conditions, parameters, and coefficients, much effort has been exhausted to give efficient and accurate solutions of the model. However, these input data are often accompanied by various sources of uncertainty, e.g., errors in estimating parameters from data, and, consequently, effectively using the solutions of the model requires an analysis of the effects of the uncertainty. The important issue is understanding how the uncertainty propagates through the mathematical model, which results in a description of the uncertainty for all outputs of the model, e.g., for all time and all space. In this chapter, we consider the effects of uncertainty in the coefficients of the differential equation and in the geometry on which the differential equation is posed. We begin by reviewing some of the standard tools for solving such problems, e.g., Monte Carlo methods, parametric and nonparametric density estimation, Karhunen-Loeve expansions, generalized polynomial chaos, and stochastic Galerkin methods.

7.1 Introduction

We introduce the PDE posed on the domain $\Omega \subset \mathbb{R}^2$,

$$\begin{cases} -\nabla \cdot (a(x;\boldsymbol{\theta})\nabla w(x;\boldsymbol{\theta})) = f(x;\boldsymbol{\theta}), & x \in \Omega, \\ w(x) = 0, & x \in \partial\Omega, \end{cases} \tag{7.1.1}$$

where $\boldsymbol{\theta}$ is a random variable or field with some given probability structure. In the case of a random field, the limitations of experiment and computation motivates replacing the field by a finite collection of independent random variables,

$$\boldsymbol{\theta}_1,\ \boldsymbol{\theta}_2,\ \boldsymbol{\theta}_3,\ \ldots\ ;\boldsymbol{\theta}_n,$$

We might assume these quantities provide a better approximation as n increases. However, it is desirable to find an approximation that is valid for small n.

We discuss studying (7.1.1) via sampling methods, e.g., Monte Carlo, and by the stochastic Galerkin method. In general, sampling methods are very simple to implement and require solving a deterministic problem for each sample. If an efficient means for solving the original problem for a fixed sample is available, sampling methods are appealing. The stochastic Galerkin method, on the other hand, requires formulating a more difficult problem, which is often a system of coupled PDEs. Not only can the task of deriving this problem be difficult, but subsequent study of it often requires the development of new solvers and methods. If these issues can be overcome, the stochastic Galerkin method eliminates the need to sample and yields the optimal accuracy by the same account of the standard Galerkin method.

The authors of [33, 34] consider the nonparametric density estimation problem of a QOFI via standard Monte Carlo methods in conjunction with Lions domain decomposition and a Neumann expansion in order to provide an efficient computational approach. A posteriori error analysis and adaptive error control algorithms are also presented. In [12], the authors present a stochastic collocation method to solve PDEs with stochastic coefficients and data under the assumption that the input data depends on a finite number of random variables. The probability density of the state of a system is studied in [20], where the authors seek to quantify the uncertainty in chemical properties during the transport of a reactive solute in a heterogeneous porous media.

In [8], the authors assume that the coefficients are described by an appropriate Karhunen-Loeve expansion and then give well-posedness results and error estimates in Sobolev spaces. The stochastic Galerkin method is used in [13] to obtain statistical moments of the solution. The so-called "worst case scenario" for elliptic PDEs with uncertainty is presented in [11].

7.2 Sample-Based Methods

A sample-based method for examining uncertainty involves sampling from the input spaces and then processing the results to compute various statistical quantities. In this section, we briefly describe a Monte Carlo sampling method for PDE with stochastic coefficients. Other sampling approaches exist, e.g., collocation and importance sampling, but are omitted for brevity.

Sampling from a known distribution

We first describe how to generate realizations of a random variable with a known distribution F via the Inverse CDF Method [66]. Assume we have a pseudo-random number generator that draws

numbers from Unif$(0,1)$. The approach for generating realizations x of a random variable X is to simply generate a realization u from Unif$(0,1)$ and then define

$$x = F_*^{-1}(u),$$

where

$$F_*^{-1}(u) = \inf_{z \in \mathbb{R}} \{F(z) \,|\, F(z) \geq u\}.$$

Letting $U \sim$ Unif$(0,1)$, we then have $F_*^{-1}(U) \sim X$. Further, since $U \sim 1-U$, $F_*^{-1}(1-U) \sim X$.

Monte Carlo methods simulate a random variable repeatedly to obtain information about the distribution of the variable. Using the realizations, we can compute the probability distribution of the output. Alternatively, we may be satisfied with some statistics, e.g. the mean. We explore the relationship between the number of realizations and the accuracy of the statistical information obtained.

We now review some basic modes of convergence.

Definition 7.2.1. Let X_n be a sequence of random variables, and let X be a random variable. Then, X_n converges to X

1. in distribution, $X_n \xrightarrow{d} X$, if, for all points x where $F(x)$ is continuous,

$$\lim_{n \to \infty} F_n(x) = F(x),$$

2. in probability, $X_n \xrightarrow{p} X$, if

$$\lim_{n \to \infty} \Pr\left(|X_n - X| \leq \varepsilon\right) = 1, \quad \forall \varepsilon > 0$$

3. almost surely, $X_n \xrightarrow{a.s.} X$, if

$$\Pr\left(\lim_{n \to \infty} X_n = X\right) = 1$$

4. in mean-square if

$$\lim_{n \to \infty} \mathbb{E}\left(|X_n - X|^2\right) = 0.$$

If X_n converges to X almost surely, the set of values such that X_n does not converge to X is a set of measure zero. Convergence in probability is a weaker notion of convergence and convergence in distribution is weaker still.

The Central Limit Theorem states that the sum of a large number of i.i.d. random variable behaves like a single normal random variable. To analyze large sets of random variables, we need the Central Limit Theorem, as well as the Law of Large Numbers.

Theorem 7.2.1 (Central Limit Theorem)**.** *Let X_i be i.i.d. random variables with $\mathbb{E}(X_i) = \mu$ and $\mathrm{Var}(X) = \sigma^2$, with $0 < \sigma^2 < \infty$. Then*

$$\lim_{n\to\infty} \Pr\left(a \leq \frac{\frac{1}{n}\sum_{i=1}^{n} X_i - \mu}{\sigma/\sqrt{n}} < b\right) = \Phi(b) - \Phi(a) = \frac{1}{\sqrt{2\pi}} \int_a^b e^{-\frac{x^2}{2}}\, \mathrm{d}x.$$

In particular,

$$\frac{\frac{1}{n}\sum_{i=1}^{n} X_i - \mu}{\sigma/\sqrt{n}} \xrightarrow{d} Z \sim N(0,1).$$

Theorem 7.2.2 (Strong Law of Large Numbers)**.** *Let X_i be i.i.d. random variables with $\mathbb{E}(X_i) = \mu$ and $\mathrm{Var}(X) = \sigma^2$, with $0 < \sigma^2 < \infty$. Then,*

$$\bar{X} = \frac{1}{n}\sum_{i=1}^{n} X_i \xrightarrow{a.s.} \mu.$$

Theorem 7.2.3 (Weak Law of Large Numbers)**.** *Let X_i be i.i.d. random variables with $\mathbb{E}(X_i) = \mu$ and $\mathrm{Var}(X) = \sigma^2$, with $0 < \sigma^2 < \infty$. Then,*

$$\bar{X} = \frac{1}{n}\sum_{i=1}^{n} X_i \xrightarrow{p} \mu.$$

Monte Carlo method

The Monte Carlo method gives a way for obtaining samples of the output space by taking random samples of the input space and solving the resulting deterministic PDEs. The general description of Monte Carlo methods is simple. For fixed N, we

1. generate N realizations of the input parameters
2. solve each of the N deterministic problems
3. use the output values to compute a cumulative probability distribution or desired statistics.

The hope is that computed statistical quantities converge to the true statistic. as $N \to \infty$.

Monte Carlo methods are specifically useful for approximating integral-based quantities, i.e.,

$$I = \int_\Omega h(\boldsymbol{\theta}) \, \mathrm{d}F(\boldsymbol{\theta}) = \int_\Omega h(\boldsymbol{\theta}) f(\boldsymbol{\theta}) \, \mathrm{d}\boldsymbol{\theta},$$

where the probability density function $f(\boldsymbol{\theta})$ is typically unknown. We select N realizations of $\boldsymbol{\theta}$ independently and consider the estimate

$$I_N = \frac{1}{N} \sum_{n=1}^{N} h(\boldsymbol{\theta}_n).$$

By the Strong Law of Large Numbers, as $N \to \infty$, $I_N \to I$ almost surely. Moreover, the error in the estimate is related to the variance of the function h and the number of samples N. In fact,

$$\mathrm{Var}\left(I_N\right) = \frac{1}{N^2} \sum_{n=1}^{N} \mathrm{Var}(h(\boldsymbol{\theta}_n)) = \frac{\mathrm{Var}(h)}{N} = \frac{\sigma^2(h)}{N}$$

so that the error in the estimate scales with $\sqrt{N}$. To see this more clearly, note

$$\lim_{N \to \infty} \Pr\left(-a \frac{\sigma(h)}{\sqrt{N}} \leq I_N - I \leq b \frac{\sigma(h)}{\sqrt{N}} \right) = \Phi(b) - \Phi(-a).$$

We are particularly interested in computing the distribution and various moments of solutions to partial differential equations with stochastic coefficients. Suppose we are interested in statistics of a QOFI computed from $w(x; \boldsymbol{\theta})$, which solves (7.1.1). Namely, let

$$Q(w; \boldsymbol{\theta}) = \int_\Omega w(x; \boldsymbol{\theta}) \psi(x) \, \mathrm{d}x$$

denote such a QOFI. Various moments, e.g., the k-th moment, of $Q(w; \boldsymbol{\theta})$ can be approximated via

$$I_N = \frac{1}{N} \sum_{n=1}^{N} (Q(w; \boldsymbol{\theta}_n))^k.$$

The Strong Law of Large Numbers gives that

$$\frac{1}{N} \sum_{n=1}^{N} (Q(w; \boldsymbol{\theta}_n))^k \overset{a.s.}{\to} \int_\Theta \left(Q(w; \boldsymbol{\theta})\right)^k \mathrm{d}P(Q(\boldsymbol{\theta})).$$

Moreover, we can estimate the distribution of $Q(w; \boldsymbol{\theta})$ by using the empirical distribution function

$$I_N = F_N(y) = \frac{1}{N} \sum_{n=1}^{N} \chi_{(-\infty, y)}(Q(w; \boldsymbol{\theta}_n)).$$

Parametric and nonparametric density estimation

Suppose $x_1, \ldots, x_n$ are data from n observations of a random variable X with an unknown distribution. We assume that the probability density function f belongs to a parameterized family, but the parameters, $\boldsymbol{\theta}$, are unknown. For example, one might assume $X \sim N(\mu, \sigma^2)$, where $\boldsymbol{\theta} = (\mu, \sigma^2)$ is unknown. We define the likelihood

$$\mathcal{L}(x_1, \ldots, x_n \mid \boldsymbol{\theta}) = f(x_1, \ldots, x_n \mid \boldsymbol{\theta}).$$

Assuming the observations are independent,

$$\mathcal{L}(x_1, \ldots, x_n \mid \boldsymbol{\theta}) = \prod_{i=1}^{n} f(x_i \mid \boldsymbol{\theta}).$$

The goal of maximum likelihood estimation is to find the parameters $\boldsymbol{\theta}$ that maximize $\mathcal{L}$, i.e.,

$$\widehat{\boldsymbol{\theta}}_{MLE} = \operatorname*{argmax}_{\boldsymbol{\theta}} \mathcal{L}(x_1, \ldots, x_n \mid \boldsymbol{\theta}).$$

Often, we instead equivalently maximize the log-likelihood $\ell = \ln(\mathcal{L})$, i.e.,

$$\widehat{\boldsymbol{\theta}}_{MLE} = \operatorname*{argmax}_{\boldsymbol{\theta}} \ell(x_1, \ldots, x_n \mid \boldsymbol{\theta}) = \operatorname*{argmax}_{\boldsymbol{\theta}} \left(\sum_{i=1}^{n} \ln(f(x_i \mid \boldsymbol{\theta})) \right).$$

The maximum likelihood estimator has the desired property of consistency, that is,

$$\widehat{\boldsymbol{\theta}}_{MLE} \xrightarrow{p} \boldsymbol{\theta},$$

as $n \to \infty$. Unfortunately, such estimators are in general biased. An estimator $\widehat{\boldsymbol{\theta}}$ for $\boldsymbol{\theta}$ is unbiased if $\mathbb{E}(\widehat{\boldsymbol{\theta}}) = \boldsymbol{\theta}$. We refer to $\mathbb{E}(\widehat{\boldsymbol{\theta}}) - \boldsymbol{\theta}$ as the bias.

We recall the likelihood

$$\mathcal{L}(x_1, \ldots, x_n \mid \boldsymbol{\theta})$$

and suppose a prior distribution on the parameters $\pi(\boldsymbol{\theta})$. An application of Bayes' theorem demonstrates that the posterior distribution is proportional to the product of the likelihood and priors, i.e,

$$\pi(\boldsymbol{\theta} \mid x_1, \ldots, x_n) \propto \mathcal{L}(x_1, \ldots, x_n \mid \boldsymbol{\theta}) \pi(\boldsymbol{\theta}).$$

In the special case that the prior is conjugate to the likelihood, closed forms for the posterior are easily found. A conjugate prior $\pi(\boldsymbol{\theta})$ to the likelihood $\pi(\cdot \mid \boldsymbol{\theta})$ is such that the posterior distribution lies in the same parameterized family as the prior.

In many applications, experience suggests that the posterior density is rarely described in parametric form. To this effect, one can consider a nonparameteric estimation of the density. We first consider the density histogram. Consider the mesh t_k, where $t_{k+1} - t_k = h$ and, consequently, the histogram is said to have bin width h. The density histogram is constructed by using blocks of width h and height $(nh)^{-1}$ and is defined

$$\bar{f}(x) = \frac{1}{nh} \sum_{k=1}^{K} \sum_{i=1}^{n} \chi_{[t_k, t_{k+1})}(x_i) \chi_{[t_k, t_{k+1})}(x),$$

where $\chi_A(x)$ is the indicator function of the set A. Notice

$$\int_{\mathbb{R}} \bar{f}(x) \, \mathrm{d}x = 1.$$

We also consider the kernel density estimator, where a kernel is a non-negative and symmetric function K such that $\int_{\mathbb{R}} K(x) \, \mathrm{d}x = 1$. Let K be some kernel function and x_i be data samples from a density f. The basic kernel estimator is

$$\bar{f} = \frac{1}{nh} \sum_{i=1}^{n} K\left(\frac{x - x_i}{h} \right),$$

where h is a parameter, often called the bandwidth, that controls the smoothing of the data. The kernel estimator $\bar{f}$ is an approximation of the density f and inherits smoothness properties of the kernel K. Again, since K integrates to 1, we have

$$\int_{\mathbb{R}} \bar{f}(x) \, \mathrm{d}x = 1.$$

A common choice for K is the Gaussian kernel $K(x) = \frac{1}{\sqrt{2\pi}} \exp\left(-\frac{x^2}{2} \right)$ so that

$$\bar{f} = \frac{1}{nh\sqrt{2\pi}} \sum_{i=1}^{n} \exp\left(-\frac{(x - x_i)^2}{2h^2} \right),$$

which is the average of n different Gaussian densities that are each centered at x_i and have variance h. In this example, it is clear that varying h will affect the smoothness of the kernel density estimator.

The empirical distribution function is defined

$$F_n(x) = \frac{1}{n} \sum_{i=1}^{n} \chi_{(-\infty, x]}(x_i).$$

Applying a simple divided difference to approximate the density f, we find

$$\bar{f} = \frac{F_n(x) - F_n(x - h)}{h} = \frac{1}{nh} \sum_{i=1}^{n} \chi_{(x_i, x_i + h]}(x),$$

which can be referred to as an empirical density function.

7.3 Stochastic Galerkin Methods

The stochastic Galerkin method [67] uses Karhunen-Loeve and generalized polynomial chaos expansions to represent the solution to and inputs for a differential equation with stochastic coefficients. Typically, a coupled system of equations must be solved to obtain the coefficients in the polynomial chaos expansion and is often done with the standard Galerkin finite element method. We first review the Karhunen-Loeve expansion and generalized polynomial chaos. Then, we present a short introduction of the stochastic Galerkin method.

Karhunen-Loeve expansion

The Karhunen-Loeve expansion represents a stochastic process as an infinite sum of orthogonal basis functions multiplied by uncorrelated random variables. Let $\omega(x;\boldsymbol{\theta})$ be a random process with

$$\overline{\omega}(x) = \mathbb{E}(\omega(x;\boldsymbol{\theta})) \quad \text{and} \quad C_\omega(x,y) = \text{Cov}(\omega(x;\boldsymbol{\theta}),\omega(y;\boldsymbol{\theta})).$$

Then, the Karhunen-Loeve expansions allows us to write

$$\omega(x;\boldsymbol{\theta}) = \overline{\omega}(x) + \sum_{k=1}^{\infty} \sqrt{\lambda_k} f_k(t)\xi_k(\boldsymbol{\theta}),$$

where f_k (λ_k) are the orthogonal eigenfunctions (eigenvalues), i.e.,

$$\int_\Omega C_\omega(x,y) f_k(y)\,\mathrm{d}y = \lambda_k f_k(x), \quad x \in \Omega.$$

The random variables $\{\xi_k(\boldsymbol{\theta})\}$ are zero-mean, unit-variance, and uncorrelated. In fact,

$$\xi_k(\boldsymbol{\theta}) = \frac{1}{\sqrt{\lambda_k}} \int_\Omega \big(\omega(x;\boldsymbol{\theta}) - \overline{\omega}(x)\big) f_k(x)\,\mathrm{d}x \tag{7.3.1}$$

We typically truncate the Karhunen-Loeve expansion to obtain a finite dimensional approximation of $\omega(x;\boldsymbol{\theta})$,

$$\omega(x;\boldsymbol{\theta}) = \overline{\omega}(x) + \sum_{k=1}^{K} \sqrt{\lambda_k} f_k(t)\xi_k(\boldsymbol{\theta}).$$

The decay rate of the eigenvalues λ_k determines when to truncate the series to obtain the desired accuracy. In general, the decay rate of the eigenvalues depends inversely on the correlation length. We now present an outline of the proof of the Karhunen-Loeve expansion.

Lemma 7.3.1. *The covariance function C_ω is bounded, symmetric, and positive definite.*

Proof. We first illustrate boundedness. Choose $x, y \in \Omega$ and notice, using Hölder's inequality,

$$\begin{aligned}
|C_\omega(x,y)| &= |\mathbb{E}\left[\omega(x;\boldsymbol{\theta})\omega(y;\boldsymbol{\theta})\right] - \overline{\omega}(x)\overline{\omega}(y)| \\
&\leq |\mathbb{E}\left[\omega(x;\boldsymbol{\theta})\omega(y;\boldsymbol{\theta})\right]| + \overline{\omega}(x)\overline{\omega}(y) \\
&\leq \left(\mathbb{E}\left[(\omega(x;\boldsymbol{\theta}))^2\right]\right)^{1/2} \cdot \left(\mathbb{E}\left[(\omega(y;\boldsymbol{\theta}))^2\right]\right)^{1/2} + \overline{\omega}(x)\overline{\omega}(y).
\end{aligned}$$

From the uniform boundedness of the second moments of $\omega(x;\boldsymbol{\theta})$, we have that C_ω is bounded. Showing symmetry is trivial as

$$C_\omega(x,y) = \mathbb{E}\left[\omega(x;\boldsymbol{\theta})\omega(y;\boldsymbol{\theta})\right] - \overline{\omega}(x)\overline{\omega}(y) = C_\omega(y,x).$$

To demonstrate positive definite, let $n \in \mathbb{N}$ be given and $x_1, \ldots, x_n \in \Omega$. We recall that the covariance matrix is positive semidefinite. Thus, by definition, C_ω is positive definite. □

Theorem 7.3.2 (Mercer's theorem)**.** *Suppose C_ω is a continuous symmetric positive definite kernel on Ω. Then there is an orthonormal basis f_k consisting of eigenfunctions such that the sequence of corresponding eigenvalues λ_k is nonnegative. The eigenfunctions corresponding to non-zero eigenvalues are continuous on Ω and*

$$C_\omega(x,y) = \sum_{n=1}^{\infty} \lambda_k f_k(x) f_k(y), \tag{7.3.2}$$

where the convergence is absolute and uniform on Ω.

Thus, C_ω admits the decomposition (7.3.2), where λ_k and f_k are the eigenvalues and orthonormal eigenfunctions, i.e., they satisfy

$$\int_\Omega C_\omega(x,y) f_k(y)\,\mathrm{d}y = \lambda_k f_k(x), \quad x \in \Omega, \tag{7.3.3}$$

and

$$\int_\Omega f_n(x) f_m(x)\,\mathrm{d}x = \delta_{nm}, \quad x \in \Omega, \tag{7.3.4}$$

We decompose $\omega(x;\boldsymbol{\theta})$ into its mean $\overline{\omega}(x)$ and a zero mean random process $\alpha(x;\boldsymbol{\theta})$,

$$\omega(x;\boldsymbol{\theta}) = \overline{\omega}(x) + \alpha(x;\boldsymbol{\theta}).$$

Note that the covariance function C_α is also given by

$$C_\alpha(x,y) = C_\omega(x,y).$$

Theorem 7.3.3 (Karhunen-Loeve Decomposition I)**.** *Let $\alpha(x;\boldsymbol{\theta}) = \omega(x;\boldsymbol{\theta}) - \overline{\omega}(x)$. Then there are random variables $\{\xi_n\}_n$ such that $\mathbb{E}\left[\xi_j(\boldsymbol{\theta})\xi_k(\boldsymbol{\theta})\right] = \delta_{jk}$, $\mathbb{E}\left[\xi_j(\boldsymbol{\theta})\right] = 0$, and*

$$\alpha(x;\boldsymbol{\theta}) = \sum_{n=1}^{\infty} \xi_n(\boldsymbol{\theta})\sqrt{\lambda_n} f_n(x), \tag{7.3.5}$$

where the sum converges in mean square uniformly in x.

Proof. From previous discussions, C_α is bounded, symmetric, and positive definite. Mercer's Theorem gives us the orthonormal eigenfunctions f_n. For non-zero eigenvalue λ_n, define

$$\xi_n(\boldsymbol{\theta}) = \frac{1}{\sqrt{\lambda_n}} \int_\Omega \alpha(x;\boldsymbol{\theta}) f_n(x)\,\mathrm{d}x.$$

Since f_n is continuous on Ω, ξ_n is integrable and

$$\mathbb{E}\left[\xi_n(\boldsymbol{\theta})\right] = 0.$$

Further,

$$\begin{aligned}
\mathbb{E}\left[\xi_j(\boldsymbol{\theta})\xi_k(\boldsymbol{\theta})\right] &= \mathbb{E}\left[\frac{1}{\sqrt{\lambda_j}}\int_\Omega \alpha(x;\boldsymbol{\theta}) f_j(x)\,\mathrm{d}x \cdot \frac{1}{\sqrt{\lambda_k}}\int_\Omega \alpha(y;\boldsymbol{\theta}) f_k(y)\,\mathrm{d}y\right] \\
&= \mathbb{E}\left[\frac{1}{\sqrt{\lambda_j\lambda_k}}\int_\Omega\int_\Omega \alpha(x;\boldsymbol{\theta})\alpha(y;\boldsymbol{\theta}) f_j(x) f_k(y)\,\mathrm{d}x\,\mathrm{d}y\right] \\
&= \frac{1}{\sqrt{\lambda_j\lambda_k}}\int_\Omega\int_\Omega \mathbb{E}\left[\alpha(x;\boldsymbol{\theta})\alpha(y;\boldsymbol{\theta})\right] f_j(x) f_k(y)\,\mathrm{d}x\,\mathrm{d}y \\
&= \frac{1}{\sqrt{\lambda_j\lambda_k}}\int_\Omega \left(\int_\Omega C_\alpha(x,y) f_j(x)\,\mathrm{d}x\right) f_k(y)\,\mathrm{d}y \\
&= \frac{\sqrt{\lambda_j}}{\sqrt{\lambda_k}}\int_\Omega f_j(y) f_k(y)\,\mathrm{d}y \\
&= \delta_{jk}.
\end{aligned}$$

Then, one can show

$$\begin{aligned}
&\mathbb{E}\left[\left(\sum_{n=1}^{N} \xi_n(\boldsymbol{\theta})\sqrt{\lambda_n} f_n(x) - \alpha(x;\boldsymbol{\theta})\right)^2\right] \\
&\qquad = \sum_{n=1}^{N} \lambda_n f_n(x)^2 - 2\sum_{n=1}^{N} \mathbb{E}\left[\xi_n(\boldsymbol{\theta})\alpha(x;\boldsymbol{\theta})\right]\sqrt{\lambda_n} f_n(x) + C_\alpha(x,x).
\end{aligned}$$

Notice

$$\mathbb{E}\left[\xi_n(\boldsymbol{\theta})\alpha(x;\boldsymbol{\theta})\right] = \sqrt{\lambda_n} f_n(x).$$

Thus,

$$\mathbb{E}\left[\left(\sum_{n=1}^{N}\xi_n(\boldsymbol{\theta})\sqrt{\lambda_n}f_n(x)-\alpha(x;\boldsymbol{\theta})\right)^2\right]=C_\alpha(x,x)-\sum_{n=1}^{N}\lambda_n f_n(x)^2.$$

The above term converges to 0 uniformly in x, completing the proof. □

Corollary 7.3.4 (Karhunen-Loeve Decomposition II)**.** *For the random process $\omega(x;\boldsymbol{\theta})$ described earlier, we can find the Karhunen-Loeve expansion*

$$\omega(x;\boldsymbol{\theta})=\overline{\omega}(x;\boldsymbol{\theta})+\sum_{n=1}^{\infty}\xi_n(\boldsymbol{\theta})\sqrt{\lambda_n}f_n(x), \tag{7.3.6}$$

where $\mathbb{E}\left[\xi_n(\boldsymbol{\theta})\right]=0$ and $\mathbb{E}\left[\xi_n(\boldsymbol{\theta})\xi_m(\boldsymbol{\theta})\right]=\delta_{nm}$.

Generalized polynomial chaos

Let Z be a random variable with distribution F and all finite moments. To keep the presentation concise, we assume that Z is absolutely continuous so that we can associate to Z a probability density function ψ. Thus,

$$\mathbb{E}(|Z|^m)=\int_{\mathbb{R}}|z|^m\psi(z)\,\mathrm{d}z<\infty,\quad m\in\mathbb{N}.$$

Definition 7.3.1. The generalized polynomial chaos basis functions are the orthogonal polynomials that satisfy

$$\mathbb{E}(\phi_m(Z)\phi_n(Z))=\gamma_n\delta_{mn},\quad m,n\in\mathbb{N},$$

where $\gamma_n=\mathbb{E}(\phi_n^2(Z))$.

Since

$$\mathbb{E}(\phi_m(Z)\phi_n(Z))=\int_{\mathbb{R}}\phi_m(z)\phi_n(z)\psi(z)\,\mathrm{d}z,$$

the functions $\{\phi_k\}$ are a set of orthogonal polynomials with respect to the weight ψ. The choice of Z, i.e., the distribution of Z, thus determines the class of orthogonal polynomials, e.g., if Z has a uniform distribution then ϕ_k is the k-th Legendre polynomials.

Consequently, the N-th order orthogonal projection of a mean square integrable function f is given by

$$\pi_N f=\sum_{k=0}^{N}\widehat{f}_k\phi_k(Z),\quad \text{where } \widehat{f}_k=\frac{1}{\gamma_k}\mathbb{E}(f(Z)\phi_k(Z)).$$

Such an approximation is said to be a strong approximation of f, e.g.,

$$\mathbb{E}((f - \pi_N f)^2) \to 0, \quad \text{as } N \to \infty.$$

In fact, the N-th order orthogonal projection is the best approximation in $\mathbb{P}_N$, the space of all polynomials of degree N, i.e.,

$$\mathbb{E}((f - \pi_N f)^2) = \inf_{g \in \mathbb{P}_N} \mathbb{E}((f - g)^2).$$

Since convergence in mean square implies weaker types of convergence, e.g., in probability and in distribution. We also have the following theorem involving weak convergence.

Theorem 7.3.5. *Let Y be a random variable with distribution F_Y and $\mathbb{E}(Y^2) < \infty$. Let Z be a random variable with distribution F_Z, and finite moments such that the generalized polynomial chaos basis functions exist. Then, defining*

$$Y_N = \sum_{k=0}^{N} a_k \phi_k(Z), \quad \textit{where} \quad a_k = \frac{1}{\gamma_k} \mathbb{E}\left(F_Y^{-1}(F_Z(Z))\phi_k(Z)\right),$$

$Y_N \xrightarrow{p} Y$ *as* $N \to \infty$.

Stochastic Galerkin finite element method

The Karhunen-Loeve expansion and generalized polynomial chaos methods play a large role in the stochastic Galerkin finite element method. We present the approach for the two-dimensional PDE

$$\begin{cases} -\nabla \cdot (a(x; Z)\nabla w(x; Z)) = f(x; Z), & x \in \Omega, \\ w(x; Z) = 0, & x \in \partial\Omega. \end{cases} \tag{7.3.7}$$

The idea is to insert an approximation of w,

$$w_N(x; Z) = \sum_{|\mathbf{k}|=0}^{N} \widehat{w}_{\mathbf{k}}(x)\phi_{\mathbf{k}}(Z), \quad \text{where} \quad \widehat{w}_{\mathbf{k}}(x) = \frac{1}{\gamma_{\mathbf{k}}} \mathbb{E}(w(x; Z)\phi_{\mathbf{k}}(Z)),$$

that is based on generalized polynomial chaos expansions. Since w is unknown, we cannot actually compute the coefficients $\widehat{w}_{\mathbf{k}}(x)$. This motivates the stochastic Galerkin finite element method, i.e., we introduce the problem: find $\widehat{v}_{\mathbf{k}}$ in

$$v_N(x; Z) = \sum_{|\mathbf{k}|=0}^{N} \widehat{v}_{\mathbf{k}}(x)\phi_{\mathbf{k}}(Z)$$

such that

$$\begin{cases} \mathbb{E}\left(-\nabla\cdot\left(a(x;Z)\nabla v_N(x;Z)\right)\phi_j(Z)\right) = \mathbb{E}\left(f(x;Z)\phi_j(Z)\right), & x\in\Omega, \\ \mathbb{E}\left(v_N(x;Z)\phi_j(Z)\right) = 0, & x\in\partial\Omega. \end{cases} \tag{7.3.8}$$

We next assume a has an Karhunen-Loeve expansion,

$$a(x;Z) = \sum_{i=0}^{N_a} \widehat{a}_i(x) Z_i,$$

where $Z_0 \equiv 1$, and we use the orthogonal projection of f,

$$\pi_N f(x;Z) = \sum_{|\ell|=0}^{N_f} \widehat{f}_\ell(x)\phi_\ell(Z).$$

Insertion of these into (7.3.8), we find for each j

$$\begin{aligned} \mathbb{E}\left(-\nabla\cdot\left(\left[\sum_{i=0}^{N_a}\widehat{a}_i(x)Z_i\right]\nabla v_N(x;Z)\right)\phi_{\mathbf{j}}(Z)\right) &= \mathbb{E}\left(\left[\sum_{\ell=0}^{N_f}\widehat{f}_\ell(x)\phi_\ell(Z)\right]\phi_{\mathbf{j}}(Z)\right) \\ &= \gamma_{\mathbf{j}}\widehat{f}_{\mathbf{j}}(x). \end{aligned}$$

Utilizing $v_N(x;Z)$ in the above and then ordering the M vectors appropriately,

$$\begin{aligned} &\mathbb{E}\left(-\nabla\cdot\left(\left[\sum_{i=0}^{N_a}\widehat{a}_i(x)Z_i\right]\left[\sum_{|\mathbf{k}|=0}^{N}\nabla\widehat{v}_{\mathbf{k}}(x)\phi_{\mathbf{k}}(Z)\right]\right)\phi_{\mathbf{j}}(Z)\right) \\ &\quad= \sum_{i=0}^{N_a}\sum_{|\mathbf{k}|=0}^{N}\mathbb{E}\left(Z_i\phi_{\mathbf{k}}(Z)\phi_{\mathbf{j}}(Z)\right)\left(-\nabla\cdot\left(\widehat{a}_i(x)\nabla\widehat{v}_{\mathbf{k}}(x)\right)\right) \\ &\quad= \sum_{k=1}^{M}\left(-\nabla\cdot\left(C_{jk}(x)\nabla\widehat{v}_k(x)\right)\right), \end{aligned}$$

where

$$C_{jk} = \sum_{i=0}^{N_a}\mathbb{E}\left(Z_i\phi_k(Z)\phi_j(Z)\right)\widehat{a}_i(x).$$

Thus, for each $j = 1,\ldots,M$, we solve

$$\sum_{k=1}^{M}\left(-\nabla\cdot\left(C_{jk}(x)\nabla\widehat{v}_k(x)\right)\right) = \gamma_j\widehat{f}_j(x),$$

which is now just a system of coupled PDEs that can be solved approximately via the standard (deterministic) Galerkin finite element procedure.

8. FORMULATION OF ELLIPTIC PROBLEMS ON UNCERTAIN DOMAINS

In several applications of boundary value problems for PDEs the geometry on which the equations are posed are uncertain. To model this uncertainty, we formulate a class of elliptic problems that are posed on stochastic domains. We demonstrate well-posedness of such problems and introduce a piecewise transformation of the domain to a deterministic reference domain. The resulting problems have stochastic coefficients, which we study via Monte Carlo and standard finite element methods.

8.1 Introduction

In many applications of boundary value problems for PDEs the geometry on which the equations are posed are uncertain. Though much work has been done in the study of PDEs with stochastic coefficients, comparatively little work exists for PDEs with stochastic domains. In fact, given a sufficiently fine spatial resolution, the physical domain on which the model is posed is almost invariably uncertain [70], e.g., due to manufacturing imperfections, the inability to obtain accurate measurements, or the approximation of the geometry from a discrete set of data points.

Early attempts investigated the effects of "rough" boundaries with a deterministic framework, e.g., using fractal boundaries. For instance, in [16, 19], heat conduction and transport across irregular boundaries in semi-infinite domains is considered. Conformal maps are used to transform the domain with an irregular boundary to that with a simple boundary so that existing tools can then be used to understand what effect such perturbations have on the transport across the boundary. In, [9, 10] the authors consider both Dirichlet and Neumann problems on a monotone sequence of domains converging to an uncertain, but fixed, domain.

The inability to accurately measure parameters, inhomogeneities, and deviations from a deterministic set of input data have deemed stochastic descriptions of the model more appropriate in many circumstances. The ensuing analysis requires both sophisticated mathematical tools, e.g., numerical approximation via finite element methods, and statistics, e.g., parameter estimation, data assimilation, and the modeling of uncertainty. In general, we consider the PDE posed on the domain

$\Omega(\boldsymbol{\theta}) \subset \mathbb{R}^2$,

$$\begin{cases} -\nabla \cdot (a(x)\nabla w(x;\boldsymbol{\theta})) = f(x), & x \in \Omega(\boldsymbol{\theta}), \\ w(x) = 0, & x \in \partial\Omega(\boldsymbol{\theta}), \end{cases} \tag{8.1.1}$$

where $\boldsymbol{\theta}$ is a random variable with some given probability structure.

The case when uncertainties are present in the coefficients of a PDE model has received much attention from numerous disciplines, e.g., biology, chemistry, and fluid dynamics. The ensuing demand for rigorous mathematical and statistical theory to accommodate the applications has been met; see [8, 11, 12, 13, 20, 33, 34, 69]. Some commonly used tools include Karhunen-Loeve expansions, generalized polynomial chaos, and stochastic collocation.

Much less attention, however, has been given to PDE models in which the boundary of the physical domain is uncertain, though this problem is equally practical in its application. Specific applications of such problems are found in transport in tubes with rough boundaries [65], aerodynamic studies in the design of wind turbines [23], heat diffusion across irregular and fractal-like surfaces [16, 19], structural analysis studies [55], acoustic scattering on rough surfaces [56, 68], seismology and oil reservoir management [13], various civil and nuclear engineering studies [11], chemical transport in rough domains [20], and understanding the effect of geometric variability on the electromechanical behavior of nanostructures [7].

One challenge for problems with stochastic domains is that the standard numerical techniques used for problems with stochastic coefficients, e.g., Karhunen-Loeve, stochastic Galerkin, and Monte Carlo, do not readily apply. For instance, standard sampling methods, e.g., Monte Carlo, face several significant challenges: a naive approach will require constructing a mesh of the domain for each realization of $\boldsymbol{\theta}$; the variational formulation requires a basis of test functions that depend on $\boldsymbol{\theta}$; and it is not clear how to perform an error analysis for multiple problems across different domains and different meshes as the error estimates will depend on $\boldsymbol{\theta}$ in some unknown way. These issues make standard Monte Carlo approaches impractical for this problem. Other techniques, e.g., Karhunen-Loeve expansions, generalized polynomial chaos, and the stochastic Galerkin method, fail for similar reasons due to the dependence of the orthogonal basis functions on $\boldsymbol{\theta}$. Consequently, new tools must be developed for problems with stochastic domains. The most popular approach is to transform the problem from the stochastic domain to a deterministic domain, which moves the dependence on $\boldsymbol{\theta}$ from the domain to the coefficients and data.

The work of [70] provides a novel approach for transforming a problem posed on a domain whose boundary is parameterized by a stochastic process to a problem posed on a deterministic domain with stochastic coefficients. The parameterization of the boundary is assumed to be well-approximated by a Karhunen-Loeve expansion, which is truncated and used to construct a stochastic transformation by solving Laplace's equation. Applying the transformation gives rise to a PDE with stochastic coefficients, which can be studied via Monte Carlo methods and stochastic Galerkin methods.

The approach described in [70] has been largely successful in many applications. For instance, the paper [65] studies flow and transport in tubes with rough surfaces. The effect of geometric variability, due to, e.g., the manufacturing process, on the electromechanical behavior of nanostructures is considered in [7]. At this scale, seemingly insignificant uncertainties, due to, e.g., etching imperfections can drastically affect the performance of the nanostructure. In [56, 68], the acoustic scattering on rough surfaces is studied. Despite its successes, however, there are several concerns and unanswered questions pertaining to this approach. Precise conditions to guarantee well-posedness of the original and transformed problems are unknown. An error analysis is not available for the effect of truncating the Karhunen-Loeve expansion, approximating the stochastic transformation, among other sources of error. Further, the description of the boundary in terms of a stochastic process requires detailed information that in some cases is not available and cannot be obtained or verified through experimentation. Instead, we often only have measurements of the domain at a finite set of points on the boundary.

We present an alternate formulation of elliptic problems on stochastic domains to the model of stochastic domains considered in [70] that describes the boundary as a stochastic process. We consider a definition of stochastic domains driven by measurements and tolerances that one might obtain in an actual experiment. Given the significant differences in the models considered in this approach and that in [70], we do not intend to argue one approach is better than the other. Instead, we note that these are two different models of a stochastic domain and each appeals to different applications.

We assume a finite number of points vary on the boundary, which is meant to represent, e.g., imposed manufacturing tolerances or actual measurements of the domain. Using a piecewise smooth transformation on a partition of the domain, we transform the problem to one posed on a deterministic domain with stochastic coefficients. The transformation is available at minimal additional cost.

We demonstrate well-posedness of both the untransformed and transformed problems. A numerical method that employs Lion's domain decomposition to deal with the non-smooth transformed coefficients and the standard finite element method is formulated. The large number of parameters and unavailability of the distributions of the stochastic coefficients make Monte Carlo and other sample-based methods appealing. Exploiting the piecewise smooth transformation allows for an efficient implementation of such Monte Carlo methods. Moreover, an a posteriori error analysis is readily available and is presented in the following chapter.

We present a simple stochastic transformation to a deterministic domain Ω that is motivated from both the work of [70] and the theory of isoparametric finite element methods in classical finite element theory. Constructing this mapping takes little additional computational effort and the resulting problem is no more complicated. All of the problems are thus transformed to PDEs on Ω with stochastic coefficients, which allows for easy comparison of results and errors across all realizations of $\boldsymbol{\theta}$.

The rest of the chapter is organized as follows. In Section 8.2, we describe a class of stochastic domains and formulate elliptic problems on them. We demonstrate well-posedness and describe how to transform the problem to one posed on a deterministic reference domain. In Section 8.3, we briefly present the finite element method and the iterative domain decomposition. We show how Monte Carlo methods will be used to approximate statistics and the distribution of a QOFI in Section 8.4.

8.2 Problem Formulation

We give a precise description of the types of stochastic domains that we consider. Then, we formulate elliptic PDEs on these domains, present well-posedness results, and then describe how to transform to a reference domain.

Description of a stochastic domain

We divide stochastic domain problems into three classes described in Fig. 8.1. We concern ourselves with the study of the first two problems only. The third class of problems can be studied by employing isoparametric finite element method techniques and the analysis found hereafter. This is left as a topic of future research.

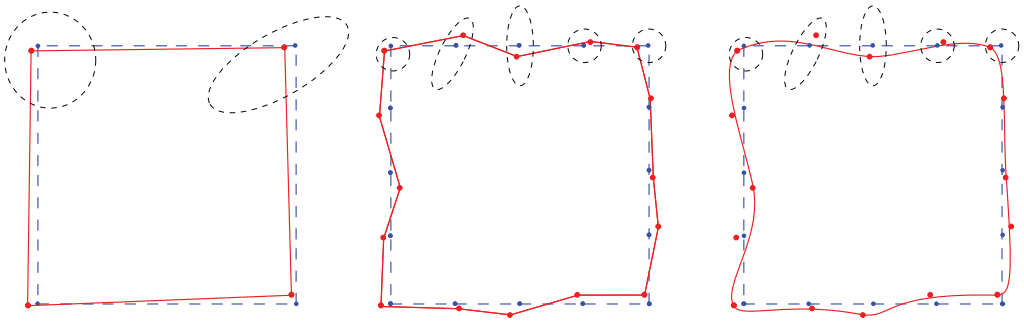

(a) (b) (c)

Fig. 8.1: Panel (a): The boundary of the domain is polygonal and includes a finite and small number of points whose position are given by a random vector $\boldsymbol{\theta}$. The perturbations may be quite large, but we require that important characteristics of the geometry do not change, e.g., convexity is preserved.
Panel (b): The boundary of the domain is polygonal and includes many points whose position are given by a random vector $\boldsymbol{\theta}$. These points are relatively close together and sufficient restrictions on the perturbations are required to guarantee well-posedness and regularity of the solutions.
Panel (c): The boundary of the domain is known to be smooth. Given a finite number of measurements of the domain, a smooth boundary is fit, e.g., a least-squares fit or a cubic spline.

The first class of problems allows perturbations that do not significantly alter the geometry, e.g., convexity. For instance, a square is very robust to perturbations at the corners, whereas perturbations along the edges easily make the domain non-convex. Such domains can be thought of in a manufacturing setting as being stamped out of a sheet of metal. The second class of problems allows many smaller perturbations that fundamentally change the original geometry. This class of problems models indents and small imperfections along the boundary. To guarantee well-posedness, non-degenerate domains, and sufficient regularity of the solutions, we impose strict restrictions on the perturbations. The third class of problems requires an additional assumption that the boundary is smooth. One can also consider this class of problems as a limit of the second class as the number of perturbed points increases. Since the boundary of the domain is smooth, well-posedness and regularity are not concerns.

Modeling assumptions

We restrict ourselves to the class of problems whose domain are defined by perturbations of a convex polygonal domain. We require that the perturbations are bounded and such that the perturbed domain remains polygonal. We assume $\boldsymbol{\theta}$ is such that there exist a bounded polygonal domain Ω^*

and a domain Ω_* with nonzero volume such that

$$\Omega_* \subseteq \Omega(\boldsymbol{\theta}) \subseteq \Omega^*, \quad \forall \boldsymbol{\theta} \in \Theta.$$

Moreover, we assume $\mathbf{0} \in \Theta$ and note that as a sequence $\boldsymbol{\theta}_i \to \mathbf{0}$ the sequence of domains $\Omega(\boldsymbol{\theta}_i)$ converge to $\Omega(\mathbf{0})$. Thus, if the perturbations are small, we expect $\Omega_* \approx \Omega^*$. Since the locations of the perturbed points are fixed, Ω_* and Ω^* limit the non-convexity that may occur.

The matrix a is defined on Ω^* and is assumed to be bounded, symmetric, and positive definite. Moreover, the entries of a are assumed to be smooth and the formulation of the coefficients is not dependent on $\boldsymbol{\theta}$, e.g., the physical characteristics of the material are not altered as $\boldsymbol{\theta}$ changes. We then have that the bilinear form

$$B_V(u,v) = (a\nabla u, \nabla v)_V = \int_V a(x)\nabla u \cdot \nabla v \,\mathrm{d}x$$

satisfies

$$|B_{\Omega(\boldsymbol{\theta})}(u,v)| \leq C_1(\boldsymbol{\theta})\|u\|_{H_0^1(\Omega(\boldsymbol{\theta}))}\|v\|_{H_0^1(\Omega(\boldsymbol{\theta}))}, \qquad \forall u, v \in H_0^1(\Omega(\boldsymbol{\theta})), \tag{8.2.1a}$$

$$B_{\Omega(\boldsymbol{\theta})}(u,u) \geq C_2(\boldsymbol{\theta})\|u\|^2_{H_0^1(\Omega(\boldsymbol{\theta}))}, \qquad \forall u \in H_0^1(\Omega(\boldsymbol{\theta})), \tag{8.2.1b}$$

for all $\boldsymbol{\theta} \in \Theta$. We assume a uniform boundedness and coercivity in the sense that, for all $\boldsymbol{\theta}$,

$$C_1(\boldsymbol{\theta}) \leq C_1 < \infty \quad \text{and} \quad C_2(\boldsymbol{\theta}) \geq C_2 > 0.$$

Consider $f \in L^2(\Omega^*)$ that is defined on Ω^* and does not depend on $\boldsymbol{\theta}$ and note that the linear functional

$$F_V(v) = \int_V f(x)v(x) \,\mathrm{d}x$$

satisfies

$$F_{\Omega(\boldsymbol{\theta})}(v) = \int_{\Omega(\boldsymbol{\theta})} f(x)v(x) \,\mathrm{d}x \leq C_3(\boldsymbol{\theta})\|v\|_{H_0^1(\Omega(\boldsymbol{\theta}))}. \tag{8.2.2}$$

Again, we assume uniform boundedness of the linear functional in the sense that, for all $\boldsymbol{\theta}$,

$$C_3(\boldsymbol{\theta}) \leq C_3 < \infty.$$

The variational formulation for (8.1.1) is: find $w \in H_0^1(\Omega(\boldsymbol{\theta}))$ such that

$$B_{\Omega(\boldsymbol{\theta})}(w,v) = F_{\Omega(\boldsymbol{\theta})}(v), \quad \forall v \in H_0^1(\Omega(\boldsymbol{\theta})). \tag{8.2.3}$$

With the uniform boundedness and coercivity of the bilinear form on the left hand side of (8.2.3) and the uniform boundedness of the linear form on the right hand side, the Lax-Milgram lemma guarantees a unique weak solution to (8.2.3) for all $\boldsymbol{\theta} \in \Theta$.

Transformation to a reference domain

We now describe how to transform the domain $\Omega(\boldsymbol{\theta})$ to a reference domain Ω. The reference domain $\Omega \subset \mathbb{R}^2$ is assumed to be a convex polygonal domain. Choosing such a domain can be somewhat arbitrary, but it is natural to take $\Omega = \Omega(\mathbf{0})$. There are several ways to transform the domain $\Omega(\boldsymbol{\theta})$ to Ω, e.g., conformal maps such as Schwarz-Christoffel transformations provide a global and smooth map. We use a piecewise transformation $\varphi : \Omega(\boldsymbol{\theta}) \to \Omega$ on a partition of $\Omega(\boldsymbol{\theta})$ into subdomains $\Omega_d(\boldsymbol{\theta})$, $d = 1, \ldots, D$, such that $\overline{\Omega(\boldsymbol{\theta})} = \bigcup_{d=1}^{D} \overline{\Omega_d(\boldsymbol{\theta})}$, i.e., $\varphi_d : \Omega_d(\boldsymbol{\theta}) \to \Omega_d$.

This partitioning of $\Omega(\boldsymbol{\theta})$ into D subdomains is not unique, though some choices have appealing benefits, which are discussed later. We thus replace the global problem (8.1.1) with an abstract domain decomposition on a partition of $\Omega(\boldsymbol{\theta})$. Let $\mathbf{n}_d$ denote the outward pointing normal vector to $\Omega_d(\boldsymbol{\theta})$ and w_d denote the solution on $\Omega_d(\boldsymbol{\theta})$. Then, (8.1.1) is equivalent to

$$\begin{cases} -\nabla \cdot (a_d(x)\nabla w_d(x;\boldsymbol{\theta})) = f_d(x), & x \in \Omega_d(\boldsymbol{\theta}), \\ w_d(x;\boldsymbol{\theta}) = 0, & x \in \partial\Omega(\boldsymbol{\theta}) \cap \partial\Omega_d(\boldsymbol{\theta}), \\ w_d(x;\boldsymbol{\theta}) = w_{\widetilde{d}}(x;\boldsymbol{\theta}), & x \in \partial\Omega_d(\boldsymbol{\theta}) \cap \partial\Omega_{\widetilde{d}}(\boldsymbol{\theta}), \quad \forall \widetilde{d} \in d', \\ \mathbf{n}_d \cdot (a_d(x)\nabla w_d(x;\boldsymbol{\theta})) = -\mathbf{n}_{\widetilde{d}} \cdot (a_d(x)\nabla w_{\widetilde{d}}(x;\boldsymbol{\theta})), & x \in \partial\Omega_d(\boldsymbol{\theta}) \cap \partial\Omega_{\widetilde{d}}(\boldsymbol{\theta}), \quad \forall \widetilde{d} \in d', \end{cases} \tag{8.2.4}$$

where d' is the set of $\{1, \ldots, D\}\backslash\{d\}$ such that $\Omega_d(\boldsymbol{\theta})$ and $\Omega_{\widetilde{d}}(\boldsymbol{\theta})$ share a boundary. The last two lines in (8.2.4) are interface conditions guaranteeing continuity of the solution and a matching flux across the boundaries.

We take $\Omega_d(\boldsymbol{\theta})$ and Ω_d to be triangular subdomains, so that we can select φ_d to be a linear map. Let $y \in \Omega_d$ denote the image of $x \in \Omega_d(\boldsymbol{\theta})$ under the map φ_d and let $\mathbf{J}_d$ denote the Jacobian of the transformation φ_d. Denote the three vertices of $\Omega_d(\boldsymbol{\theta})$ with $\mathbf{r}_{d,1}$, $\mathbf{r}_{d,2}$, and $\mathbf{r}_{d,3}$. and the three vertices of Ω_d with $\mathbf{s}_{d,1}$, $\mathbf{s}_{d,2}$, and $\mathbf{s}_{d,3}$. We note that

$$\varphi_d(x) = \mathbf{J}_d(x - \mathbf{r}_{d,1}) + \mathbf{s}_{d,1}, \tag{8.2.5}$$

where $\mathbf{J}_d$ is given by

$$\mathbf{J}_d = \begin{pmatrix} \mathbf{s}_{d,2} - \mathbf{s}_{d,1} & -(\mathbf{s}_{d,3} - \mathbf{s}_{d,1}) \end{pmatrix} \begin{pmatrix} \mathbf{r}_{d,2} - \mathbf{r}_{d,1} & -(\mathbf{r}_{d,3} - \mathbf{r}_{d,1}) \end{pmatrix}^{-1} = \mathbf{S}_d \mathbf{R}_d^{-1}.$$

Both $\mathbf{S}_d$ and $\mathbf{R}_d$ are invertible since $\Omega_d(\boldsymbol{\theta})$ and Ω_d are each non-degenerate triangles.

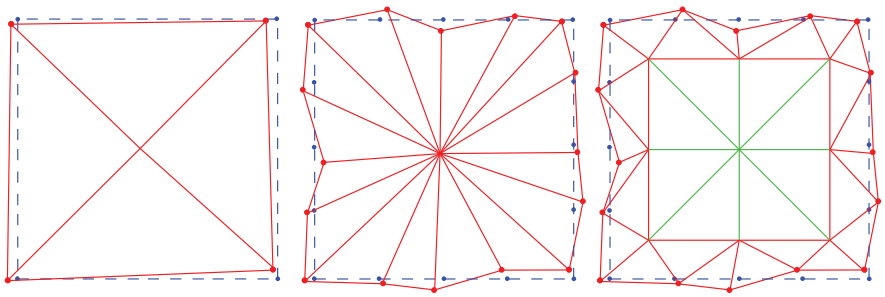

(a) (b) (c)

Fig. 8.2: A realization of the random domain $\Omega(\boldsymbol{\theta})$ (solid) and the reference domain Ω (dashed) for different numbers of perturbed points. Two different partitions for identical domains are considered in panels (b) and (c), respectively.

Then, using (8.2.5) in (8.2.4),

$$\begin{cases} -\nabla\cdot(\mathbf{A}_d(y)\nabla u_d(y;\boldsymbol{\theta})) = F_d(y), & y\in\Omega_d, \\ u_d(y;\boldsymbol{\theta}) = 0, & y\in\partial\Omega\cap\partial\Omega_d, \\ u_d(y;\boldsymbol{\theta}) = u_{\widetilde{d}}(y;\boldsymbol{\theta}), & y\in\partial\Omega_d\cap\partial\Omega_{\widetilde{d}}, \quad \forall\widetilde{d}\in d', \\ \mathbf{n}_d\cdot(\mathbf{A}_d(y)\nabla u_d(y;\boldsymbol{\theta})) = -\mathbf{n}_{\widetilde{d}}\cdot(\mathbf{A}_{\widetilde{d}}(y)\nabla u_{\widetilde{d}}(y;\boldsymbol{\theta})), & y\in\partial\Omega_d\cap\partial\Omega_{\widetilde{d}}, \quad \forall\widetilde{d}\in d', \end{cases} \tag{8.2.6}$$

where $u_d(y;\boldsymbol{\theta}) = w_d(\varphi_d^{-1}(y);\boldsymbol{\theta})$,

$$\mathbf{A}_d(y) = \mathbf{J}_d^{\top} a_d(\varphi_d^{-1}(y))\mathbf{J}_d, \quad \text{and} \quad F_d(y) = f_d(\varphi_d^{-1}(y)).$$

We require the partition to be such that

$$0 < M_* \le \inf_{\boldsymbol{\theta}\in\Theta}\inf_d |\det(\mathbf{J}_d)| \le \sup_{\boldsymbol{\theta}\in\Theta}\sup_d |\det(\mathbf{J}_d)| \le M^* < \infty. \tag{8.2.7}$$

In practice, one might specify M_* and M^* a priori, which thus limits the possible mapping grids and resulting maps. It is appealing to select mapping grids such that M^* is small and M_* is large.

Lemma 8.2.1 (Ciarlet)**.** *Let Ω_d and $\Omega_d(\boldsymbol{\theta})$ be such that $\varphi_d : \Omega_d(\boldsymbol{\theta}) \to \Omega_d$ is a linear map, e.g., $\varphi_d(x) = \mathbf{J}_d x + c$, where $c\in\mathbb{R}^2$. Let $\kappa_d = diam(\Omega_d)$ and $\kappa_d(\boldsymbol{\theta}) = diam(\Omega_d(\boldsymbol{\theta}))$. Further, define $\rho_d = \sup\{diam(S)\,|\,S\subseteq\Omega_d\}$ and $\rho_d(\boldsymbol{\theta}) = \sup\{diam(S)\,|\,S\subseteq\Omega_d(\boldsymbol{\theta})\}$. Then,*

$$\|\mathbf{J}_d\| \le \frac{\kappa_d}{\rho_d(\boldsymbol{\theta})} \quad \textit{and} \quad \|\mathbf{J}_d^{-1}\| \le \frac{\kappa_d(\boldsymbol{\theta})}{\rho_d}.$$

Let $w : \Omega_d(\boldsymbol{\theta}) \to \mathbb{R}$ and define $u = w\circ\varphi_d^{-1}$. Then, if $w\in W^{m,2}(\Omega(\boldsymbol{\theta}))$ for integer $m\ge 0$, then $u\in W^{m,2}(\Omega)$ and

$$|u|_{W^{m,2}(\Omega_d)} \le C\|\mathbf{J}_d^{-1}\|^m\cdot|\det(\mathbf{J}_d)|^{1/2}\cdot|w|_{W^{m,2}(\Omega_d(\boldsymbol{\theta}))}.$$

Theorem 8.2.2. *For each d, the matrix $\mathbf{A}_d$ is symmetric and positive definite. Further,*

$$B_\Omega(u,v) = \sum_{d=1}^{D} \int_{\Omega_d} \mathbf{A}_d(y)\nabla u \cdot \nabla v \, \mathrm{d}y$$

is bounded and coercive and

$$F_\Omega(v) = \sum_{d=1}^{D} \int_{\Omega_d} F_d(y)v(y) \, \mathrm{d}y$$

is boundedc. Consequently, the Lax-Milgram Lemma grants, for a given $\boldsymbol{\theta}$, (8.2.6) *is well-posed. Moreover, the set of problems is uniformly well-posed in the sense that*

$$\inf_{\boldsymbol{\theta}} B_\Omega(u,u) \geq C_1 \|u\|^2_{H^1(\Omega)}$$
$$\sup_{\boldsymbol{\theta}} B_\Omega(u,v) \leq C_2 \|u\|_{H^1(\Omega)} \|v\|_{H^1(\Omega)}$$

and

$$\sup_{\boldsymbol{\theta}} F_\Omega(v) \leq C_3 \|u\|_{H^1(\Omega)} \|v\|_{H^1(\Omega)},$$

where $C_1 > 0$ and $C_2, C_3 < \infty$.

Proof. We see that $\mathbf{A}_d$ is symmetric and positive definite since

$$\mathbf{x}^\top \mathbf{A}_d \mathbf{x} = (\mathbf{J}_d \mathbf{x})^\top a_d(\varphi_d^{-1}(y))(\mathbf{J}_d \mathbf{x}) \geq 0,$$

with equality only when $\mathbf{J}_d \mathbf{x} = \mathbf{0}$, i.e., $\mathbf{x} = \mathbf{0}$. Since $\mathbf{A}_d$ is positive definite,

$$\begin{aligned} B_\Omega(u,u) &= \sum_{d=1}^{D} \int_{\Omega_d} \mathbf{A}_d(y)\nabla u \cdot \nabla u \, \mathrm{d}y \\ &\geq \sum_{d=1}^{D} C_1^d(\boldsymbol{\theta}) \|u\|^2_{H^1(\Omega_d)} \\ &\geq C_1(\boldsymbol{\theta}) \|u\|^2_{H^1(\Omega)}, \end{aligned}$$

which shows coercivity. We demonstrate boundedness, we have

$$\begin{aligned} |B_\Omega(u,v)| &\leq \sum_{d=1}^{D} \left| \int_{\Omega_d} \mathbf{A}_d(y)\nabla u \cdot \nabla v \, \mathrm{d}y \right| \\ &\leq \sum_{d=1}^{D} \|\mathbf{A}_d\| \cdot \|u\|_{H^1(\Omega_d)} \cdot \|v\|_{H^1(\Omega_d)} \\ &\leq \sum_{d=1}^{D} C_2^d(\boldsymbol{\theta}) \|u\|_{H^1(\Omega_d)} \cdot \|v\|_{H^1(\Omega_d)} \\ &\leq C_2(\boldsymbol{\theta}) \|u\|_{H^1(\Omega)} \cdot \|v\|_{H^1(\Omega)}, \end{aligned}$$

where $C_2(\boldsymbol{\theta}) = \left(\frac{\kappa_d}{\rho_d(\boldsymbol{\theta})}\right)^2 \max_{x\in\Omega^*} |a(x)|$. Similarly,

$$\begin{aligned} |F_{\Omega_d}(v)| &\leq \sum_{d=1}^{D} \left| \int_{\Omega_d} f_d(\varphi_d^{-1}(y)) v(y)\, \mathrm{d}y \right| \\ &\leq \sum_{d=1}^{D} C_3^d(\boldsymbol{\theta}) \|v\|_{H^1(\Omega_d)} \\ &\leq C_3(\boldsymbol{\theta}) \|v\|_{H^1(\Omega)}. \end{aligned}$$

The Lax-Milgram Lemma gives well-posedness of the transformed problem for a fixed $\boldsymbol{\theta}$. The assumption (8.2.7) gives the existence of C_1 and C_2, whereas $C_3 = \max_{x\in\Omega^*} |f(x)|$, completing the proof. □

Effect of the transformation

As mentioned previously, the choice of partition and thus the transformations, is somewhat arbitrary. We now discuss the effect of the choice made and its implications in the numerical method. The following example illustrates this fact by considering poorly chosen mapping grids. We show how the function $f(x, y) = 2 + \sin(3\pi x)\sin(3\pi y)$ is transformed from a randomly perturbed domain to the unit square. We consider a mapping grid similar to that in Fig. 8.2, but where the center of the "X" is placed at three different points. We show how this transformation affects the transformed function. As the center of the "X" approaches the corner of the domain, the function f is conpressed non-uniformly. The total variation of f increases dramatically, which will then require finite element refinement or better quadrature.

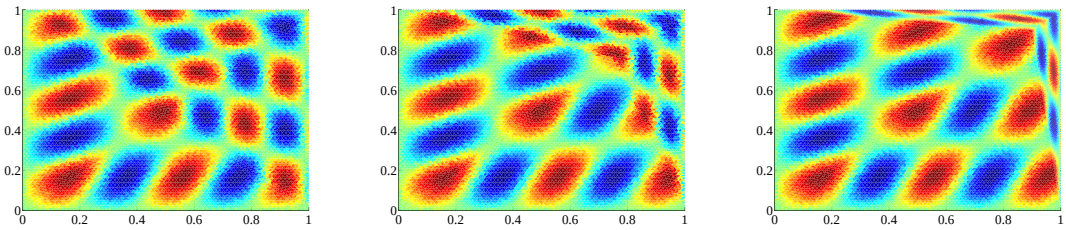

(a) (b) (c)

Fig. 8.3: Center of the "X" at $(0.5, 0.5)$ (a), at $(0.75, 0.75)$ (b), and $(0.9, 0.9)$ (c).

Although it is not immediately clear how to find an optimal mapping grid, certain characteristics are desired. For instance, choosing restrictive bounds M_* and M^* on $\det(J_d)$ guarantees that

a subdomain will not undergo a non-proportionate amount of stretching and shrinking under the transformation, see Fig. 8.3(c). More importantly, we require that the transformation increases the total variation of the coefficients and data as little as possible, see Fig. 8.3(a) as opposed to Fig. 8.3(b,c). With these motivations, we introduce the following constrained optimization problem to find the desired mapping grid: find φ such that

$$\sup_{\boldsymbol{\theta}\in\Theta}\max_{d}\left(\int_{\Omega_d}|\nabla a_d(\varphi_d^{-1}(y))|+|\nabla f_d(\varphi_d^{-1}(y))|\,\mathrm{d}y\right)$$

is minimized subject to the constraints on $\det(J_d)$. In general, this is a difficult optimization problem, but an approximation will suffice. For instance, we can fix $\Omega(\boldsymbol{\theta})=\Omega^*$ and pose the problem: find φ such that

$$\max_{d}\left(\int_{\Omega_d}|\nabla a_d(\varphi_d^{-1}(y))|+|\nabla f_d(\varphi_d^{-1}(y))|\,\mathrm{d}y\right)$$

is minimized subject to constraints on the $\det(J_d)$. Further yet, for a mesh such as that found in Fig. 8.2(a,b), we need only to locate to the center of the mesh. Similarly, for a mesh such as that found in Fig. 8.2(c), we need only to determine the scale factor of the boundary of the domain. Both of these problems are one-dimensional optimization problems that are much more tractable.

8.3 Finite Element Method and Domain Decomposition

Let U denote the finite element approximation of u so that the finite element formulation reads: find $U\in V_{0,h}^{(1)}$ such that

$$\begin{cases}\displaystyle\int_{\Omega_d}\mathbf{A}_d(y)\nabla U_d(y;\boldsymbol{\theta})\cdot\nabla v\,\mathrm{d}y=\int_{\Omega_d}F_d(y)v(y)\,\mathrm{d}y, & \forall v\in V_{0,h}^{(1)}\\ U_d(y;\boldsymbol{\theta})=0, & y\in\partial\Omega\cap\partial\Omega_d,\\ U_d(y;\boldsymbol{\theta})=U_{\widetilde{d}}(y;\boldsymbol{\theta}), & y\in\partial\Omega_d\cap\partial\Omega_{\widetilde{d}},\quad\forall\widetilde{d}\in d',\\ \mathbf{n}_d\cdot(\mathbf{A}_d(y)\nabla U_d(y;\boldsymbol{\theta}))=-\mathbf{n}_{\widetilde{d}}\cdot(\mathbf{A}_{\widetilde{d}}(y)\nabla U_{\widetilde{d}}(y;\boldsymbol{\theta})), & y\in\partial\Omega_d\cap\partial\Omega_{\widetilde{d}},\quad\forall\widetilde{d}\in d'.\end{cases}\tag{8.3.1}$$

To approximate U, we employ I iterations of Lion's domain decomposition algorithm, resulting in U^I. That is, given a set of initial guesses $\{U_d^0,\,d=1,\ldots,D\}$, we solve for $i=1,2,\ldots,I$,

$$\begin{aligned}&(\mathbf{A}_d(y)\nabla U_d^i,\nabla v)_d+\sum_{\widetilde{d}\in d'}\left(\frac{1}{\lambda}\langle U_d^i,v\rangle_{d\cap\widetilde{d}}-\langle\mathbf{n}_{\widetilde{d}}\cdot\mathbf{A}_d(y)\nabla U_d^i,v\rangle_{d\cap\widetilde{d}}\right)\\&\qquad=(F_d(y),\nabla v)_d+\sum_{\widetilde{d}\in d'}\left(\frac{1}{\lambda}\langle U_d^{i-1},v\rangle_{d\cap\widetilde{d}}-\langle\mathbf{n}_{\widetilde{d}}\cdot\mathbf{A}_d(y)\nabla U_d^{i-1},v\rangle_{d\cap\widetilde{d}}\right),\end{aligned}\tag{8.3.2}$$

where

$$(f,g)_d = \int_{\Omega_d} f(x)g(x)\,\mathrm{d}x \quad \text{and} \quad \langle f,g\rangle_{d\cap\widetilde{d}} = f(x)g(x)\,\Big|_{d\cap\widetilde{d}}.$$

The parameter λ can be chosen to improve convergence of the iterative method.

The matrix form of (8.3.2) reads, on each subdomain Ω_d,

$$\mathbf{M}_d U_d^i = \mathbf{b}_d^{i-1},$$

where

$$(\mathbf{M}_d)_{k,\ell} = (\mathbf{A}_d(y)\nabla\xi_d^k, \nabla\xi_d^\ell)_d + \sum_{\widetilde{d}\in d'}\left(\frac{1}{\lambda}\langle\xi_d^k,\xi_d^\ell\rangle_{d\cap\widetilde{d}} - \langle \mathbf{n}_{\widetilde{d}}\cdot\mathbf{A}_d(y)\nabla\xi_d^k,\xi_d^\ell\rangle_{d\cap\widetilde{d}}\right)$$

$$(\mathbf{b}_d^{i-1})_k = (F_d,\xi_d^k)_d + \sum_{\widetilde{d}\in d'}\left(\frac{1}{\lambda}\langle U_d^{i-1},\xi_d^k\rangle_{d\cap\widetilde{d}} - \langle \mathbf{n}_{\widetilde{d}}\cdot\mathbf{A}_d(y)\nabla U_d^{i-1},\xi_d^k\rangle_{d\cap\widetilde{d}}\right).$$

The numerical method is described in Algorithm 8.1.

Algorithm 8.1: Finite element method and domain decomposition for a single realization of $\boldsymbol{\theta}$

for $i = 1,\ldots,I$ *(number of iterations)* **do**
  for $d = 1,\ldots,D$ *(number of subdomains)* **do**
    solve $U_d^i = (\mathbf{M}_d)^{-1}\mathbf{b}_d^{i-1}$
  end
end

8.4 Monte Carlo Methods

Monte Carlo methods are specifically useful in computing integral-based quantities, i.e.,

$$I = \int_\Omega h(\boldsymbol{\theta})\,\mathrm{d}F(\boldsymbol{\theta}) = \int_\Omega h(\boldsymbol{\theta})f(\boldsymbol{\theta})\,\mathrm{d}\boldsymbol{\theta},$$

where the probability density function $f(\boldsymbol{\theta})$ is typically unknown. We select N realizations of $\boldsymbol{\theta}$ independently and consider the estimate

$$I_N = \frac{1}{N}\sum_{n=1}^N h(\boldsymbol{\theta}_n).$$

By the Strong Law of Large Numbers, as $N\to\infty$, $I_N \to I$ almost surely. Moreover, the error in the estimate is related to the variance of the function h and the number of samples N. In fact,

$$\mathrm{Var}\,(I_N) = \frac{1}{N^2}\sum_{n=1}^N \mathrm{Var}(h(\boldsymbol{\theta}_n)) = \frac{\mathrm{Var}(h)}{N} = \frac{\sigma^2(h)}{N}$$

so that the error in the estimate scales with $\sqrt{N}$. To see this more clearly, note

$$\lim_{N\to\infty} \Pr\left(-a\frac{\sigma(h)}{\sqrt{N}} \leq I_N - I \leq b\frac{\sigma(h)}{\sqrt{N}}\right) = \Phi(b) - \Phi(-a).$$

We are particularly interested in computing the distribution and statistics of solutions to partial differential equations with stochastic coefficients. Suppose we are interested in statistics of a QOFI computed from $w(x;\boldsymbol{\theta})$, which solves (7.1.1). Namely, let

$$Q(w;\boldsymbol{\theta}) = \int_\Omega w(x;\boldsymbol{\theta})\psi(x)\,\mathrm{d}x$$

denote such a QOFI. Various moments, e.g., the k-th moment, of $Q(w;\boldsymbol{\theta})$ can be approximated via

$$I_N = \frac{1}{N}\sum_{n=1}^{N}(Q(w;\boldsymbol{\theta}_n))^k.$$

The Strong Law of Large Numbers gives that

$$\frac{1}{N}\sum_{n=1}^{N}(Q(w;\boldsymbol{\theta}_n))^k \overset{a.s.}{\to} \int_\Theta (Q(w;\boldsymbol{\theta}))^k\,\mathrm{d}P(Q(\boldsymbol{\theta})).$$

Moreover, we can estimate the distribution of $Q(w;\boldsymbol{\theta})$ by using the empirical distribution function

$$I_N = \frac{1}{N}\sum_{n=1}^{N}\chi_{(-\infty,y)}(Q(w;\boldsymbol{\theta}_n)).$$

8.5 Summary

In several applications of boundary value problems for PDEs the geometry on which the equations are posed are uncertain. To model this uncertainty, we formulate a class of elliptic problems that are posed on stochastic domains. We demonstrate well-posedness of such problems and introduce a piecewise transformation of the domain to a deterministic reference domain. The resulting problems have stochastic coefficients, which we study via Monte Carlo and standard finite element methods. In the next chapter, we consider the nonparametric density estimation problem for a QOFI.

9. A POSTERIORI ERROR ANALYSIS FOR ELLIPTIC PROBLEMS ON UNCERTAIN DOMAINS

In this chapter, we consider the nonparametric density estimation problem for a QOFI computed from solutions of the elliptic PDEs with stochastic domains that were formulated in the previous chapter. We use a simple Monte Carlo sampling procedure to estimate statistics and the distribution of the QOFI. Several aspects of the problem formulation are exploited, e.g., localizing the effect of the stochastic domain to the boundary subdomains, to improve the efficiency of the Monte Carlo sampling method so that many samples can be obtained to approximate the distribution at a reasonable cost. We present an a posteriori error analysis for each sample and for the empirical distribution function obtained from the samples. The a posteriori error estimate for the computed probability distribution reflects both deterministic and statistical sources of error including the effects of the transformation.

9.1 Introduction

We consider the PDE on $\Omega(\boldsymbol{\theta})$

$$\begin{cases} -\nabla \cdot (a(x)\nabla w(x;\boldsymbol{\theta})) = f(x), & x \in \Omega(\boldsymbol{\theta}), \\ w(x;\boldsymbol{\theta}) = 0, & x \in \partial\Omega(\boldsymbol{\theta}), \end{cases} \tag{9.1.1}$$

where $\boldsymbol{\theta}$ is a random variable with some given probability structure and $\Omega(\boldsymbol{\theta}) \subset \mathbb{R}^2$ is a polygonal domain whose boundary nodes depend on the random variable $\boldsymbol{\theta}$. We use the formulation of the problem presented in the previous chapter, which we briefly summarize at this time.

A piecewise transformation $\varphi : \Omega(\boldsymbol{\theta}) \to \Omega$ on a partition of $\Omega(\boldsymbol{\theta})$ into subdomains $\Omega_d(\boldsymbol{\theta})$, $d = 1, \ldots, D$, such that $\overline{\Omega(\boldsymbol{\theta})} = \bigcup_{d=1}^{D} \overline{\Omega_d(\boldsymbol{\theta})}$, i.e., $\varphi_d : \Omega_d(\boldsymbol{\theta}) \to \Omega_d$ is used to transform the problem (9.1.1) to

$$\begin{cases} -\nabla \cdot (\mathbf{A}_d(y)\nabla u_d(y;\boldsymbol{\theta})) = F_d(y), & y \in \Omega_d, \\ u_d(y;\boldsymbol{\theta}) = 0, & y \in \partial\Omega \cap \partial\Omega_d, \\ u_d(y;\boldsymbol{\theta}) = u_{\widetilde{d}}(y), & y \in \partial\Omega_d \cap \partial\Omega_{\widetilde{d}}, \quad \forall \widetilde{d} \in d', \\ \mathbf{n}_d \cdot (\mathbf{A}_d(y)\nabla u_d(y;\boldsymbol{\theta})) = -\mathbf{n}_{\widetilde{d}} \cdot (\mathbf{A}_{\widetilde{d}}(y)\nabla u_{\widetilde{d}}(y;\boldsymbol{\theta})), & y \in \partial\Omega_d \cap \partial\Omega_{\widetilde{d}}, \quad \forall \widetilde{d} \in d', \end{cases} \tag{9.1.2}$$

where $u_d(y;\boldsymbol{\theta}) = w_d(\varphi_d^{-1}(y);\boldsymbol{\theta})$,

$$\mathbf{A}_d(y) = \mathbf{J}_d^\top a_d(\varphi_d^{-1}(y))\mathbf{J}_d, \quad \text{and} \quad F_d(v) = f_d(\varphi_d^{-1}(y)).$$

In Fig. 9.1, we present three such partitions of both the domain Ω and realizations of the stochastic domain $\Omega(\boldsymbol{\theta})$. We seek to compute the distribution of a QOFI computed as a linear functional of the

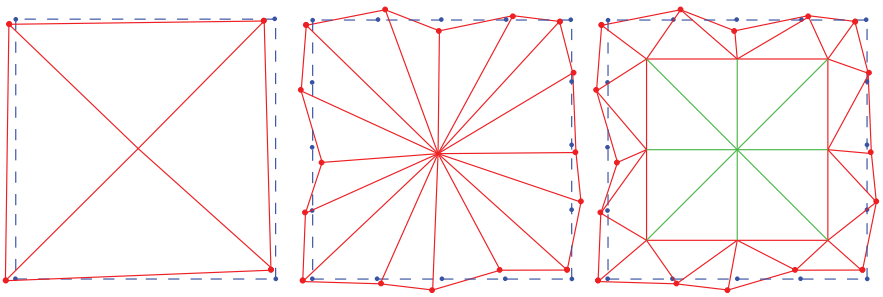

(a) (b) (c)

Fig. 9.1: A realization of the random domain $\Omega(\boldsymbol{\theta})$ (solid) and the reference domain Ω (dashed) for different numbers of perturbed points. Three different partitions are considered.

solution of (9.1.1), i.e.,

$$Q(w;\boldsymbol{\theta}) = (w,\psi)_{\Omega(\boldsymbol{\theta})} = \int_{\Omega(\boldsymbol{\theta})} w(x;\boldsymbol{\theta})\psi(x)\,\mathrm{d}x,$$

where ψ defines the QOFI. Using the transformation, we define the QOFI in terms of the transformed variables via

$$Q(u;\boldsymbol{\theta}) = \sum_{d=1}^{D} \int_{\Omega_d} u_d(y;\boldsymbol{\theta})\psi_d(\varphi_d^{-1}(y))\det\left(\mathbf{J}_d\right)^{-1}\mathrm{d}y.$$

We then employ Monte Carlo sampling methods to sample the output QOFI and then construct estimates of various statistics and of the distribution of the QOFI.

We show how to localize the effects of randomness to the boundary subdomains and utilize a Neumann series to make several of the necessary deterministic computations independent of the number of samples. We further demonstrate that a single finite element mesh can be used for all realizations and, consequently, Monte Carlo sampling methods can be performed with reduced computational expense. We then present an a posteriori error analysis for each sample and for the estimated distribution of the QOFI, which includes errors due to the finite element discretization, the domain decomposition iteration, quadrature, and finite sampling.

9.2 A Posteriori Error Analysis for a Single Realization

We present the finite element method and domain decomposition algorithm for a single realization. Then, we give an a posteriori error analysis for a single realization. The error analysis includes the effects of the finite element discretization, quadrature, and the domain decomposition algorithm.

Finite element method and domain decomposition

Let U denote the finite element approximation of u so that the finite element formulation reads: find $U \in V_{0,h}^{(1)}$ such that

$$\begin{cases} \displaystyle\int_{\Omega_d} \mathbf{A}_d(y)\nabla U_d(y;\boldsymbol{\theta})\cdot\nabla v\,\mathrm{d}y = \int_{\Omega_d} F_d(y)v(y)\,\mathrm{d}y, & \forall v \in V_{0,h}^{(1)} \\ U_d(y;\boldsymbol{\theta}) = 0, & y \in \partial\Omega \cap \partial\Omega_d, \\ U_d(y;\boldsymbol{\theta}) = U_{\widetilde{d}}(y;\boldsymbol{\theta}), & y \in \partial\Omega_d \cap \partial\Omega_{\widetilde{d}}, \quad \forall \widetilde{d} \in d', \\ \mathbf{n}_d \cdot (\mathbf{A}_d(y)\nabla U_d(y;\boldsymbol{\theta})) = -\mathbf{n}_{\widetilde{d}}\cdot(\mathbf{A}_{\widetilde{d}}(y)\nabla U_{\widetilde{d}}(y;\boldsymbol{\theta})), & y \in \partial\Omega_d \cap \partial\Omega_{\widetilde{d}}, \quad \forall \widetilde{d} \in d'. \end{cases} \tag{9.2.1}$$

To approximate U, we employ I iterations of Lion's domain decomposition algorithm, resulting in U^I. That is, given a set of initial guesses $\{U_d^0,\ d = 1,\ldots,D\}$, we solve for $i = 1, 2, \ldots, I$,

$$\begin{aligned} &(\mathbf{A}_d(y)\nabla U_d^i, \nabla v)_d + \sum_{\widetilde{d}\in d'}\left(\frac{1}{\lambda}\langle U_d^i, v\rangle_{d\cap\widetilde{d}} - \langle \mathbf{n}_{\widetilde{d}}\cdot\mathbf{A}_d(y)\nabla U_d^i, v\rangle_{d\cap\widetilde{d}}\right) \\ &\qquad = (F_d(y),\nabla v)_d + \sum_{\widetilde{d}\in d'}\left(\frac{1}{\lambda}\langle U_d^{i-1}, v\rangle_{d\cap\widetilde{d}} - \langle \mathbf{n}_{\widetilde{d}}\cdot\mathbf{A}_d(y)\nabla U_d^{i-1}, v\rangle_{d\cap\widetilde{d}}\right), \end{aligned} \tag{9.2.2}$$

where

$$(f,g)_d = \int_{\Omega_d} f(x)g(x)\,\mathrm{d}x \quad \text{and} \quad \langle f,g\rangle_{d\cap\widetilde{d}} = f(x)g(x)\Big|_{d\cap\widetilde{d}}.$$

The parameter λ can be chosen to improve convergence of the iterative method.

The matrix form of (9.2.2) reads, on each subdomain Ω_d,

$$\mathbf{M}_d U_d^i = \mathbf{b}_d^{i-1},$$

where

$$\begin{aligned} (\mathbf{M}_d)_{k,\ell} &= (\mathbf{A}_d(y)\nabla\xi_d^k, \nabla\xi_d^\ell)_d + \sum_{\widetilde{d}\in d'}\left(\frac{1}{\lambda}\langle\xi_d^k,\xi_d^\ell\rangle_{d\cap\widetilde{d}} - \langle\mathbf{n}_{\widetilde{d}}\cdot\mathbf{A}_d(y)\nabla\xi_d^k,\xi_d^\ell\rangle_{d\cap\widetilde{d}}\right) \\ (\mathbf{b}_d^{i-1})_k &= (F_d,\xi_d^k)_d + \sum_{\widetilde{d}\in d'}\left(\frac{1}{\lambda}\langle U_d^{i-1},\xi_d^k\rangle_{d\cap\widetilde{d}} - \langle\mathbf{n}_{\widetilde{d}}\cdot\mathbf{A}_d(y)\nabla U_d^{i-1},\xi_d^k\rangle_{d\cap\widetilde{d}}\right). \end{aligned}$$

We refer the reader to Algorithm 8.1.

We now introduce the dual problems for the problem (9.1.2). To begin, we let ψ define a QOFI, i.e.,

$$\begin{aligned} Q(w;\boldsymbol{\theta}) &= \int_{\Omega(\boldsymbol{\theta})} w(x;\boldsymbol{\theta})\psi(x)\,\mathrm{d}x \\ &= \sum_{d=1}^{D} \int_{\Omega_d(\boldsymbol{\theta})} w_d(x;\boldsymbol{\theta})\psi_d(x)\,\mathrm{d}x. \end{aligned} \tag{9.2.3}$$

There is a little ambiguity in defining an appropriate QOFI on $\Omega(\boldsymbol{\theta})$. It is most intuitive to consider QOFIs that are either specific to a reference domain or are somehow independent of the domain, e.g., $\psi = \delta(x)$, where $x \in \Omega_*$, is reasonable, but $\psi = \delta(x)$ for $x \notin \Omega_*$ is not. Moreover, several choices of ψ will not only measure the effect of the domain on the QOFI, but will also measure the size of the domain, e.g., $\psi = 1$.

We rewrite (9.2.3) using φ_d and define

$$Q(u;\boldsymbol{\theta}) = \sum_{d=1}^{D} \int_{\Omega_d} u_d(y;\boldsymbol{\theta})\psi_d(\varphi_d^{-1}(y)) \det\left(\mathbf{J}_d\right)^{-1} \mathrm{d}y. \tag{9.2.4}$$

We use the same partition of Ω and pose the dual problem as an abstract domain decomposition over the partition, i.e.,

$$\begin{cases} \displaystyle\int_{\Omega_d} \mathbf{A}_d(y)\nabla\eta_d(y;\boldsymbol{\theta})\cdot\nabla v\,\mathrm{d}y = \int_{\Omega_d} \Psi_d(y)v(y)\,\mathrm{d}y, & \forall v \in V_{0,h}^{(1)} \\ \eta_d(y;\boldsymbol{\theta}) = 0, & y \in \partial\Omega \cap \partial\Omega_d, \\ \eta_d(y;\boldsymbol{\theta}) = \eta_{\widetilde{d}}(y;\boldsymbol{\theta}), & y \in \partial\Omega_d \cap \partial\Omega_{\widetilde{d}}, \quad \forall \widetilde{d} \in d', \\ \mathbf{n}_d \cdot (\mathbf{A}_d(y)\nabla\eta_d(y;\boldsymbol{\theta})) = -\mathbf{n}_{\widetilde{d}} \cdot (\mathbf{A}_{\widetilde{d}}(y)\nabla\eta_{\widetilde{d}}(y;\boldsymbol{\theta})), & y \in \partial\Omega_d \cap \partial\Omega_{\widetilde{d}}, \quad \forall \widetilde{d} \in d', \end{cases} \tag{9.2.5}$$

where

$$\Psi_d(y) = \psi(\varphi_d^{-1}(y)) \det\left(\mathbf{J}_d\right)^{-1}.$$

Standard techniques show

$$Q(u;\boldsymbol{\theta}) = \sum_{d=1}^{D} \int_{\Omega_d} F_d(y)\eta_d(y)\,\mathrm{d}y. \tag{9.2.6}$$

The numerical method gives an approximation of $Q(u;\boldsymbol{\theta})$, namely

$$Q(U^I;\boldsymbol{\theta}) = \sum_{d=1}^{D} (U_d^I, \Psi_d)_d.$$

For a given realization of $\boldsymbol{\theta}$, we are thus interested in the error

$$Q(u;\boldsymbol{\theta}) - Q(U^I;\boldsymbol{\theta}) = \sum_{d=1}^{D} \left[(u_d - U_d, \Psi_d)_d + (U_d - U_d^I, \Psi_d)_d \right].$$

To understand the error due to the finite element method, we compute

$$\begin{aligned} E_1 &= \sum_{d=1}^{D} (u_d - U_d, \Psi_d)_d \\ &= \sum_{d=1}^{D} \int_{\Omega_d} (u_d - U_d)\Psi_d(y)\,\mathrm{d}y \\ &= \sum_{d=1}^{D} \left[\int_{\Omega_d} F_d(y)\eta_d\,\mathrm{d}y - \int_{\Omega_d} \mathbf{A}_d(y)\nabla\eta_d \cdot \nabla U_d\,\mathrm{d}y \right], \end{aligned}$$

which, by Galerkin orthogonality, is equal to

$$E_1 = \sum_{d=1}^{D} \left[\int_{\Omega_d} F_d(y)(\eta_d - \pi_h\eta_d)\,\mathrm{d}y - \int_{\Omega_d} \mathbf{A}_d(y)\nabla U_d \cdot \nabla(\eta_d - \pi_h\eta_d)\,\mathrm{d}y \right].$$

Then, letting Ω_d^j, $j = 1, \ldots, N_d$, be the j-th element in the subdomain Ω_d, we have

$$E_1 = \sum_{d=1}^{D} \sum_{j=1}^{N_d} \left[\int_{\Omega_d^j} F_d(y)(\eta_d - \pi_h\eta_d)\,\mathrm{d}y - \int_{\Omega_d^j} \mathbf{A}_d(y)\nabla U_d \cdot \nabla(\eta_d - \pi_h\eta_d)\,\mathrm{d}y \right]. \tag{9.2.7}$$

In practice, we approximate (9.2.7) by replacing U with U^I, i.e.,

$$E_1 \approx \sum_{d=1}^{D} \sum_{j=1}^{N_d} \left[\int_{\Omega_d^j} F_d(y)(\eta_d - \pi_h\eta_d)\,\mathrm{d}y - \int_{\Omega_d^j} \mathbf{A}_d(y)\nabla U_d^I \cdot \nabla(\eta_d - \pi_h\eta_d)\,\mathrm{d}y \right]. \tag{9.2.8}$$

To understand the error due to Lion's domain decomposition, we compute

$$E_2 = \sum_{d=1}^{D} (U_d - U_d^I, \Psi_d)_d. \tag{9.2.9}$$

Again, we must approximate (9.2.9) and a reasonable choice is

$$E_2 \approx \sum_{d=1}^{D} \sum_{j=1}^{N_d} \left[\int_{\Omega_d^j} \left(U_d^{I+\Delta I} - U_d^I \right) \Psi_d(y)\,\mathrm{d}y \right], \tag{9.2.10}$$

where $\Delta I \in \mathbb{N}$ is chosen to be sufficiently large.

When quadrature is used, we obtain the solution $\widetilde{U}$ to

$$\begin{cases} \displaystyle\int_{\Omega_d} \overline{\mathbf{A}_d(y)}\nabla\widetilde{U}_d(y;\boldsymbol{\theta})\cdot\nabla v\,\mathrm{d}y = \int_{\Omega_d}\overline{F_d(y)}v(y)\,\mathrm{d}y, & \forall v\in V_{0,h}^{(1)} \\ \widetilde{U}_d(y;\boldsymbol{\theta}) = 0, & y\in\partial\Omega\cap\partial\Omega_d, \\ \widetilde{U}_d(y;\boldsymbol{\theta}) = \widetilde{U}_{\widetilde{d}}(y;\boldsymbol{\theta}), & y\in\partial\Omega_d\cap\partial\Omega_{\widetilde{d}},\quad \forall\widetilde{d}\in d', \\ \mathbf{n}_d\cdot(\mathbf{A}_d(y)\nabla\widetilde{U}_d(y;\boldsymbol{\theta})) = -\mathbf{n}_{\widetilde{d}}\cdot(\mathbf{A}_{\widetilde{d}}(y)\nabla\widetilde{U}_{\widetilde{d}}(y;\boldsymbol{\theta})), & y\in\partial\Omega_d\cap\partial\Omega_{\widetilde{d}},\quad \forall\widetilde{d}\in d', \end{cases} \tag{9.2.11}$$

where the notation $\overline{g}$ represents the appropriate projection of g so that

$$\int_T \overline{g(y)}\,\mathrm{d}y$$

gives the desired quadrature of g on the triangular element T.

We note

$$\begin{aligned} Q(u;\boldsymbol{\theta}) - Q(\widetilde{U}^I;\boldsymbol{\theta}) &= (Q(u;\boldsymbol{\theta}) - Q(U;\boldsymbol{\theta})) \\ &\quad + (Q(U;\boldsymbol{\theta}) - Q(U^I;\boldsymbol{\theta})) \\ &\quad + (Q(U^I;\boldsymbol{\theta}) - Q(\widetilde{U}^I;\boldsymbol{\theta}) \end{aligned}$$

and, mimicking earlier work,

$$\begin{aligned} &Q(u;\boldsymbol{\theta}) - Q(\widetilde{U}^I;\boldsymbol{\theta}) \\ &\quad = \sum_{d=1}^{D}\left[\int_{\Omega_d} F_d(y)(\eta_d - \pi_h\eta_d)\,\mathrm{d}y - \int_{\Omega_d}\mathbf{A}_d(y)\nabla\widetilde{U}_d\cdot\nabla(\eta_d-\pi_h\eta_d)\,\mathrm{d}y\right] \\ &\qquad + \sum_{d=1}^{D}\int_{\Omega_d}\mathbf{A}_d(y)\nabla\left(\widetilde{U}_d - \widetilde{U}_d^I\right)\cdot\nabla\eta_d\,\mathrm{d}y \\ &\qquad\quad + \sum_{d=1}^{D}\left[\int_{\Omega_d}\left(F_d(y) - \overline{F_d(y)}\right)\pi_h\eta_d\,\mathrm{d}y - \int_{\Omega_d}\left(\mathbf{A}_d(y) - \overline{\mathbf{A}_d(y)}\right)\nabla\widetilde{U}_d\cdot\nabla\pi_h\eta_d\,\mathrm{d}y\right]. \end{aligned}$$

Then, letting Ω_d^j, $j=1,\ldots,N_d$ be the j-th element in the subdomain Ω_d, we have

$$\begin{aligned} &Q(u;\boldsymbol{\theta}) - Q(\widetilde{U}^I;\boldsymbol{\theta}) \\ &\quad = \sum_{d=1}^{D}\sum_{j=1}^{N_d}\left[\int_{\Omega_d^j} F_d(y)(\eta_d - \pi_h\eta_d)\,\mathrm{d}y - \int_{\Omega_d^j}\mathbf{A}_d(y)\nabla\widetilde{U}_d\cdot\nabla(\eta_d-\pi_h\eta_d)\,\mathrm{d}y\right] \\ &\qquad + \sum_{d=1}^{D}\sum_{j=1}^{N_d}\int_{\Omega_d^j}\mathbf{A}_d(y)\nabla\left(\widetilde{U}_d - \widetilde{U}_d^I\right)\cdot\nabla\eta_d\,\mathrm{d}y \\ &\qquad\quad + \sum_{d=1}^{D}\sum_{j=1}^{N_d}\left[\int_{\Omega_d^j}\left(F_d(y) - \overline{F_d(y)}\right)\pi_h\eta_d\,\mathrm{d}y - \int_{\Omega_d^j}\left(\mathbf{A}_d(y) - \overline{\mathbf{A}_d(y)}\right)\nabla\widetilde{U}_d\cdot\nabla\pi_h\eta_d\,\mathrm{d}y\right]. \end{aligned}$$

The first two terms in (9.2.12) are the finite element and domain decomposition errors we have already treated. The third term in (9.2.12),

$$E_3 = \sum_{d=1}^{D} \sum_{j=1}^{N_d} \left[\int_{\Omega_d^j} \left(F_d(y) - \overline{F_d(y)} \right) \pi_h \eta_d \, \mathrm{d}y - \int_{\Omega_d^j} \left(\mathbf{A}_d(y) - \overline{\mathbf{A}_d(y)} \right) \nabla \widetilde{U}_d \cdot \nabla \pi_h \eta_d \, \mathrm{d}y \right], \tag{9.2.12}$$

is the error due to quadrature. In practice, we approximate (9.2.12) via

$$E_3 \approx \sum_{d=1}^{D} \sum_{j=1}^{N_d} \left[\int_{\Omega_d^j} \left(F_d(y) - \overline{F_d(y)} \right) \pi_h \eta_d \, \mathrm{d}y - \int_{\Omega_d^j} \left(\mathbf{A}_d(y) - \overline{\mathbf{A}_d(y)} \right) \nabla U_d^I \cdot \nabla \pi_h \eta_d \, \mathrm{d}y \right], \tag{9.2.13}$$

If the error E_3 is large, it suggests we need to improve the quadrature, which might be better to improve the quadrature instead of refining the finite element mesh (which can also be used to reduce quadrature error). For clarity, we ignore the effect of quadrature for the duration of the chapter.

9.3 An Efficient Monte Carlo Algorithm for Many Realizations

In order to obtain estimates of statistics and the distribution of the QOFI, we must obtain N independent realizations of $Q(u;\boldsymbol{\theta})$. We describe ways to exploit the finite element and domain decomposition formulations in order to make the Monte Carlo efficient. The results are binned according to the empirical distribution function and we perform an a posteriori error analysis on the resulting estimate of the distribution.

A global finite element mesh and initialization

Monte Carlo methods are computationally tractable for this problem largely because of the ability to use a single finite element mesh for all realizations $\boldsymbol{\theta}^n$, i.e., the need to mesh and perform mesh refinement for each realization has been eliminated. This also allows for an intuitive and straightforward approach for comparing numerical methods and the associated errors for each realization $\boldsymbol{\theta}^n$. For an illustration, we refer to Fig. 9.2. Take $a = \mathbf{Id}$, $f(x,y) = 2000x(1-x) + 2000y(1-y)$, and $\psi(x,y) = \frac{100}{\pi} \exp\left(-50(x-0.8)^2 - 50(y-0.75)^2\right)$. We then refine the mesh if the element error contribution is larger than 0.005. Notice that the element-wise error contributions vary between $\Omega(\boldsymbol{\theta})$ and Ω in some complicated way that does not depends solely on h or the number of elements.

The problem at hand is to determine whether such a global finite element mesh exists and then to find it. The global bounds on the boundedness and coercivity in Theorem 8.2.2 suggest the

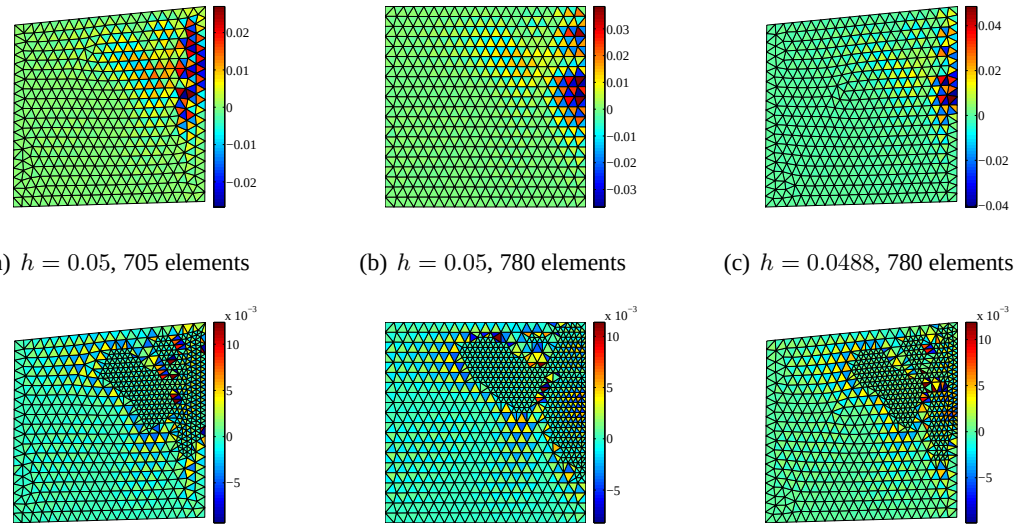

(a) $h = 0.05$, 705 elements (b) $h = 0.05$, 780 elements (c) $h = 0.0488$, 780 elements

(d) refinement of (a) (e) refinement of (b) (f) refinement of (c)

Fig. 9.2: Comparison of numerical errors between $\boldsymbol{\theta} = \mathbf{0}$ (center) and a small perturbation $\boldsymbol{\theta}$ (left, right). Center: we fix $h = 0.05$ so that there are 780 elements. Left: $h = 0.05$, but there are 705 elements. Right: $h = 0.0488$, which gives 780 elements.

existence of such a mesh, but we also must be able to construct it. We take a very simple approach to constructing such a mesh, described in Algorithm 9.1. This can be done in the initialization of the code and is thus independent of the number of samples. During the Monte Carlo sampling, if a realization is encountered that does not satisfy the error tolerance, we refine adaptively and continue using the new mesh.

Algorithm 9.1: Finding the global finite element mesh

start with initial (uniform) mesh
adaptively refine mesh to solve a set of test problems sufficiently accurately
use the resulting mesh

Algorithm 9.1 is demonstrated in the following example. For this illustration, we take $a = \mathbf{Id}$, $f(x, y) = 200x(1-x) + 200y(1-y)$, and $\psi(x, y) = \frac{100}{\pi} \exp\left(-50(x - 0.75)^2 - 50(y - 0.75)^2\right)$. In Fig. 9.3, we show the required meshes to solve the problem on Ω_*, $\Omega(\mathbf{0})$, Ω^*, and all three simultaneously.

We also use the numerical solution for $\Omega(\boldsymbol{\theta}) = \Omega(\mathbf{0})$ to initialize the Lion's domain decomposition algorithm. Further, for all $\boldsymbol{\theta}$, especially $\boldsymbol{\theta}$ small, this initialization will reduce the number of iterations in the domain decomposition algorithm and, thus, lead to gains in efficiency and reduction of numerical errors.

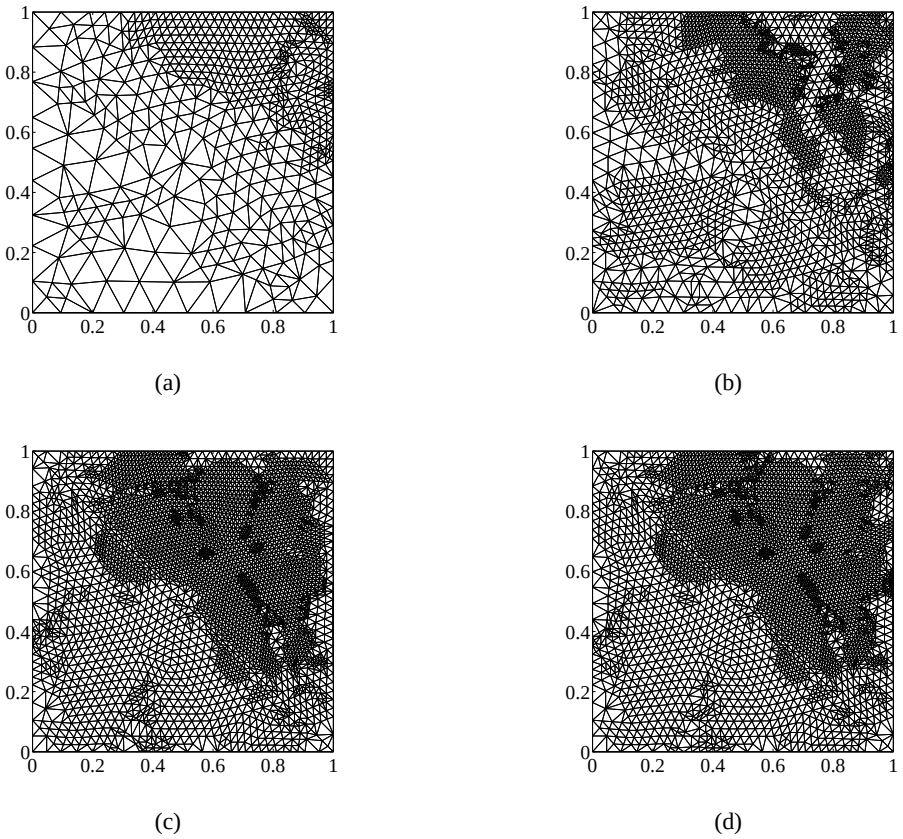

Fig. 9.3: Mesh required to solve the problem on Ω_* (a), $\Omega(\mathbf{0})$ (b), Ω^* (c), and all three (d).

Monte Carlo simulation

We now describe the Monte Carlo sampling and numerical solution of the PDEs in detail, which is presented in Algorithm 9.2. We use a superscript n in the established notation to denote the n-th realization of $\boldsymbol{\theta}$. The matrix form of (9.2.2) reads, on each subdomain Ω_d,

$$\mathbf{M}_d^n U_d^{i,n} = \mathbf{b}_d^{i-1,n},$$

where

$$(\mathbf{M}_d^n)_{k,\ell} = (\mathbf{A}_d^n(y)\nabla\xi_d^k, \nabla\xi_d^\ell)_d + \sum_{\widetilde{d}\in d'} \left(\frac{1}{\lambda}\langle \xi_d^k, \xi_d^\ell \rangle_{d\cap\widetilde{d}} - \langle \mathbf{n}_{\widetilde{d}} \cdot \mathbf{A}_d^n(y)\nabla\xi_d^k, \xi_d^\ell \rangle_{d\cap\widetilde{d}} \right)$$

$$(\mathbf{b}_d^{i-1,n})_k = (F_d^n, \xi_d^k)_d + \sum_{\widetilde{d}\in d'} \left(\frac{1}{\lambda}\langle U_d^{i-1,n}, \xi_d^k \rangle_{d\cap\widetilde{d}} - \langle \mathbf{n}_{\widetilde{d}} \cdot \mathbf{A}_d^n(y)\nabla U_d^{i-1,n}, \xi_d^k \rangle_{d\cap\widetilde{d}} \right).$$

Algorithm 9.2: Finite element method and domain decomposition for a Monte Carlo simulation

for $n = 1, \ldots, N$ *(number of samples)* **do**
  for $i = 1, \ldots, I$ *(number of iterations)* **do**
    for $d = 1, \ldots, D$ *(number of subdomains)* **do**
      solve $U_d^{i,n} = (\mathbf{M}_d^n)^{-1}\mathbf{b}_d^{i-1,n}$
    end
  end
end

Localizing the effect of uncertainty to the boundary subdomains

Motivation for localizing the effect of the perturbations to the boundary subdomains is found in comparing Fig. 9.1(b,c). The shape and size of the subdomains in Fig. 9.1(c) are more appealing, which has implications in the efficiency of the domain decomposition method. Since the effect of the perturbations is localized to the boundary elements, we are also able to choose φ in such a way that $\varphi_d = \mathbf{Id}_d$ on *many* $d \in \{1, \ldots, D\}$. Such a choice implies $\mathbf{A}_d^n = a_d$, for all n. This allows us to precompute several of the matrix inverses and, in turn, make them independent of n. Further, $F_d^n = f_d$ so that we can precompute

$$(F_d^n, \xi_d^k)_d = (f_d, \xi_d^k)_d$$

as well. This is illustrated in Fig. 9.1 and described in Algorithm 9.3.

Algorithm 9.3: Monte Carlo simulation with localized randomness to the boundary subdomains

```
for d = 1, ..., D do
    if φ_d = Id_d then
        precompute (M_d)^{-1} and (F_d, ξ_d^k)_d
    end
end
for n = 1, ..., N (number of samples) do
    for i = 1, ..., I (number of iterations) do
        for d = 1, ..., D (number of subdomains) do
            solve U_d^{i,n} = (M_d)^{-1} b_d^{i-1,n}
        end
    end
end
```

Neumann series

We now write

$$\mathbf{A}_d(y) = a_d(y) + \mathbb{A}_d(y),$$

where

$$\begin{aligned}\mathbb{A}_d(y) &= \mathbf{J}_d^\top a_d(\varphi_d^{-1}(y))\mathbf{J}_d - a_d(y) \\ &= \underbrace{a_d(\varphi_d^{-1}(y)) - a_d(y)}_{\mathbb{A}_d^{(1)}(y)} + \underbrace{\mathbf{J}_d^\top a_d(\varphi_d^{-1}(y))\mathbf{J}_d - a_d(\varphi_d^{-1}(y))}_{\mathbb{A}_d^{(2)}(y)}.\end{aligned}$$

In the case that $\mathbb{A}_d(y)$ is a polynomial, the work of [33, 34] readily applies. It is useful to interpret $\mathbb{A}_d(y)$ as the perturbation in the diffusion coefficient from $\boldsymbol{\theta}$. Further, $\mathbb{A}_d^{(1)}(y)$ can be interpreted as describing how $a_d(y)$ contributes to the perturbation, whereas $\mathbb{A}_d^{(2)}(y)$ describes how $\varphi_d(y)$ contributes the perturbation. In theory, if $\varphi_d \approx \mathbf{Id}_d$ and the entries of a vary sufficiently much in space, then $\mathbb{A}_d^{(1)}(y)$ will dominate $\mathbb{A}_d^{(2)}(y)$.

Remark 9.3.1. *There are a two important cases to consider:*

1. *if $\varphi_d = \mathbf{Id}_d$, then $\mathbb{A}_d = \mathbf{0}$ and $\mathbf{A}_d(y) = a_d(y)$*
2. *if $a(y)$ is a piecewise constant matrix, i.e., $a_d(y) = a_d$, then $\mathbb{A}_d^{(1)}(y) = \mathbf{0}$ and $\mathbb{A}_d^{(2)}(y) = \mathbf{J}_d^\top a_d \mathbf{J}_d - a_d$*

We again consider the matrix form of (9.2.2). That is, on each subdomain Ω_d,

$$(\mathbf{K}_d^a + \mathbf{K}_d^n)U_d^{i,n} = \mathbf{b}_d^{i-1,n},$$

where

$$\begin{aligned}
(\mathbf{K}_d^a)_{k,\ell} &= (a_d(y)\nabla\xi_d^k, \nabla\xi_d^\ell)_d + \sum_{\widetilde{d}\in d'}\left(\frac{1}{\lambda}\langle\xi_d^k, \xi_d^\ell\rangle_{d\cap\widetilde{d}} - \langle \mathbf{n}_{\widetilde{d}}\cdot a_d(y)\nabla\xi_d^k, \xi_d^\ell\rangle_{d\cap\widetilde{d}}\right)\\
(\mathbf{K}_d^n)_{k,\ell} &= (\mathbb{A}_d^n(y)\nabla\xi_d^k, \nabla\xi_d^\ell)_d - \sum_{\widetilde{d}\in d'}\langle \mathbf{n}_{\widetilde{d}}\cdot \mathbb{A}_d^n(y)\nabla\xi_d^k, \xi_d^\ell\rangle_{d\cap\widetilde{d}}\\
(\mathbf{b}_d^{i-1,n})_k &= (F_d^n, \xi_d^k)_d + \sum_{\widetilde{d}\in d'}\left(\frac{1}{\lambda}\langle U_d^{i-1,n}, \xi_d^k\rangle_{d\cap\widetilde{d}} - \langle \mathbf{n}_{\widetilde{d}}\cdot \mathbf{A}_d^n(y)\nabla U_d^{i-1,n}, \xi_d^k\rangle_{d\cap\widetilde{d}}\right).
\end{aligned}$$

The ability to separate the elliptic coefficient into a deterministic piece and a perturbation can be exploited by the Neumann series. We first assume

$$\|(\mathbf{K}_d^a)^{-1}\mathbf{K}_d^n\| < 1,$$

so that

$$\begin{aligned}
(\mathbf{K}_d^a + \mathbf{K}_d^n)^{-1} &= (\mathbf{Id}_d + (\mathbf{K}_d^a)^{-1}\mathbf{K}_d^n)^{-1}(\mathbf{K}_d^a)^{-1}\\
&= \left[\sum_{p=0}^{\infty}\left(-(\mathbf{K}_d^a)^{-1}\mathbf{K}_d^n\right)^p\right](\mathbf{K}_d^a)^{-1}.
\end{aligned}$$

We define $U_{d,P}^{i,n}$ to be

$$U_{d,P}^{i,n} = \left[\sum_{p=0}^{P}\left(-(\mathbf{K}_d^a)^{-1}\mathbf{K}_d^n\right)^p\right](\mathbf{K}_d^a)^{-1}\mathbf{b}_{d,P}^{I-1,n}.$$

Note in Algorithm 9.4 that the number of inverses is independent of N.

Algorithm 9.4: Monte Carlo simulation with Neumann series

for $d = 1, \ldots, D$ **do**
  precompute $\mathbf{K}_d^a$
  if $\varphi_d = \mathbf{Id}_d$ **then**
    precompute $(\mathbf{K}_d^a)^{-1}$ and $(F_d, \xi_d^k)_d$
  end
end
for $n = 1, \ldots, N$ *(number of samples)* **do**
  for $i = 1, \ldots, I$ *(number of iterations)* **do**
    for $d = 1, \ldots, D$ *(number of subdomains)* **do**
      if $\varphi_d = \mathbf{Id}_d$ **then**
        solve $U_{d,P}^{i,n} = (\mathbf{K}_d^a)^{-1}\mathbf{b}_d^{i-1,n}$
      else
        solve $U_{d,P}^{i,n} = \left[\sum_{p=0}^{P}\left(-(\mathbf{K}_d^a)^{-1}\mathbf{K}_d^n\right)^p\right](\mathbf{K}_d^a)^{-1}\mathbf{b}_d^{i-1,n}$
      end
    end
  end
end

We are now concerned with the error associated with the Neumann expansion,

$$E_4 = \sum_{d=1}^{D}(U_d^{I,n} - U_{d,P}^{I,n}, \Psi_d)_d, \tag{9.3.1}$$

which may be approximated

$$E_4 \approx \sum_{d=1}^{D}\sum_{j=1}^{N_d}\left[\int_{\Omega_d^j}\left(U_{d,P+\Delta P}^{I,n} - U_{d,P}^{I,n}\right)\Psi_d(y)\,\mathrm{d}y\right], \tag{9.3.2}$$

for sufficiently large ΔP.

9.4 Estimating the Distribution of a Quantity of Interest

We now treat the approximation of the probability distribution function and the associated error. The probability distribution function of $Q(u;\boldsymbol{\theta})$ is given by

$$P(t) = \Pr(Q(u;\boldsymbol{\theta}) \le t).$$

We only have the approximations $U^{I,n}$ (or $U_P^{I,n}$) so that, given N realizations of $\boldsymbol{\theta}$, $\{\boldsymbol{\theta}^n\}_{n=1}^N$, we use the *estimated* empirical distribution function

$$\widehat{P}_N(t) = \frac{1}{N}\sum_{n=1}^{N}\chi_{(-\infty,t)}(Q(U^{I,n};\boldsymbol{\theta})),$$

which approximates the true empirical distribution function

$$P_N(t) = \frac{1}{N}\sum_{n=1}^{N} \chi_{(-\infty,t)}(Q(u^n;\boldsymbol{\theta})).$$

We are then interested in the error

$$|P(t) - \widehat{P}_N(t)| \le \underbrace{|P(t) - P_N(t)|}_{\text{sampling}} + \underbrace{|P_N(t) - \widehat{P}_N(t)|}_{\text{numerical}}, \tag{9.4.1}$$

where the first term on the right of (9.4.1) is the sampling error.

The empirical distribution P_N is an unbiased estimator of P since

$$\mathbb{E}(P_N(t)) = \frac{1}{N}\sum_{n=1}^{N} \mathbb{E}(\chi_{(-\infty,t]}(Q(u^n;\boldsymbol{\theta}))) = \frac{1}{N}\sum_{n=1}^{N} \Pr(Q(u;\boldsymbol{\theta}) \le t) = P(t).$$

Further,

$$\mathrm{Var}(P_N(t)) = \frac{P(t)(1-P(t))}{N}.$$

The Strong Law of Large Numbers gives

$$P_N(t) \overset{a.s.}{\to} P(t), \quad \forall t,$$

i.e., the estimator $P_N(t)$ is consistent. Further, the Central Limit Theorem gives

$$\sqrt{N}(P_N(t) - P(t)) \overset{d}{\to} N(0, P(t)(1-P(t))).$$

Thus, taking N sufficiently large will make the first term on the right of (9.4.1) arbitrarily small with arbitrarily high probability.

The second term on the right of (9.4.1) is

$$\begin{aligned} |P_N(t) - \widehat{P}_N(t)| &= \left| \frac{1}{N}\sum_{n=1}^{N} \left(\chi_{(-\infty,t)}(Q(u^n)) - \chi_{(-\infty,t)}(Q(U_P^{I,n})) \right) \right| \\ &= \left| \frac{1}{N}\sum_{n=1}^{N} \left(\chi_{(-\infty,t)}(Q(u^n)) - \chi_{(-\infty,t+e^n)}(Q(u^n)) \right) \right|, \end{aligned}$$

where we have defined $e^n = Q(u^n) - Q(U_P^{I,n})$, and then,

$$\begin{aligned} |P_N(t) - \widehat{P}_N(t)| &\le \left| \frac{1}{N}\sum_{n=1}^{N} \left(\chi_{(t-|e^n|,t+|e^n|)}(Q(u^n)) \right) \right| \\ &\le \left| \frac{1}{N}\sum_{n=1}^{N} \left(\chi_{(t-e,t+e)}(Q(u^n)) \right) \right| \\ &= |P_N(t+e) - P_N(t-e)|, \end{aligned}$$

where $e = \max_n |e^n|$. Consequently, by making e sufficiently small, we can make the second term on the right of (9.4.1) arbitrarily small. We note that the quantity e, and each e^n, involves contributions due to the finite element discretization, the domain decomposition algorithm, Neumann expansion, and quadrature.

9.5 Numerical Experiments

We now consider a numerical example that demonstrates both adaptive mesh refinement via an a posteriori error analysis and the approximation of statistics from Monte Carlo simulations. We consider the domain $\Omega = (0,1) \times (0,1)$ and perturbations $\boldsymbol{\theta}_i = \text{Unif}(-0.02, 0.02) \times \text{Unif}(-0.02, 0.02)$ at each corner of the square. We assume that $a = 1$ and $f(x,y) = 2000x(1-x) + 2000y(1-y)$. The QOFI is defined by $\psi(x,y) = \frac{100}{\pi} \exp\left(-50(x-0.9)^2 - 50(y-0.75)^2\right)$, which approximates a weighted average in a neighborhood of the point $(0.9, 0.75)$. In Fig. 9.4, the transformed problem is solved for one realization of $\boldsymbol{\theta}$ via the domain decomposition and finite element formulations described previously. The QOFI is approximated to be 32.140. We refine the mesh at elements such

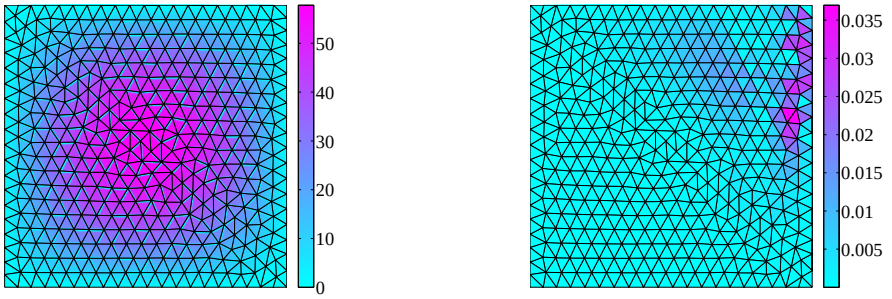

(a) (b)

Fig. 9.4: Solution (left) and element-wise finite element error (right) on a uniform mesh.

that the error contributions is larger than 0.004. The solution is then found on the refined mesh and is shown in Fig. 9.5. The QOFI is approximated to be 32.265 on the refined mesh. Notice that the element-wise error contributions have been reduced by roughly a factor of three.

To approximate the distribution of the QOFI and various subsequent statistics, we employ the Monte Carlo simulation algorithm for 10,000 realizations. In Fig. 9.6, we plot the approximate empirical distribution function and the density histogram. That latter is compared to a normal distribution with mean 31.362 and variance 3.491, which were both computed from the simulations.

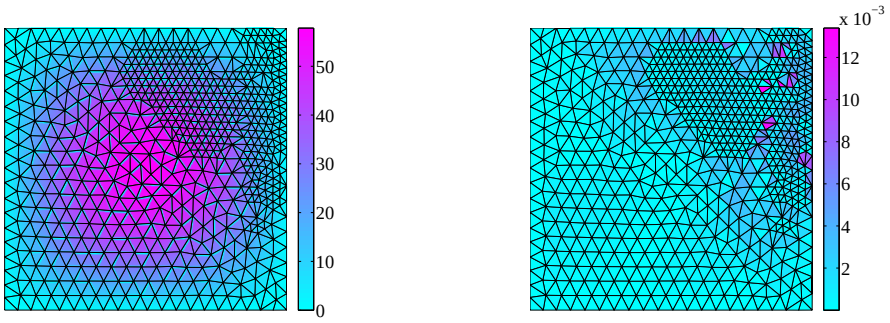

(a) (b)

Fig. 9.5: Solution (left) and element-wise finite element error (right) on a refinement of the mesh.

The purpose of such a comparison is not to argue that the distribution of the QOFI is normal, which is clearly not the case because the density is known to have compact support. Fig. 9.6 demonstrates that the density of the QOFI is right-skewed, e.g., the median was approximated to be 31.339.

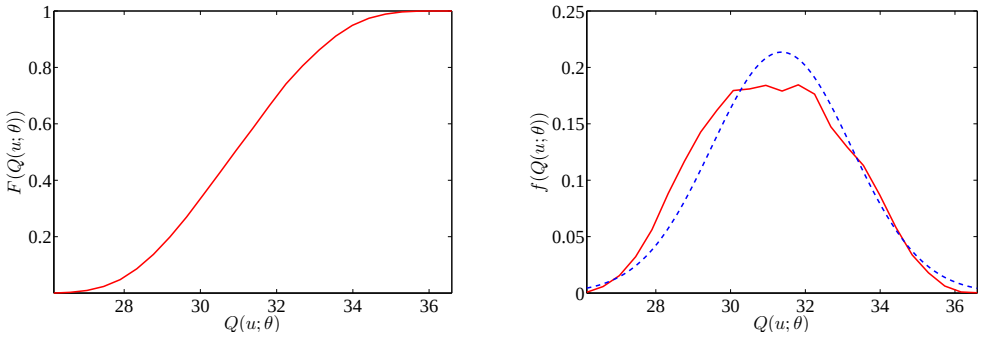

(a) (b)

Fig. 9.6: Approximate empirical distribution function and density of the QOFI defined by $\psi(x,y) = \frac{100}{\pi}\exp\left(-50(x-0.9)^2 - 50(y-0.75)^2\right)$. The results of 10,000 realizations in a Monte Carlo algorithm were used.

We now investigate the dependence of the QOFI on the uncertainty at different corners of the domain. Since the QOFI is localized near the corner $(1,1)$, hereafter referred to as corner 3, we expect the sensitivity of Q to be large relative to the other corners, e.g., corner 1, i.e., $(0,0)$. In Fig. 9.7, we plot Q against the x and y components of the perturbations at corners 1 and 3. There is no statistically significant relationship between the two for corner 1, whereas a strong relationship exists for corner 3. As θ_1 increases, the QOFI increases, which is expected because the QOFI is located farther from the homogeneous Dirichlet condition for increasing $\boldsymbol{\theta}_1$.

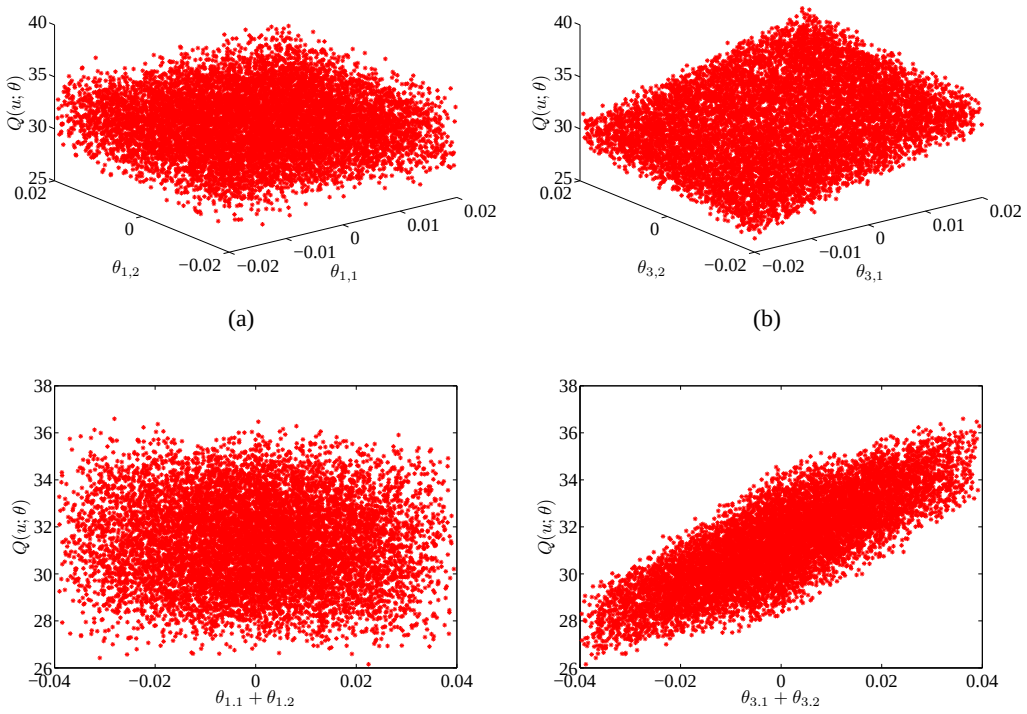

Fig. 9.7: The QOFI defined by $\psi(x,y) = \frac{100}{\pi}\exp\left(-50(x-0.9)^2 - 50(y-0.75)^2\right)$ plotted against the perturbations at corners 1 and 3.

We now consider a different QOFI defined by $\psi(x, y) = 1$ and, again, employ the Monte Carlo simulation algorithm for 10,000 realizations. In Fig. 9.8, we plot the approximate empirical distribution function and the density histogram. That latter is compared to a normal distribution with mean 27.351 and variance 0.599, which were both computed from the simulations. As with the other QOFI, the density of the QOFI has compact support and is right-skewed.

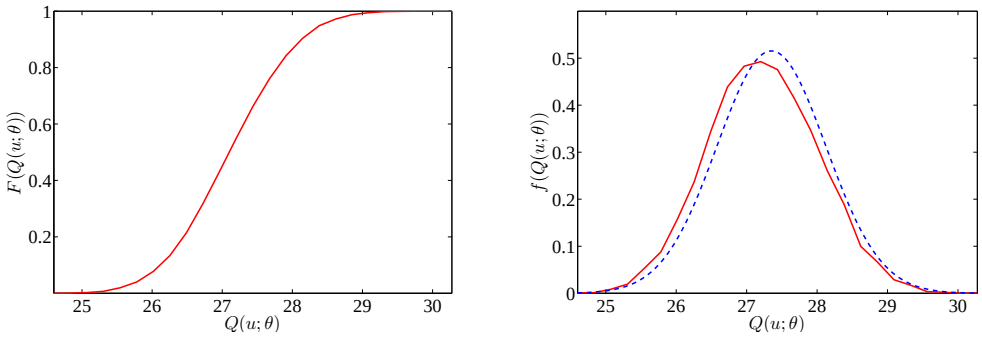

(a) (b)

Fig. 9.8: Approximate empirical distribution function and density of the QOFI defined by $\psi(x, y) = 1$. The results of 10,000 realizations in a Monte Carlo algorithm were used.

We now investigate the dependence of the QOFI on the uncertainty at different corners. Since the QOFI is the average of the solution over the entire domain, we expect the sensitivity of Q to be similar across the four corners, which is verified in Fig. 9.9. If the perturbations are such that the resulting domain is larger in size, the QOFI tends to increase as well.

9.6 Summary

We consider the nonparametric density estimation problem for a QOFI computed from solutions of the elliptic PDEs with stochastic domains that were formulated in the previous chapter. We consider several measures to improve the efficiency of the Monte Carlo sampling method so that many samples can be obtained to approximate the distribution at a reasonable cost. An a posteriori error analysis is presented for each sample and for the empirical distribution function obtained from the samples. The a posteriori error estimate for the computed probability distribution reflects both deterministic and statistical sources of error including the effects of the transformation.

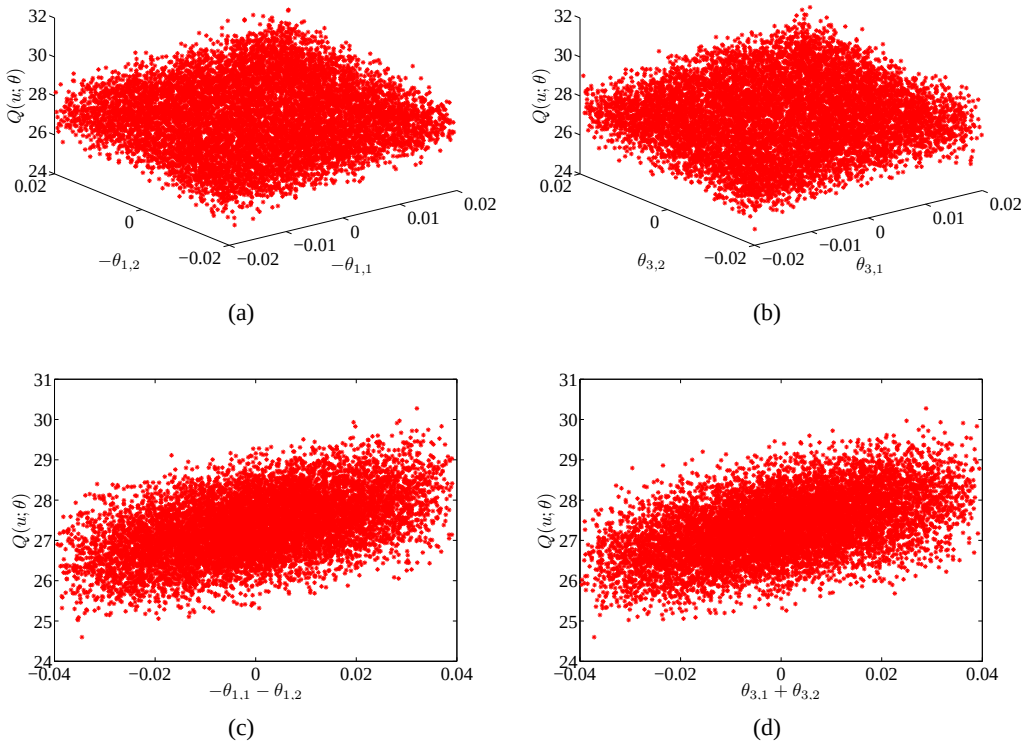

Fig. 9.9: The QOFI defined by $\psi(x, y) = 1$ plotted against the perturbations at corners 1 and 3.

10. CONCLUSION

In the first part of this dissertation, we study the nonlocal diffusion equation with so-called Lévy measure ν as the master equation for a pure-jump Lévy process. In the case $\nu \in L^1(\mathbb{R})$, a relationship to fractional diffusion is established in a limit of vanishing nonlocality, which implies the convergence of a compound Poisson process to a stable process. In the case $\nu \notin L^1$, an equivalence with fractional diffusion is reviewed and the smoothing of the nonlocal operator is shown to correspond precisely to the activity of the underlying Lévy process and the variation of its sample paths. We introduce volume-constrained nonlocal diffusion equations and demonstrate that they are the master equations for Lévy processes restricted to a bounded domain. The ensuing variational formulation and conforming finite element method provide a powerful tool for studying both Lévy processes and fractional diffusion on bounded, non-simple geometries with volume constraints.

In the second part of this dissertation, we consider the problem of estimating the distribution of a quantity of interest computed from the solution of an elliptic partial differential equation posed on a domain $\Omega(\boldsymbol{\theta}) \subset \mathbb{R}^2$ with a randomly perturbed boundary, where $\boldsymbol{\theta}$ is a random vector with given probability structure. We construct a piecewise smooth transformation from a partition of $\Omega(\boldsymbol{\theta})$ to a reference domain Ω in order to avoid the complications associated with solving the problems on $\Omega(\boldsymbol{\theta})$. The domain decomposition formulation is exploited by localizing the effect of the randomness to boundary elements in order to achieve a computationally efficient Monte Carlo sampling procedure. An a posteriori error analysis for the approximate distribution, which includes a deterministic error for each sample and a stochastic error from the effect of sampling, is also presented. We thus provide an efficient means to estimate the distribution of a quantity of interest via a Monte Carlo sampling procedure while also providing a posteriori error estimates for each sample.

BIBLIOGRAPHY

[1] F. Andreu, J. M. Mazón, J. D. Rossi, and J. Toledo. A nonlocal p-Laplacian evolution equation with Neumann boundary conditions. *Journal de Mathmatiques Pures et Appliqus*, 90(2):201 – 227, 2008.

[2] F. Andreu, J. M. Mazón, J. D. Rossi, and J. Toledo. A nonlocal p-Laplacian evolution equation with nonhomogeneous Dirichlet boundary conditions. *SIAM Journal on Mathematical Analysis*, 40(5):1815–1851, 2009.

[3] F. Andreu, J. M. Mazón, J. D. Rossi, and J. Toledo. *Nonlocal Diffusion Problems*, volume 165 of *Mathematical Surveys and Monographs*. American Mathematical Society, 2010.

[4] D. Applebaum. *Lévy Processes and Stochastic Calculus*, volume 93 of *Cambridge studies in advanced mathematics*. Cambridge, 2004.

[5] G. L. Aranovich and M. D. Donohue. Eliminating the mean-free-path inconsistency in classical phenomenological model of diffusion for fluids. *Physica A: Statistical Mechanics and its Applications*, 373:119–141, 2007.

[6] G. L. Aranovich and M. D. Donohue. Diffusion in fluids with large mean free paths: Nonclassical behavior between Knudsen and Fickian limits. *Physica A: Statistical Mechanics and its Applications*, 388:3355–3370, 2009.

[7] M. Arnst and R. Ghanem. Probabilistic Electromechanical Modeling of Nanostructures with Random Geometry. *Journal of Computational and Theoretical Nanoscience*, 6(10):2256–2272, 2009.

[8] I. Babuška and P. Chatzipantelidis. On solving elliptic stochastic partial differential equations. *Computer Methods in Applied Mechanics and Engineering*, 191(37-38):4093–4122, 2002.

[9] I. Babuška and J. Chleboun. Effects of uncertainties in the domain on the solution of Neumann boundary value problems in two spatial dimensions. *Mathematics of Computation*, 71(240):1339–1370, 2002.

[10] I. Babuška and J. Chleboun. Effects of uncertainties in the domain on the solution of Dirichlet boundary value problems. *Numerische Mathematik*, 93(4):583–610, 2003.

[11] I. Babuška, F. Nobile, and R. Tempone. Worst case scenario analysis for elliptic problems with uncertainty. *Numerische Mathematik*, 101(2):185–219, 2005.

[12] I. Babuška, F. Nobile, and R. Tempone. A stochastic collocation method for elliptic partial differential equations with random input data. *Siam J. Numer. Anal*, 45(3):1005–1034, 2007.

[13] I. Babuška, R. Tempone, and G. E. Zouraris. Galerkin finite element approximations of stochastic elliptic partial differential equations. *Siam J. Numer. Anal*, 42(2):800–825, 2004.

[14] K. Barmak, M. Emelianenko, D. Golovaty, D. Kinderlehrer, and S. Taasan. Towards a statistical theory of texture evolution in polycrystals. *SIAM Journal on Scientific Computing*, 30(6):3150–3169, 2008.

[15] S. K. Bhowmik. Stability and convergence analysis of a one step approximation of a linear partial integro-differential equation. *Numerical Methods for Partial Differential Equations*, 2010.

[16] M. G. Blyth and C. Pozrikidis. Heat conduction across irregular and fractal-like surfaces. *International Journal of Heat and Mass Transfer*, 46(8):1329–1339, 2003.

[17] F. Bobaru and M. Duangpanya. The peridynamic formulation for transient heat conduction. *International Journal of Heat and Mass Transfer*, 53(19–20):4047–4059, 2010.

[18] K. Bogdan, T. Byczkowski, T. Kulczycki, M. Ryznar, R. Song, and Z. Vondraček. *Potential analysis of stable processes and its extensions*, volume 1980. Springer Verlag, 2009.

[19] M. Brady and C. Pozrikidis. Diffusive transport across irregular and fractal walls. *Proceedings: Mathematical and Physical Sciences*, 442(1916):571–583, 1993.

[20] S. Broyda, M. Dentz, and D. M. Tartakovsky. Probability density functions for advective–reactive transport in radial flow. *Stochastic Environmental Research and Risk Assessment*, pages 1–8, 2010.

[21] N. Burch and R. B. Lehoucq. Classical, nonlocal, and fractional diffusion equations on bounded domains. *International Journal for Multiscale Computational Engineering*, 2011.

[22] N. Burch and R. B. Lehoucq. Continuous-time random walks on bounded domains. *Phys. Rev. E*, 83(1), 2011. Copyright 2011 by the American Physical Society.

[23] C. Canuto and D. Fransos. Numerical solution of partial differential equations in random domains: an application to Wind Engineering. 2009.

[24] C. Carrillo and P. Fife. Spatial effects in discrete generation population models. *Journal of Mathematical Biology*, 50(2):161–188, 2005.

[25] C. Cattaneo. Sulla conduzione del calore. *Atti Sem. Mat. Fis. Univ. Modena*, 3(3):21, 1948.

[26] E. Chasseigne, M. Chaves, and J. D. Rossi. Asymptotic behavior for nonlocal diffusion equations. *Journal de mathématiques pures et appliquées*, 86(3):271–291, 2006.

[27] X. Chen and M. Gunzburger. Continuous and discontinuous finite element methods for a peridynamics model of mechanics. *Computer Methods in Applied Mechanics and Engineering*, 2010.

[28] M. Dentz, A. Cortis, H. Scher, and B. Berkowitz. Time behavior of solute transport in heterogeneous media: Transition from anomalous to normal transport. *Advances in Water Resources*, 27(2):155–173, 2004.

[29] Q. Du, M. Gunzburger, R. B. Lehoucq, and K. Zhou. Analysis and approximation of nonlocal diffusion problems with volume constraints.

[30] A. Einstein. *Investigations on the Theory of the Brownian Movement*. Dover Pubns, 1956.

[31] E. Emmrich and O. Weckner. The peridynamic equation of motion in non-local elasticity theory. In *III European Conference on Computational Mechanics. Solids, Structures and Coupled Problems in Engineering, Lisbon, Springer*, volume 19, 2006.

[32] V. J. Ervin and J. P. Roop. Variational formulation for the stationary fractional advection dispersion equation. *Numerical Methods for Partial Differential Equations*, 22:558–576, 2005.

[33] D. Estep, A. Malqvist, and S. Tavener. Nonparametric density estimation for randomly perturbed elliptic problems I: computational methods, a posteriori analysis, and adaptive error control. *SIAM Journal on Scientific Computing*, pages 08–00261, 2008.

[34] D. Estep, A. Malqvist, and S. Tavener. Nonparametric density estimation for randomly perturbed elliptic problems II: Applications and adaptive modeling. *International Journal for Numerical Methods in Engineering*, 2009.

[35] G. Gilboa and S. Osher. Nonlocal operators with applications to image processing. *UCLA CAM Report*, pages 07–23, 2007.

[36] M. Gunzburger and R. B. Lehoucq. A nonlocal vector calculus with application to nonlocal boundary value problems. *Multiscale Modeling and Simulation*, 8:1581–1598, 2010.

[37] L. I. Ignat and J. D. Rossi. Decay estimates for nonlocal problems via energy methods. *J. Math. Pures Appl.*, 92:163–187, 2009.

[38] S. Jespersen, R. Metzler, and H. C. Fogedby. Levy flights in external force fields: Langevin and fractional Fokker-Planck equations and their solutions. *Physical Review - Series E*, 59:2736–2745, 1999.

[39] D. D. Joseph and L. Preziosi. Heat waves. *Reviews of Modern Physics*, 61(1):41–73, 1989.

[40] D. Jou, J. Casas-Vázquez, and M. Criado-Sancho. *Thermodynamics of fluids under flow*. Springer-Verlag New York Inc, 2001.

[41] V. M. Kenkre, E. W. Montroll, and M. F. Shlesinger. Generalized master equations for continuous-time random walks. *Journal of Statistical Physics*, 9(1):45–50, 1973.

[42] J. Klafler and I. M. Sokolov. Anomalous diffusion spreads its wings. *Physics World*, 18(8):29, 2005.

[43] J. Klafter, M. F. Shlesinger, and G. Zumofen. Beyond brownian motion. *Physics Today*, 49:33, 1996.

[44] N. Krepysheva, L. Di Pietro, and M. C. Néel. Fractional diffusion and reflective boundary condition. *Physica A: Statistical Mechanics and its Applications*, 368(2):355–361, 2006.

[45] G. Lebon, D. Jou, and J. Casas-Vázquez. *Understanding Non-equilibrium Thermodynamics: Foundations, Applications, Frontiers*. Springer Verlag, 2007.

[46] R. B. Lehoucq and O. Anatole von Lilienfeld. Translation of Walter Noll's "Derivation of the Fundamental Equations of Continuum Thermodynamics from Statistical Mechanics". *Journal of Elasticity*, 100:1–20, 2010.

[47] F. Mainardi, M. Raberto, R. Gorenflo, and E. Scalas. Fractional calculus and continuous-time finance II: the waiting-time distribution. *Physica A: Statistical Mechanics and its Applications*, 287(3-4):468–481, 2000.

[48] M. M. Meerschaert, J. Mortensen, and S. W. Wheatcraft. Fractional vector calculus for fractional advection-dispersion. *Physica A: Statistical Mechanics and its Applications*, 367:181–190, 2006.

[49] R. Metzler and J. Klafter. The random walk's guide to anomalous diffusion: a fractional dynamics approach. *Physics Reports*, 339(1), 2001.

[50] B. Milligen, I. Calvo, and R. Sánchez. Continuous time random walks in finite domains and general boundary conditions: some formal considerations. *Journal of Physics A: Mathematical and Theoretical*, 41:215004, 2008.

[51] W. Min, G. Luo, B. J. Cherayil, S. C. Kou, and X. S. Xie. Observation of a power-law memory kernel for fluctuations within a single protein molecule. *Physical review letters*, 94(19):198302, 2005.

[52] E. W. Montroll and G. H. Weiss. Random walks on lattices. II. *Journal of Mathematical Physics*, 6:167, 1965.

[53] S. P. Neuman and D. M. Tartakovsky. Perspective on theories of non-Fickian transport in heterogeneous media. *Advances in Water Resources*, 32:670–680, 2009.

[54] W. Noll. Die Herleitung der Grundgleichungen der Thermomechanik der Kontinua aus der statistischen Mechanik. *Indiana Univ. Math. J.*, 4:627–646, 1955. Original publishing journal was the J. Rational Mech. Anal. See the English translation [46].

[55] A. Nouy, A. Clement, F. Schoefs, and N. Moès. An extended stochastic finite element method for solving stochastic partial differential equations on random domains. *Computer Methods in Applied Mechanics and Engineering*, 197(51-52):4663–4682, 2008.

[56] R. M. Oba. Global boundary flattening transforms for acoustic propagation under rough sea surfaces. *The Journal of the Acoustical Society of America*, 128:39, 2010.

[57] B. K. Øksendal. *Stochastic differential equations: an introduction with applications*. Springer, 2003.

[58] A. Papapantoleon. An introduction to Lévy processes with applications in finance. *Lecture Notes*, 2006.

[59] P. Paradisi, R. Cesari, F. Mainardi, A. Maurizi, and F. Tampieri. A generalized Fick's law to describe non-local transport effects. *Physics and Chemistry of the Earth, Part B: Hydrology, Oceans and Atmosphere*, 26(4):275–279, 2001.

[60] I. Podlubny. Fractional differential equations, 1999.

[61] I. Podlubny, A. Chechkin, T. Skovranek, Y. Q. Chen, and B. M. Vinagre Jara. Matrix approach to discrete fractional calculus II: Partial fractional differential equations. *Journal of Computational Physics*, 228:3137–3153, 2009.

[62] G. Ramos-Fernandez, J. L. Mateos, O. Miramontes, G. Cocho, H. Larralde, and B. Ayala-Orozco. Lévy walk patterns in the foraging movements of spider monkeys (Ateles geoffroyi). *Behavioral Ecology and Sociobiology*, 55(3):223–230, 2004.

[63] R. Schumer, D. A. Benson, M. M. Meerschaert, and B. Baeumer. Multiscaling fractional advection-dispersion equations and their solutions. *Water Resour. Res.*, 39(1):1022, 2003.

[64] I. M. Sokolov and J. Klafter. From diffusion to anomalous diffusion: A century after Einsteins Brownian motion. *Chaos: An Interdisciplinary Journal of Nonlinear Science*, 15:026103, 2005.

[65] D. M. Tartakovsky and D. Xiu. Stochastic analysis of transport in tubes with rough walls. *Journal of Computational Physics*, 217(1):248–259, 2006.

[66] D.D. Wackerly, W. Mendenhall, and R.L. Scheaffer. *Mathematical statistics with applications*. Thomson, Brooks/Cole, 2008.

[67] D. Xiu. *Numerical Methods for Stochastic Computations: A Spectral Method Approach*. Princeton Univ Pr, 2010.

[68] D. Xiu and J. Shen. An efficient spectral method for acoustic scattering from rough surfaces. *Communications in computational physics*, 2:54–72, 2007.

[69] D. Xiu and D. M. Tartakovsky. A two-scale nonperturbative approach to uncertainty analysis of diffusion in random composites. *Multiscale Model. Simul*, 2(4):662–674, 2004.

[70] D. Xiu and D.M. Tartakovsky. Numerical methods for differential equations in random domains. *SIAM Journal on Scientific Computing*, 28(3):1167–1185, 2007.

[71] H. Zhang, F. Liu, and V. Anh. Numerical approximation of Lévy-Feller diffusion equation and its probability interpretation. *Journal of Computational and Applied Mathematics*, 206(2):1098–1115, 2007.

[72] K. Zhou and Q. Du. Mathematical and numerical analysis of linear peridynamic models with nonlocal boundary conditions. *SIAM J. Num. Anal*, 48(5):1759–1780, 2010.

[73] A. Zoia, A. Rosso, and M. Kardar. Fractional Laplacian in bounded domains. *Physical Review E*, 76(2):21116, 2007.